1-1-2013

Formulation Devlopment Of Mesoporous Silica Nanoparticles As An Injectable Delivery System

Amit S. Wani
Wayne State University,

FORMULATION DEVELOPMENT OF MESOPOROUS SILICA NANOPARTICLES AS AN INJECTABLE DELIVERY SYSTEM

by

AMIT WANI

DISSERTATION

Submitted to the Graduate School

of Wayne State University,

Detroit, Michigan

in partial fulfillment of the requirements

for the degree of

DOCTOR OF PHILOSOPHY

2013

MAJOR: PHARMACEUTICAL SCIENCES

Approved by:

_____

Advisor Date

_____

_____

_____

DEDICATION

I would like to dedicate this dissertation to my mom, Rekha Wani and dad, Suresh Wani for their continuous support and motivation.

ACKNOWLEDGEMENTS

I would like to express my deepest gratitude and sincere thanks to my PhD advisor, Prof. David Oupický for his continuous support and encouragement, and most importantly being patient with me. I sincerely thank of him for standing by me through thick and thin during this incredible journey.

During this process of acknowledgement writing, I have been thinking what is the one thing that Dr. Oupický gave me and I thought, he made me think critically. As Socrates once said, "I cannot teach anybody anything, I can only make them think." Dr. Oupický motivated me to think and ask critical questions and I will be deeply indebted him for this. I cherish every moment I have spent with him. Every meeting with him not only thought me about drug delivery but also tantamount to a lesson in a day-to-day life. I not only think of him as a PhD mentor but a real life advisor whom I will definitely bank on for suggestions in the future.

I would also like to thank my committee members, Profs. Stephanie Brock (Department of Chemistry), Joshua Reineke and Deepak Bhalla for their professional suggestions and guidance. I specifically thank Prof. Stephanie Brock for valuable comments during committee meetings. I still remember her "Bread and Butter" comment, which was a true revelation and extremely motivating. I also thank Dr. Brock's group members Raja and Layan for providing mesoporous silica nanoparticles for the project without which none of my work would have been accomplished. Special thank goes to Raja for the optimization of silica synthesis process and for his support during the first phase of the project. I am grateful to DLAR for providing animal

handling training and for all help. I also thank Dr. Lisa Polin from the Karmanos Cancer Institute for the training of the development of MDA-MB-231 tumor model.

I am obliged to the Department of Pharmaceutical Sciences for giving me the opportunity in this exciting graduate program. I specifically thank department Chair, Dr. George Corcoran for providing me great support in this incredible journey. I also thank then department graduate officer, Dr. Hanley Abramson for providing me great opportunity and help in the beginning of my studies at Wayne State University.

Finally yet importantly, I would like to thank my friends and family without whose support this journey might not have been fruitful. I would also like to acknowledge my maternal grandfather, Bapu S. Wani for his blessings whose life-struggle inspired me since childhood.

TABLES OF CONTENT

LIST OF TABLES

LIST OF FIGURES

LIST OF SCHEMES

CHAPTER 1

INTRODUCTION

1.1 Nanoparticles and cancer chemotherapy

Nanotechnology has great potential in the cancer therapy as it may provide enhanced efficacy and reduced side effects over conventional treatments such as radiation and chemotherapy (Farokhzad and Langer, 2009; Schroeder et al., 2012). These features are mainly due to the improved solubility of hydrophobic drugs (Ensign et al., 2012), ability to encapsulate drug combinations (Milane et al., 2011a), decreased drug resistance (Jabr-Milane et al., 2008), higher accumulation of drugs in tumors (SchÃ¤dlich et al., 2011) and active intracellular delivery of nanoparticles in the tumor cells (Panyam and Labhasetwar, 2003). Various strategies have been investigated to localize nanoparticles at tumor sites, including passive tumor targeting by Enhanced Permeation and Retention (EPR) effect (Greish, 2007; Matsumura and Maeda, 1986) and active targeting by attaching targeting moieties that bind to receptors which are specifically over-expressed in cancer cells (Brigger et al., 2002). Based on these strategies, nanoparticles have been investigated to kill tumor cells and to spare healthy tissues but much success has not been accomplished yet. The main reasons for the limiting success are variable drug release pattern, low drug loading capacity of nanoparticles, aggregation of nanoparticles, which leads to increase in the uptake by reticuloendothelial (RES) system, and limitations to combine with other emerging therapies such as gene therapy (Brannon-Peppas, 1995; Dobrovolskaia et al., 2008; Schroeder et al., 2012). Different types of nanocarriers such as polymeric nanoparticles, micelles, liposomes and inorganic nanoparticles haven been investigated to address these complex problems but search for the “magic bullet” is still on (Farokhzad and Langer, 2009; Nasongkla et al., 2006; Schroeder et al., 2012).

1.2 Mesoporous Silica Nanoparticles

Since discovery of M415 material family by Mobil Corporation scientists in 1992 and the application of MCM-41 materials in the drug delivery by Vallet Regi et al. in 2000 (Vallet-Regi et al., 2000), mesoporous silicas have been widely investigated as a reservoir for controlled drug delivery and theranostics (Zhang et al., 2012), and as a platform for drug-gene combinations (Chen et al., 2009a). Feasibility of adjusting the pore size of nanoparticles offers a versatile platform for inclusion of drug molecules in the silica matrix despite of differences in their physicochemical properties (Lu et al., 2007a; Wani et al., 2012). Generally, polymer matrices have been reported as controlled drug delivery systems which encapsulate drugs (Farokhzad and Langer, 2009) as well as act as a crystallization inhibitor for guest molecules (Panyam et al., 2004). Heterogeneous distribution of drug molecules in the polymeric matrix affects the release rate between different samples (Huang and Brazel, 2001). Materials with homogenous porosity would facilitate homogenous drug distribution and much improvement in the drug release would be expected (Vallet-Regi et al., 2000). Well defined, homogenous porous structure of mesoporous silica fulfills these parameters and presents an interesting alternative for the polymeric devices.

Mesoporous silica offers high surface area, easy surface functionalization, high drug loading capacity, compatibility with hydrophilic as well as hydrophobic drug molecules, amorphization of pharmaceuticals and high biocompatibility all of which may play an important role in the oral as well as injectable formulations (Bhattarai et al., 2010; Meng et al., 2011a; Qian and Bogner, 2011). In this section, I will present a current status of mesoporous silica nanoparticles (MSN) as oral and injectable drug delivery systems.

1.2.1 Current status of MSN in drug delivery

1.2.1.1 MSN as oral drug delivery systems

Oral administration of drugs is simplest, easiest and most common route of administration. During absorption of drugs from GI tract, drug molecules enter into liver via portal circulation called “First Pass”. During this process, drugs may be metabolized in the liver before being bioavailable and hence, first pass metabolism is the biggest challenge and disadvantage of oral drug delivery. However, not all drugs are orally bioavailable. This includes poorly soluble drugs, large molecules, highly charged compounds or drugs susceptible to degradation by stomach acid or various enzymes in the GI tract. Formulation development strategies play an important role in facilitating absorption of such molecules from the GI tract (Ensign et al., 2012). Rate of dissolution is a rate-limiting step for poorly soluble class II drugs (Biopharmaceutical Classification System) and selection of physical form (crystalline or amorphous) of drug candidate by solid-state characterization is important for oral bioavailability (Panyam et al., 2004; Takano et al., 2008). In general, amorphous drugs are thermodynamically unstable, especially in the presence of water, with decrease in the glass transition temperature (Tg), transformation of amorphous-to-crystalline form have been widely reported (Qian and Bogner, 2011; Yu, 2001). Because of the above mentioned issues, amorphous forms are rarely chosen for the development of solid dosage forms. However, polymorphs (different crystal structure but the same chemical composition) create profound implications on formulation development with significantly different solubility, dissolution rate, compactibility, hygroscopicity, physical and chemical stability (Kawakami, 2012). Polymorph that gives higher solubility and faster dissolution rate is usually a preferred candidate for oral delivery. However, it is worth noting that polymorph with the high solubility and faster dissolution rate is also a

metastable (i.e. high-energy form) and conversion of metastable to thermodynamically more stable polymorph is often possible, resulting in lower oral bioavailability. For example, in the case of ritonavir, an antiretroviral agent, the most stable form appeared after two years after launch of the product due to conformational polymorphism which resulted in formation of polymorph with distinct differences in the solubility pattern and threatened sale of the product (Bauer et al., 2001; Kawakami, 2012). Therefore, companies prefer to select most thermodynamically stable polymorph for formulation development.

Various strategies such as salts, prodrugs, particle size reduction, solubilizing excipients, microemulsions, co-solvents and cyclodextrin-based inclusion complexes have been widely investigated to increase solubility and dissolution rate to achieve satisfactory absorption and bioavailability (Davis and Brewster, 2004; Kawakami, 2012). Amorphization (crystalline-to-amorphous transformation) of active pharmaceutical ingredients (API) is an actively pursued area of research. Ordered structure of a crystal may be disrupted by solid dispersion, supercooling, dehydration, milling, and annealing of metastable crystalline forms (Kawakami, 2012; Qian and Bogner, 2011; Willart and Descamps, 2008). As mentioned above, such amorphous forms are present in the higher energy state and spontaneous re-crystallization over time might negate the solubility advantage. However, formulators should take care in selecting such amorphization technique to achieve required physical and chemical stabilities from the therapeutic standpoint. Out of the above-mentioned approaches, solid dispersion has been proved to be the most successful in enhancing dissolution profile and solubility (Panyam et al., 2004; Qian and Bogner, 2011). In general, solid dispersion technology can be classified into eutectic mixtures, solid solutions and physical mixture of microcrystalline drug dispersed in the polymeric carrier. When drug is molecularly dispersed in polymer, driving force for drug

crystallization is reduced and polymers kinetically act as a crystallization inhibitor by lowering the mobility of drug molecules. Widely used solid dispersion agents are polyethylene glycol (PEG), polyvinylpyrrolidone (PVP), sugars, and urea. It is generally believed that solid dispersions can enhance the dissolution rate through one or combination of the following factors:

(a) Increasing surface area: a drug exists as fine crystalline particles in a solid dispersion, which drastically increases surface area of the drug compared to conventional formulation

(b) Surface modification through intimate contact with hydrophilic carrier: when eutectic mixture or physical mixture is formed, surface properties of drug molecules are modified with hydrophilic polymer such that it wets surface more easily.

(c) Increased solubility through formation of solid solution: In case of solid solution, hydrophilic carrier molecules are replaced with drug molecules or interstitial positioning of drug molecules in the polymer carrier lattice to form a one phase system. Such drug forms a molecular dispersion and is present in a molecular state called as a “solid solution” the step of drug dissolution is bypassed.

Disadvantage of solid dispersion strategies are mainly related to their physical stability (Serajuddin, 1999). Physical treatments such as pulverization and ageing may destabilize the system and changes can occur in the crystalline profile and a dissolution rate. Moisture absorption and temperature are critical factors in destabilizing high-energy, metastable forms, causing phase separation, crystal growth or conversion to stable crystalline form during storage, which may result in variable oral bioavailability. Selection of material which will give single phase system with drug molecules that will remain miscible with the material is important for long-term physical stability and there is a need for thermally and chemically stable material

which will act as an amorphization platform for poorly soluble class II drugs (Qian and Bogner, 2011).

Mesoporous silica offers large surface area (e.g. greater than 500 m^2/g), well ordered porous structure, high pore volume (approximately 1 cm^3/g), high mechanical strength, thermal and chemical stability, and resistance to microbial attack as compared to their polymeric counterparts (Bhattarai et al., 2010; Qian and Bogner, 2011; Rosenholm et al., 2010b). Large surface area allows adsorption of drug molecules into nanosized capillaries, thus decreasing overall Gibbs free energy and stabilizing the system at a lower free energy state. The adsorbed molecules are present in the amorphous form in the silica matrix because the silica matrix prevents crystal growth and nucleation due to the pore size-constraint effect. Amorphous porous silica system will crystallize only when thermodynamic states of the system are perturbed (Martens et al., 2008; Qian and Bogner, 2011). Mesoporous silica is thus an interesting excipient which may act as a crystallization inhibitor as well as a conventional glidant to improve flow properties, thus facilitating dual function in the development of oral dosage forms. By controlling surface functionalization, silica can be used in the immediate as well as controlled release solid dosage formulations. Efforts have been made to improve oral bioavailability of itaconazole, a triazole antimycotic compound, which has low aqueous solubility (less than 1 ng/ml at pH = 7) (Mellaerts et al., 2008b). Mellaerts and co-workers prepared solid dispersion of itraconazole using mesoporous silica and found that molecularly dispersed itraconzaole was present in the amorphous form, which was confirmed by the absence of Tm and Tg in the tested formulation. Dissolution studies of the mesoporous silica-based intraconazole formulation showed higher solubility of the amorphous formulation when compared with pure crystalline itraconazole (Mellaerts et al., 2007). Based on the similar principle, solubility improvement was

observed for wide range of compounds when formulated with porous silicas, including carbamazepine (Thomas et al., 2010), carvedilol (Hu et al., 2012), diazepam, indomethacin, grisofulvin, ketoconazole (Van Speybroeck et al., 2009), ibuprofen (Martens et al., 2008), nifedipine and telmisartan (Zhang et al., 2010a). The unique phase transformation of drugs in the presence of mesoporous materials can be advantageous in formulating and delivering poorly soluble class II drugs to improve oral bioavailability. MSN-based solid dispersion is a potential way to solve stability-related problems and a suitable alternative to polymer-based solid dispersion technique. More work is needed to elucidate detailed mechanism of amorphization and to promote the use of MSN in oral delivery systems.

1.2.1.2 MSN as injectable delivery systems

Another important aspect of mesoporous silicas is their potential as a colloidally-stable injectable formulation because of the easy surface functionalization, biocompatibility, controlled rate of degradation, and control over particle size and shape during synthesis (Bhattarai et al., 2010; Chen et al., 2009a; Rosenholm et al., 2010b). Generally, particles below 200 nm are suitable for intravenous administration and simple but robust method of MSN synthesis facilitates desired particle size with homogenous porous structure. Suitable properties of injectable nanoparticle formulations include limited aggregation, long circulation time, biodegradability, absence of dose dumping, and ability to home to the targeted site (Farokhzad and Langer, 2009; Schroeder et al., 2012). An optimal delivery system for effective anticancer therapy should be able to reach desired tumor site with minimal loss of activity while in the circulation. After reaching the tumor tissue, particles should enable a controlled delivery of cargo in the active form. Surface functionalization of MSN with PEG and tumor targeting ligands may have the potential to satisfy the above-mentioned requirements.

Nanoparticles without surface modification are usually rapidly cleared from the circulation by RES based on the nanoparticles size and surface properties such as charge, and hydrophobicity (Fox et al., 2009). The fate of systemically administered particles can be controlled by adjusting particle size, particle shape and surface functionalization (Yu et al., 2012). Nanoparticles can be surface functionalized to achieve passive or active targeting by controlling size of the nanoparticles or by attaching targeting ligands (Rosenholm et al., 2010b; Schroeder et al., 2012). Incorporation of PEG also enables passive targeting to tumors via EPR effect (van Vlerken et al., 2007). PEG is a hydrophilic polymer, which helps to reduce charge on the particles and provides "stealth" coating for camouflaging particles from macrophages. On this topic, Nel and co-workers investigated effect of particle size reduction and polymer coating of MSN on passive accumulation in KB-31 luc xenograft model and reported enhanced rate of tumor shrinking with doxorubicin loaded MSN compared to free doxorubicin (Meng et al., 2011a). On the same note, passive targeting can also be achieved by controlling shape of the nanoparticles. Ghandehari and co-workers reported that rod-shaped gold nanoparticles accumulate at higher concentration in the tumor compared to spherical shaped gold nanoparticles which may be due to less recognition by macrophages, increase in the circulation time and higher tumor cell uptake (Arnida et al., 2011).

Active targeting can be achieved by conjugating targeting antibodies, peptides, aptamers and ligands overexpressed on cancer cells to the surface of nanoparticles (Rosenholm et al., 2010b). Surface functionalized nanoparticles can overcome P-gp- mediated drug resistance by avoiding recognition by P-gp because being enveloped in an endosome when entering cell, leading to higher intracellular drug concentration (Chavanpatil et al., 2006). Zink and co-workers functionalized camptothecin loaded MSN with folate and observed enhanced cytotoxicity with

about 60% cell death after 24 h for PANC 1 cells, however, non-targeted particles showed cytotoxicity of about 30% after 24 h (Liong et al., 2008). Successful active targeting of MSN was also reported by Rosenholm et al. who conjugated anti-cancer drug, methotrexate, which is structurally similar to folate, on the surface of MSN. In this way, methotrexate was able to act dually as a targeting ligand as well as a chemotherapeutic agent. They observed that methotrexate-MSN induced apoptotic cell death in cancerous HeLa cells while significantly less apoptosis was observed with the non-cancerous HEK-293 cells at the similar biological concentrations (Rosenholm et al., 2010a). The same authors also reported that the level of cancer cell apoptosis induced by MSN conjugated with methotrexate was significantly higher than the corresponding concentration of free methotrexate. Overall, mesoporous silica materials satisfy many of the pre-requisites for passive and active targeting mechanisms in tumor delivery.

MSN has been extensively investigated for controlled release of anti-cancer drugs (Li et al., 2010; Lu et al., 2007a; Meng et al., 2011a; Meng et al., 2010a; Wani et al., 2012), DNA (Bhattarai et al., 2010), siRNA (Chen et al., 2009a) as well as proteins (Lin et al., 2008). Controlled release was achieved by modifying MSN with various stimuli responsive barriers which protect the cargo from unwanted leakage during circulation but allow release of the content in response to specific stimulus at the targeted site. Effects of stimulus such as pH, temperature and redox gradient on controlled drug release have been widely studied (Bhattarai et al., 2010; Singh et al., 2011). Table 1 shows examples of such strategies capable of controlling release of guest molecules. Reliable controlled release of loaded cargo at physiological condition is a challenging endeavor and care should be taken in selecting the stimulus for particular application and disease condition. Though most of the below mentioned strategies worked in vitro, less effort has been invested in extrapolating these strategies towards preclinical setting.

Singh et al. reported that increase in the release of doxorubicin in response to proteases present at the tumor site *in vivo* and showed higher cellular apoptosis signifying importance of stimuli responsive delivery (Singh et al., 2011).

Table 1. Strategies capable of controlling release of guest molecules from MSN by specific stimulus

Stimulus	Capping barrier	Cargo	Application	Reference
Temperature	PNIPAM	Doxorubicin	Human sarcoma	(Singh et al., 2011)
Redox (DTT)	poly(2-diethylamino) ethyl methacrylate)	Rhodamine B	N.A.	(Kotsuchibashi et al., 2012)
pH	Chitosan	Ibuprofen	N.A.	(Popat et al., 2012)
Magnetic	Fe_3O_4	Fluorescein	N.A.	(Giri et al., 2005)
Redox (GSH)	β-cyclodextrin	Doxorubicin	Adenocarcinoma	(Kim et al., 2010)
pH	PDMAEMA	Chloroquine	Breast cancer	(Bhattarai et al., 2010)
pH	Polyethyleneimine/β-cyclodextrin polyseudorotaxane	Calcein	N.A.	(Park et al., 2007)
Protease	PNIPAM-co-PEG	Doxorubicin	Human sarcoma	(Singh et al., 2011)
Redox (H_2O_2)	IgG	Metal chelator	Alzheimer	(Geng et al., 2012)
Ultrasound	Chitosan	Ibuprofen	N.A.	(Depan et al., 2010)

N.A. Application is not reported

Polypseudorotaxane formation between cyclodextrin (CD) and PEI-b-PEG-b-PEI polymer undergoes selective complexation and decomplexation between CD and PEI as a function of pH. It served as a template for MSN to control the release of loaded cargo (Park et al., 2007). Calcein, a fluorescent molecule, was encapsulated into CD-MSN and controlled release of calcein as a function of pH was reported. Validity of such sophisticated mechanism needs to be verified with biologically important molecules in *in vitro* as well as in vivo settings.

Table 1 confirms that easy surface functionalization makes MSN a suitable platform to develop as a stimuli-responsive delivery system. To take advantage of this promising delivery system, it is necessary to focus on the physicochemical parameters of MSN that controls drug loading, drug release and overall biological outcome.

1.2.2 Physicochemical aspects of MSN

The ultimate goal of nanoparticles in anti-cancer therapy is to improve killing of cancer cells and to spare non-cancerous or healthy cells and tissues. To achieve such efficient targeted therapy, it is important to understand how physicochemical aspects of MSN such as particle synthesis, particle size, particle shape, surface functionalization, hydrolytic stability, redispersibility affect biological outcome.

1.2.2.1 Particle synthesis

In case of MSN, the particle size range of interest for targeted intracellular delivery is about 50-200 nm as large particles can be excreted out by immune systems and smaller particles are too difficult to synthesize as a consequence of inherent mesoporosity. Monodisperse particles are also preferred as it allows uniform biodistribution and homogenous release profile in the body (Farokhzad and Langer, 2009; Schroeder et al., 2012; Xie and Smith, 2010). Therefore, chemical synthesis methods have been widely used to prepare mesoporous silicas as opposed to physical methods such as spray-drying which results in large particles with wide particle size distribution (Rosenholm et al., 2010b). In most synthesis procedures, tetraethoxysilane (TEOS) has been used as a silica precursor. Cetyl trimethyl ammonium bromide (CTAB), a cationic ammonium salt, has been used as a structure-directing agent (Bhattarai et al., 2010; Giri et al., 2005). This sol-gel synthesis often referred as Stöber method leads to particles with pore size of

2-4 nm and cylindrical mesostructure arranged in a hexagonal fashion. Simple MSN synthesis also allows incorporation of functional groups by reacting respective functional silanes with the silica precursor. Selection of pore size of MSN depends upon the size of encapsulated cargo. Considering loading of anti-cancer small molecules, pore size of 2-4 nm is sufficient, however, recently efforts have been made in increasing pore size of MSN to accommodate macromolecules such as DNA and proteins (Gao et al., 2009; Slowing et al., 2007). Pore size modification can be easily achieved by the addition of pore swelling agent, trimethylbenzene (TMB), during condensation. However, care should be taken in such a way that TMB is preferentially solubilize in alcoholic solvent rather than encapsulated in micellar surfactant to achieve desired pore size (Rosenholm et al., 2010b; Slowing et al., 2007). The largest pore size for MSN is reported to be 20 nm (Gao et al., 2009). In this case, MSN was synthesized in acidic condition rather than alkaline condition with polymeric ABA block copolymer surfactant as the structure-directing agent. However, particle size distribution for these MSN are broader compared to MSN synthesized by alkaline condition.

A key important step in obtaining well-dispersed nanoparticles is the removal of surfactant template. Template removal is normally performed by acid hydrolysis, as thermal decomposition leads to the loss of surface functional groups present on the mesoporous structure. MSN obtained with thermal decomposition process also lead to inter-particle condensation and may increase the overall particle size distribution. It is worth noting that care should be taken in removal of CTAB completely as CTAB is cytotoxic and may hampered use to such system in the biological condition. Shi and co-workers recently reported a modified method of MSN synthesis to achieve highly dispersed particles with particle size as low as 25 nm with excellent colloidal stability (Pan et al., 2012). They incorporated hexadecyl trimetyl ammonium chloride (CTAC) as

a structure directing agent in a silica precursor. Size of the nanoparticles was controlled by addition of triethanolamine (TEA), with lower TEA content (0.02g) giving larger MSN (105 nm) while higher TEA content (0.08g) giving smaller particle size of 25 nm. However, surface area of particles decreased from 561 to 391 cm^2/g with decrease in the particle size from 105 nm to 25 nm. Similarly, Lin and co-workers reported a synthesis of rod shaped mesoporous silica nanoparticles by modifying conventional MSN synthesis and its application in controlled drug delivery confirming flexibility of material in obtaining desired particle size and shape (Giri et al., 2005). At the same time, surface modification of the mesoporous channels and/or external particle surfaces with various functional groups also gives more temporal control over manipulation of surface properties for controlled drug delivery and biomedical applications (Bhattarai et al., 2010; Giri et al., 2005; Rosenholm et al., 2010b; Slowing et al., 2007; Wani et al., 2012).

1.2.2.2 MSN hydrolytic stability

Another important aspect of nanoparticles used in drug delivery is their chemical stability in endogenous conditions. Particle dissolution profile is important to determine as it controls (i) drug release and (ii) overall drug circulation time *in vivo*. From toxicological point of view, it is important to understand degradation profile of MSN in aqueous conditions as it may help to elucidate long-term toxicity associated with nanoparticle accumulation. However, it is quite surprising that limited number of systematic studies have focused on the dissolution profile of MSN in the biological environment. Generally, exterior surface of MSN contains functional groups, targeting ligands and protective polymeric layers and it is necessary to understand MSN dissolution rate as faster degradation of particles may dissociate surface functionalities prior it reaches targeted site. Furthermore, hydrolytic stability is important for the Active Pharmaceutical

Ingredient (API) physical state as faster degradation of nanoparticles may change amorphization profile of the API due to the changes in the mesoporous structure. Walcarious et al. investigated dissolution profile of unmodified and amino- functionalized silica at different pH (Etienne and Walcarius, 2003). They found that amino-modified MSN dissolved at a faster rate than conventional silica under simulated biological conditions. The same group also reported that amine group dissociation reached plateau after 4 h indicating not all surface functionalities are dissociated from particles and signifies role of surface charge in increasing the rate of dissolution. Onida and co-workers investigated dissolution profile of mesoporous silica with

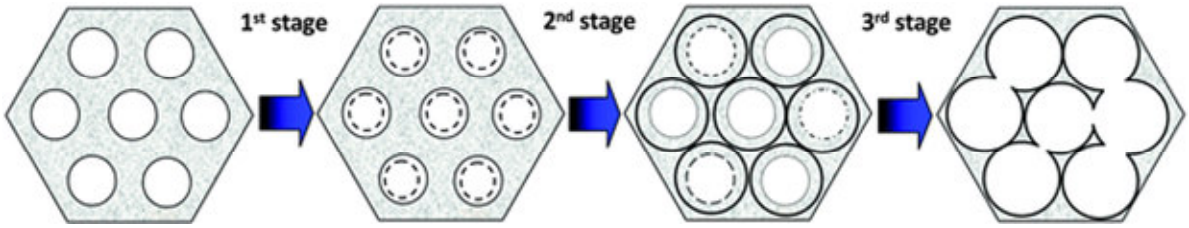

Scheme 1. Schematic illustration of the degradation profile of mesoporous silica in SBF proposed by He et al. The initial fast bulk degradation is retarded by the formation of Ca/Mg-silicate layer (stage 2) followed by a slow diffusion-controlled degradation behavior over several days (stage 3). Adapted from (He et al., 2010a).

particle size ranging from 200 to 800 nm in the simulated body fluid (Mortera et al., 2010). They found a rapid decrease in the mesopore volume during the first hour of incubation, while XRD confirmed the presence of mesoporous structure in the particles. Authors concluded that the dissolved silica re-deposited on the porous opening gradually closing the pores. Authors supported their claim by drug release measurements, where the drug release rate attained plateau at the same time when mesoporous volume was strongly diminished. Similarly, He et al. reported a three stage degradation behavior of MSN in simulated body fluid (Scheme 1) (He et al., 2010a). This study revealed rapid initial bulk degradation, followed by the deposition of calcium/magnesium silicate layer which drastically decreased the degradation rate. The third

stage involved a maintained slow diffusion of dissolved silica species, while the whole sample was degraded after 15 days of incubation. Interestingly, particle morphology remained intact after 24 h, even though etching and enlargement of pores was clearly observed. On the same note, Oupický and co-workers also observed degradation of silica with intact particle morphology after 24 h of incubation in biologically relevant media (Bhattarai et al., 2010). The hydrolysis of particles as a function of particle size under *in vivo* condition is important to understand as small particles may disintegrate faster than larger particles and this may affect clearance mechanism for different particle size silica. These results clearly highlight the need for detailed particle disintegration studies in relation to drug delivery application of MSN.

1.2.2.3 Drug loading

Large surface area, tunable pore size and pore volume make mesoporous silica an ideal candidate to load large amount of drug molecules in the porous structure. Based on the available literature, drug loading procedures can be classified as: (i) adsorption from solution, (ii) incipient wetness impregnation and (iii) melting of mixture of drug and mesoporous silica (Mellaerts et al., 2008a). MSN are suitable for hydrophilic as well as hydrophobic compounds and based on API solubility, drug-loading process can be performed in the organic solvent or water. Selection of loading method generally depends on the availability of API, its solubility profile and physicochemical properties.

In adsorption from solution method, slurry of API is usually stirred in presence of porous material to allow drug adsorption, followed by centrifugation or filtration to separate drug-loaded particles from solution. Although this is a widely used method, adsorption of drug molecules, in fact, is a low yielding process. Generally, drug molecules adsorb in a monolayer fashion which

can be modeled using Langmuir adsoprtion isotherm (Qian and Bogner, 2011; Rosenholm et al., 2010b). This is because after the first monolayer on the silica surface, succeeding drug layers are associated more closely with the solvent. Similarly, monolayer formation was also observed during protein adsorption from aqueous solutions (Vinu et al., 2004). For hydrophilic drugs, adjustment of pH is required to yield high drug loading levels than what is possible from organic media (Ma et al., 2011; Salonen et al., 2005). Zink and co-workers studied the effect of pH on loading of doxorubicin and found that higher loading was observed at neutral than at acidic pH (Meng et al., 2010a). Many studies have highlighted the possibility of using adsorption from solution method for hydrophilic as well as hydrophobic drugs (Bhattarai et al., 2010; Li et al., 2010; Liu et al., 2012; Meng et al., 2011a; Wani et al., 2012).

In incipient wetness method, measured concentration of drug solution is generally added into mesoporous silica to achieve sufficient surface wetting and solvent is evaporated at elevated temperature (Mellaerts et al., 2008a; Qian and Bogner, 2011). This method gives more control over drug loading as different concentrations of drug solution may be prepared to control drug loading degree based on the need of the specific application. Solubility of drug molecule in the selected solvent may limit the loading efficiency of this method. As incipient wetness allows direct control over the amount of drug to be transferred from solution to porous silica, it may compromise amorphization of drug molecules based on the rate of evaporation. There is a need to study the effect of speed of evaporation on solid state of the loaded molecules. In both of the above-mentioned methods, selection of solvent is very important as it contributes to the efficiency of drug loading.

The third method, heating or melting method, involves heating of drug-silica mixture up to the melting point of drug molecules allowing drug to enter into porous nano-confinement.

However, melted drugs often adsorb on the exterior surface of MSN, blocking access to the porous structure. Martens and co-worker loaded intraconazole by melt method and found that mesoporous volume, total pore volume and mesopore size was similar to that of the empty particle indicating melt method has little effect on porosity (Martens et al., 2008). They speculate that high viscosity of molten intraconazole may impede the flow of liquid into the pores. In addition, heating of mixture may lead to decomposition of the drug and functional groups in MSN, hence the melting method is less applicable in drug loading for MSN.

1.2.2.4 MSN formulation

In this section, development of MSN formulations of small molecules is first discussed, followed by the colloidal stability approaches and drug release mechanism. Selection of MSN properties strictly depends upon the physicochemical properties of API. Formulators should follow the following steps in developing MSN formulations:

(1) Determine physicochemical properties of API such as pKa, log P, molecular weight and molecular size.

(2) Determine solubility of API. For hydrophilic compounds, effect of pH on solubility should be determined.

(3) Select pore size, surface functionalization, based on physicochemical properties of API

(4) Route of administration (rod shape particle may be useful for improvement in the total blood circulation time) and the specific need of the application (PEGylation, polymer modification, attachment of targeted moiety and imaging agent)

(5) Selection of drug loading method based on physicochemical properties and solubility profile of API

(6) Loading of drug molecules into MSN

(7) Investigate the effect of pre and post-surface modifications such as PEGylation, polymer attachment on drug loading

(8) Determination of loading of MSN by HPLC and TGA

(9) Characterization of drug-loaded MSN by DLS, DSC, PXRD, TEM

The above mentioned steps are summarized in Scheme 2.

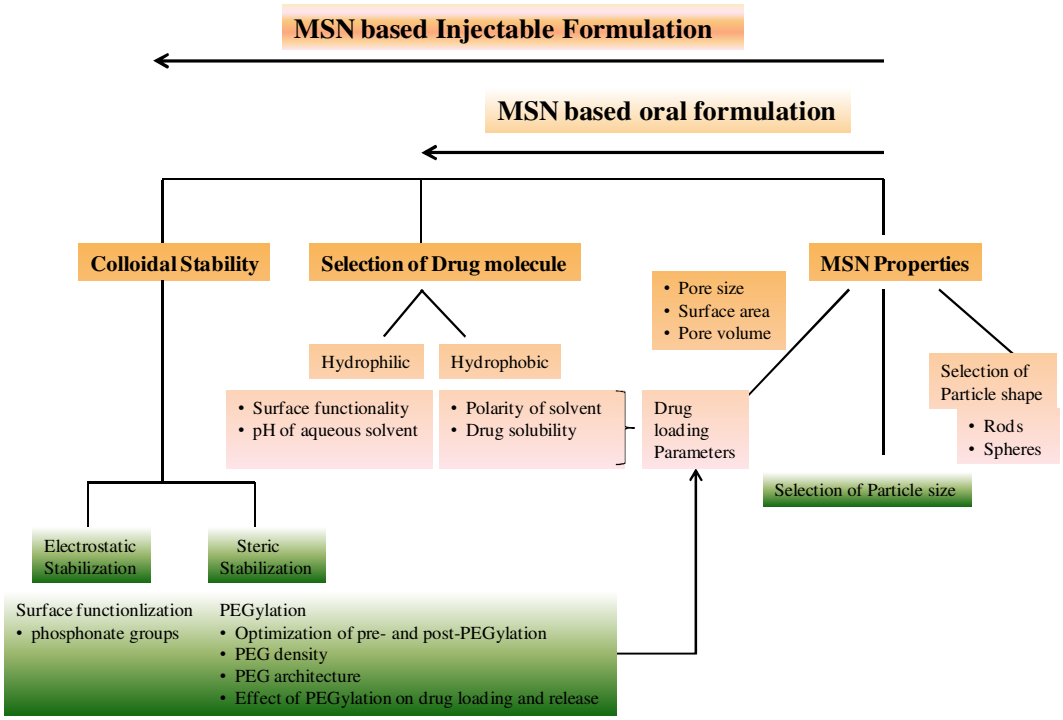

Scheme 2. Schematic representation of development of MSN based injectable formulation

The aggregation of unmodified MSN in solution leads to erroneous *in vivo* profile. The aggregates or particles with sizes above ~200 nm in diameter are readily bound with opsonin proteins and cleared by liver and spleen decreasing concentration of drug in the blood compartment. Opsonin proteins are more likely to bind to hydrophobic or charged particles than

hydrophilic or neutral particles, which accelerates rate of elimination by liver and spleen (Farokhzad and Langer, 2009; Fox et al., 2009). On this topic, it is necessary to develop long-circulating, colloidally stable particles to take full advantage of particulate delivery system. Colloidal particles are generally stabilized by electrostatic or steric stabilization. If attractive forces such as Van der Waals forces prevail over repulsive forces such as electrostatic forces, particle aggregate in clusters. Aqueous suspensions are widely stabilized by electrostatic stabilization, achieved by the repulsion of equally charged particles. It is considered that electrostatic stabilization results from the formation of electric double layer on the particle surface and is a function of pH and the ionic strength of the solution. The strength of repulsive forces decreases with the increase in the distance between particles. In this case, determination of isoelectric point of nanoparticles is important as at this pH the net particle charge is zero. It is considered that aqueous suspensions with absolute values of zeta potential above 30 mV are physically stabilized by electrostatic stabilization. In case of MSN, presence of high surface concentration of silanol groups can lead to formation of siloxane bridges between the particles making colloidal stability a challenge (Rosenholm et al., 2010b). Phosphonate modification of MSN can overcome the aggregation, making the particles more dispersible (Lu et al., 2007a). On the same note, it is reported that amino-functionalized MSN have higher redispersibility compared to thiol-modified MSN, suggesting importance in the selection of surface functionality (Rosenholm et al., 2010b). Polymer modification of MSN by cationic polymers such as PEI also leads to higher zeta potential making particles more electrostatically stable (Bergman et al., 2008). Under *in vivo* condition, electrostatic stabilization is less efficient due to the adsorption of proteins on the charged particle surface which makes particles more recognizable to the immune system.

Steric stabilization is another approach of achieving highly stable aqueous suspensions by adsorption or covalent attachment of polymers to the surface of MSN. In steric stabilization, polymer chains prevent particles to get close in the range of attractive Van der Waals forces. Hydrophilic polymers such as PEG have been widely used to stabilize particles by steric stabilization. Sometimes particles are stabilized by electrostatic as well as steric stabilization which is called electrosteric stabilization. Ya et al. reported that increase in the molecular weight of chitosan increases the thickness of chitosan layer attached to poly(butyl cyanoacrylate) nanoparticles which resulted in an increase in the steric repulsive energy and the electrostatic repulsive energy, and increased the potential energy between the two particles (Yang et al., 2000). The electrosteric principle has been reported for dextran-modified nanoparticles as well as other polymeric surfactants (Douglas et al., 1985). Effect of polymeric layer on drug loading and release has to be examined when aiming for sterically stabilized mesoporous silica.

1.2.3 Cellular aspects of MSN

1.2.3.1 Cell uptake

Studies of the interactions between inorganic nanoparticles and mammalian cells have shown great potential in using these materials in various biomedical applications such as drug and gene delivery (Chen et al., 2009a), disease diagnosis (Brigger et al., 2002), cell type recognition and imaging (Slowing et al., 2007). The physicochemical properties such as surface chemistry, particle size, and particle shape of MSN play key roles in determining biological behavior of the particles, and these critical parameters need to be considered when developing MSN for targeted drug delivery. The uptake of nonfunctionalized, negatively charged MSN by cells has been found to occur through non-specific adsorptive endocytosis. Lin and co-workers investigated effect of surface functionalities on uptake of MSN in HeLa cells and found higher

cell uptake for FITC and aminopropyl-functionalized MSN than for guanidinopropyl and folate-aminopropyl-functionalized MSN (Slowing et al., 2006a). They reported that FITC and aminopropyl-MSN had higher endosomal escape compared to other functionalized particles. Interestingly, aspect ratio which controls shape of the particles has shown to limit the rate of cell uptake (high aspect ratio = high and fast cell uptake) (Huang et al., 2010). Nel and co-workers recently investigated the effect of MSN aspect ratio MSN on HeLa cell uptake and found that rod shaped particles showed higher cell uptake through micropinocytosis compared to spherical MSN (Meng et al., 2011b). Such accumulating results suggest that spherical nanocarriers may not be the optimal delivery system due to poor cell uptake and unsatisfactory biodistribution compared to particles with higher aspect ratios (Arnida et al., 2011). Available evidences suggest that optimization of the shape of nanoparticles is essential to achieve long circulating nanocarriers after intra venous administration.

1.2.3.2 Cytotoxicity

In vitro toxicity studies are often using as preliminary screening process before determining safety of biomaterial *in vivo*. Parameters such as surface chemistry, particle size, charge and particle shape affects particle aggregation, protein adsorption on particles, interaction at the cell-particle interfaces and intracellular particle trafficking are all critical determinants of cellular toxicity and *in vivo* behavior (Rosenholm et al., 2010b; SchÃ¤dlich et al., 2011; Slowing et al., 2006a). Toxicity studies based on these parameters have indeed been reported for mesoporous silica to some extent but more extensively for non-porous silica. The studies demonstrated size dependent toxicity of silica nanoparticles on endothelial cells (Napierska et al., 2009). Particles above 100 nm showed very little toxicity while sub-50 nm particles induced greater cell death. Dosage of particles is a critical determinant for cellular toxicity and reported

"safe concentration" for MSN is up to 100 μg/ml (Slowing et al., 2007; Wani et al., 2012). Particle toxicity is also influenced by surface charge. It has been demonstrated that positively charged amino-functionalized mesoporous silica has lower cellular toxicity compared to negatively charged unmodified MSN in *in vitro* conditions (Tao et al., 2009). On the same note, Pasqua and co-workers reported that thiol and amino functionalized MSN induced higher cell death compared to unmodified mesoporous silica (Di Pasqua et al., 2008). These reports suggest that critical evaluation of toxicity of MSN is needed before its preclinical application.

1.2.3.3 Intracellular delivery of drugs and genes by MSN

The optimal intracellular delivery system should not only be endocytosed at higher rate but also be capable of releasing cargo efficiently at the right intracellular target. MSN is a versatile platform which has successfully transported hydrophobic molecules such as PTX, camptothecin (Lu et al., 2007a), hydrophilic drugs such as doxorubicin(Chen et al., 2009a; Singh et al., 2011), membrane impermeable proteins such as cytochrome (Slowing et al., 2007) and various genes and siRNAs (Bhattarai et al., 2010) to the intracellular environment. Intracellular trafficking of particles is an area of interest as it may allow monitoring of real time delivery and location. Based on the mode of action of the drug and the route of intracellular trafficking it may possible to develop optimal delivery system. Due to the difficulties in the quantifying intracellularly released drug, the intracellular drug release efficiency is often measured in terms of cell viability as a function of treatment with MSN loaded with cytotoxic drugs. However, it has been showed that the amount of fluorescent doxorubicin delivered to cells can be quantified by flow cytometry and HPLC but such methods are limited to inherent fluorescence of drug molecules (Chen et al., 2009a). Fluorescent tagging is a viable option to quantify and to monitor intracellular trafficking of nanoparticles but question of dissociation of tag from the

nanoparticles or the drug always being raised during analysis of such results. However, *in vitro* cell uptake, toxicity and intracellular trafficking studies show credibility of the delivery system and may help to conclude *in vivo* results.

1.2.4 *In vivo* aspects of MSN

In the case of cancer, the ultimate goal of the delivery system is to kill cancer cells or to make them more susceptible to the treatment with minimum damage to the healthy cells. Aggregation of nanoparticles accelerate accumulation of nanoparticles in the healthy organs, disruption of biological membranes and unwanted activation of immune response favoring critical evaluation of physicochemical parameters of nanomaterials to decrease biodistribution to healthy organs (Brigger et al., 2002; Farokhzad and Langer, 2009; Fox et al., 2009; Schroeder et al., 2012). *In vivo* aspects of MSN mainly involve determination of toxicological profile of the nanoparticles and their degradation products and its ability to act as a tool to deliver chemotherapeutics to the tumors.

1.2.4.1 Biocompatibility of MSN *in vivo*

Although many reports suggest low toxicity of MSN in the *in vitro* studies, it is important to assess toxicity and biocompatibility of MSN *in vivo* for crucial design of these nanomaterials for biomedical applications. Ghandehari and co-workers extensively evaluated *in vivo* toxicity in mice of MSN using particles with different geometry, size, porosity and surface charge (Arnida et al., 2011; Yu et al., 2012). They found that non-porous silica (bare or amino modified) had a high maximum tolerated dose (MTD) between 100-150 mg/kg body weight. Surprisingly mesoporous silica had a lower safety threshold with MTD between 30 to 65 mg/kg irrespective of the geometry. It has been reported that intravenous injection of MSN at a dose of 6 mg/mouse

(approximately 240 mg/kg) was too toxic and animal died immediately after injection (Hudson et al., 2008). Interestingly, toxicity of MSN was alleviated by amine surface functionalization, resulting in a 2-3 fold increase in the MTDs to 100-150 mg/kg (Yu et al., 2012). This study confirmed that surface functionalization is an important way to improve biocompatibility of MSN *in vivo*. It was observed that among animals showing adverse reactions, renal damage was the major adverse effect of MSN demonstrated by sharply increased blood urea nitrogen levels. Extensive damage to the heart and lung was observed with the non-porous Stöber nanoparticles (Arnida et al., 2011; Yu et al., 2012). Porosity is also an important parameter that influences toxicity. Mesoporous silica materials greatly reduced hemolytic activity compared to amorphous non-porous silica but still showed dose dependent hemolysis (Lin and Haynes, 2010; Rosenholm et al., 2010b; Yu et al., 2012). The hemolytic activity did not seem to be attributed to the effective surface charge. Thus, it was concluded that observed hemolysis was attributed to the strong electrostatic interaction between silanol of silica and trimethylammonium head group of RBC's membrane lipid (Rosenholm et al., 2010b). PEGylation of MSN is also a favorable approach to prevent hemolysis and to improve blood compatibility. PEG forms a hydrophilic stealth layer on the particle surface preventing interaction of the silanol groups with RBC (Lin and Haynes, 2010). Given the complexity of biological environment, it is important to address toxicological concerns early in the development of biocompatible materials.

CHAPTER 2

SURFACE FUNCTIONALIZATION OF MESOPOROUS SILICA NANOPARTICLES CONROLS LOADING AND RELEASE BEHAVIOR OF MITOXANTRONE

Please note that the content of this chapter was published in the Pharmaceutical Research (Wani et al. 2012). As the first author, I performed all the work in the paper except the nanoparticle synthesis (contributed by Dr. E. Mutthuswamy, the second author) and the characterization of mesoporous silica nanoparticles (contributed by Layan, the third author). All the authors agreed with including their work in this dissertation.

2.1 Introduction

Therapeutic strategies based on nanoparticle drug delivery systems aim to improve the anti-proliferative activity of anticancer drugs by localizing them in a controlled fashion at the tumor site (Davis et al., 2008). Mesoporous silica nanoparticles (MSN), such as Mobile Composition Matter number 41 (MCM-41), are silica particles containing pores with diameters in the 1.5-20 nm range. MSN have been proposed as a suitable platform for biomedical applications, including drug and gene delivery (Chen et al., 2009b; Lu et al., 2007a; Slowing et al., 2008; Xia et al., 2009b). MSN offer several advantages in drug delivery over polymeric nanoparticles, including tunable pore size, large surface area, high drug loading capacity, ability to encapsulate hydrophilic as well as hydrophobic drugs, and easy surface functionalization. Existing evidence suggests that silica materials, including MSN, are biocompatible and bioresorbable (Viitala et al., 2005). Numerous studies described easy hydrolysis and dissolution of porous silica particles in simulated physiologic conditions (Finnie et al., 2009; Galarneau et

al., 2007; Lin and Haynes, 2010). The particles are typically hydrolyzed into silicic acid, which is known to undergo renal elimination in vivo (Jugdaohsingh et al., 2000).

Hydrophobic polymeric nanoparticles efficiently encapsulate hydrophobic drugs but are usually ill suited for encapsulation of large amounts of relatively hydrophilic drugs. Available reports show, for example, that only about 5% of doxorubicin can be loaded in poly(lactic-co-glycolic) acid nanoparticles (Park et al., 2009b). In addition, delivery of hydrophilic drugs by hydrophobic polyester nanoparticles is subject to a potentially dangerous dose-dumping. Like polymeric nanoparticles, MSN are able to improve solubility and achieve controlled release of poorly soluble hydrophobic drugs (e.g. camptothecin, PTX) (Lu et al., 2007b; Xia et al., 2009b), attributable to their well-defined porosities and versatile surface chemistry. MSN have also been successfully developed for delivery of water soluble drugs (e.g. doxorubicin.HCl) with an excellent drug loading capacity (~40% w/w loading) (Chen et al., 2009b; Meng et al., 2011a; Meng et al., 2010b). Park et al. reported that electrostatic interactions between positively charged doxorubicin and negatively charged porous silica nanoparticles were responsible for the dramatically enhanced loading (Park et al., 2009a). Controlled release of hydrophilic molecules, such as adenosine triphosphate has been achieved by tailoring the pore size of microporous and mesoporous materials (Slowing et al., 2007). In addition, studies on tuning of pore wall properties such as by silylation of the silica matrix to make it more hydrophobic (Qu et al., 2006) or amine modification to achieve positively charged surface (Munoz et al., 2003) reveal that release of hydrophilic drugs can be easily adjusted.

Another important aspect of mesoporous silica is amorphization or crystalline-to-amorphous transformation of active pharmaceutical ingredient in the porous nanoconfinement. Mesoporous silica exerts a strong confinement effect on drug crystallization due to its large

surface area (greater than 500 m^2/g) with high surface free energy and higher pore volume (e.g., approximately $1cm^3/g$). The small pore size may prevent drug molecule nucleation by preventing the formation of supercritical nuclei beyond critical nucleus size. In addition, the strong adsorption and interaction of drug molecules on the surface of mesoporous silica may also hinder the ordering of drug molecules necessary for crystallization. It has been reported that porous structure has a size-constraint effect on nucleation and crystal growth (Jackson and McKenna, 1996; Qian and Bogner, 2011). Jacson et al. investigated effect of pore size (4 to 73 nm) of porous adsorbent on adsorption of crystalline o-terphenyl and found that crystalline-to-amorphous transformation while decreasing pore size with lowest pore size particles (4 nm) preventing crystallization completely (Jackson and McKenna, 1996).

MTX (Figure 1) is an anthraquinone derivative that has been extensively investigated for the treatment of breast and prostate cancer but its clinical application has been limited due to severe cardiotoxicity (van Dalen et al., 2004). Solid lipid nanoparticles (Lu et al., 2006), liposomes (Law et al., 1996) and polyester nanoparticles (Chen et al., 2009c) have been investigated to improve MTX formulation but limited drug loading capacity and poorly controlled release hindered their utility. Electrostatic interaction of MTX with silica matrix has been reported very recently (Ma et al., 2011) but systematic investigation of the effect of surface functionalization of MSN on MTX loading and release has not yet been reported. The goal of the present study was to investigate the effect of surface functionalization of mesoporous silica on crystallization behavior of MTX with focus on optimization of surface functionality for achieving amorphous MTX formulations with controlled rate of release. We predicted that surface functionalization of MSN will serve as a simple and robust way of controlling MTX

delivery without the need for introducing of any complex mechanism of drug release control into the design of MSN.

2.2 Materials

Tetraethylorthosilicate (TEOS), 3-mercaptopropyltrimethoxysilane (MPTMS), 3-aminopropyltriethoxysilane (APTES), *N*-cetyltrimethylammonium bromide (CTAB), hydrochloric acid, and sulfuric acid were purchased from Sigma-Aldrich (St. Louis, MO). Mitoxantrone dihydrochloride (MTX) was purchased from SantaCruz Biotechnology Inc. (Santa Cruz, CA). Roswell Park Memorial Institute (RPMI), phosphate buffered saline (PBS), fetal bovine serum (FBS) were purchased from Invitrogen (Grand Island, NJ). Cell titer 96 Aqueous One solution cell proliferation assay (MTS reagent) was purchased from Promega (Madison, WI).

2.3 Methods

2.3.1 Synthesis of mesoporous silica nanoparticles (MSN)

SH-, mixed SH/NH_2- (50:50) and NH_2-functionalized MSN were synthesized by co-condensation of TEOS, MPTMS and APTMS using modified surfactant-templated base catalyzed method reported previously (Bhattarai et al., 2010). In a typical synthesis of mixed SH/NH_2-MSN, 1.0 g of CTAB was dissolved in 480 mL of de-ionized water made basic by the addition of 3.5 mL of 2.0 M NaOH, and the temperature raised to 80 °C. To this solution, 5.0 mL TEOS was injected at a rate of ~1.0 mL/min using a syringe pump while stirring. The injection of TEOS was immediately followed by drop-wise addition of MPTMS (1.3 mmol) and APTES (1.3 mmol), to achieve a molar ratio of TEOS:MPTMS:APTES of 8.7:1:1. The dispersion was maintained at 80 °C for about 2 h and the final product was isolated by centrifugation. The isolated product was washed with excess deionized water and methanol and dried in vacuum.

Removal of the CTAB template was carried out by refluxing the dried product in acidic methanol solution (18 mL of 12 M HCl, 20 mL of methanol) overnight. The particles were isolated by centrifugation, washed with methanol and de-ionized water, and dried overnight under active vacuum in a dessicator to yield a free flowing white powder. Synthesis of SH-MSN and NH_2-MSN was carried out using the same procedure using either 2.6 mmol of MPTMS or 2.6 mmol APTES alone.

2.3.2 Characterization of MSN

The morphology and size of nanoparticles were characterized by transmission electron microscopy (TEM) on a JEOL 2010 Analytical Electron Microscope at 200 kV. TEM samples were prepared by placing a drop of a sonicated aqueous solution of MSN on a carbon-coated copper grid. The surface area, average pore size, cumulative pore volume, and pore size distributions were determined from nitrogen adsorption/desorption isotherms acquired at 77 K using a 30 s equilibrium interval on an ASAP 2010 Micromeritics porosimeter. The surface areas were computed using the Brunauer-Emmett-Teller (BET) model. The cumulative pore volumes and the pore size distribution was obtained from density functional theory (DFT) modeling using the DFT package of the Micromeritics V2.00 software over the entire range of the adsorption isotherm. The content of thiol and amino groups in the MSN was determined from the sulfur and nitrogen content in MSN measured by elemental analysis (Atlantic Microlabs Inc., Norcross, GA).

2.3.3 MTX loading

In a typical experiment, 667 μL of 4.5 mg/mL of MTX in PBS (pH 7.4) was added to 10 mg of dry MSN. The mixture was sonicated for 30 min and kept stirring on a magnetic stirplate for 24 h. Then, drug loaded particles were centrifuged at 14,100 g for 10 min. After

centrifugation, MTX loaded MSN were vacuum dried overnight. The amount of MTX loaded in MSN was estimated from the MTX concentration difference in the original solution and the supernatant after loading in MSN. MTX concentration was determined by absorbance at 658 nm. Drug loading is expressed as % w/w = 100*(weight of MTX in MSN)/[(weight of MTX in MSN) + (weight of MSN)]. The content of MTX in MSN was also determined by thermogravimetric analysis (TGA) under air (Perkin-Elmer Pyris 1, 10 °C/min), subtracting the mass lost during analysis of empty modified MSN particles.

2.3.4 Zeta Potential measurement

The measurement of zeta potential of SH-MSN, SH/NH_2–MSN, and NH_2-MSN with and without MTX loading was performed using a ZetaPlus Particle Size and Zeta Potential Analyzer (Brookhaven Instruments) equipped with a 35-mW solid state red laser (658 nm) at 25 ºC. Scattered light was detected at 90°. Samples were prepared by suspending 200 μg of particles in 2 mL PBS (pH 7.4). Zeta potential values were calculated from measured velocities using the Smoluchowski equation and results are expressed as the mean ± S.D. of 5 runs.

2.3.5 *In Vitro* Release of MTX

Release of MTX from MSN was analyzed by suspending a known mass of the particles in 2 mL of appropriate release medium (PBS, pH 7.4, or 0.2 M sodium acetate buffer, pH 4.5). At each pre-determined time point, MSN were centrifuged at 14,100 g for 10 min. One mL of supernatant was removed and replaced with 1 mL of fresh release media. The media volumes and drug concentrations were selected so that sink conditions were maintained during the entire experiment. The concentration of MTX in the supernatant was determined from absorbance at 658 nm using a standard absorbance vs. concentration curve constructed for MTX in the corresponding release buffer. Because only 1 mL of the release media was removed at each time

point, the amount of released MTX was corrected for MTX remaining in the release medium from the previous time point.

2.3.6 Characterization of crystalline/amorphous state of MTX in MSN

The crystalline state of MTX loaded in MSN was determined by differential scanning calorimetry (DSC) and X-ray powder diffraction (XRD). In the DSC analysis, 3-4 mg of sample was packed in hermetically sealed aluminum pans and heated under dry nitrogen purge using MDSC Model 2920 (TA instruments, New Castle, DE) equipped with a refrigerated cooling system. Samples were heated from 0 to 250 °C at a heating rate of 10 °C/minute. Thermograms were analyzed using Universal Analysis 2000 software (TA Instruments, New Castle, DE). The powder XRD patterns were obtained on Rigaku D/MAX-2200PC diffractometer at 40 kV and 40 mA (Cu Kα radiation). Data were obtained from 5° to 30° (diffraction angle 2θ) at a scanning speed of 3°/min at room temperature.

2.3.7 Self-quenching of MTX fluorescence in MSN

Effect of MTX loading in MSN on self-quenching of the MTX fluorescence was studied by fluorescence spectroscopy using a Fluoromax-3 (Horiba Jobin Yvon Inc.). 6.9 μg/mL of MTX, either free or loaded in MSN, was suspended in PBS (pH 7.4). The excitation wavelength was set to 607 nm and emission spectra were recorded from 650 to 750 nm.

2.3.8 Cell Culture

Triple negative MDA-MB-231 human breast cancer cell line was a kind gift from Dr. Jing Li, Karmanos Cancer Institute, Detroit MI. The cells were maintained in Hyclone's RPMI medium supplemented with 2.05 mM L-glutamine, 10% FBS and 1% penicillin. Cells were maintained in an incubator at 37 °C with 5% CO_2.

2.3.9 Cell Viability

Cytotoxicity of drug-loaded MSN was determined by the CellTiter 96® Aqueous Cell Proliferation Assay and compared with that of empty MSN. Five thousand MDA-MB-231 cells were seeded in a 96-well plate. One day after reaching confluence, the cytotoxicity of the different surface modified MSN formulations was evaluated by incubating the cells in 100 µL of RPMI/FBS with increasing MSN concentrations. The medium was removed after 72 h and replaced with a mixture of 100 µL fresh RPMI and 20 µL MTS reagent solution. The cells were incubated for 2 h at 37 °C. The absorbance of each well was then measured at 490 nm to determine cell viability. The results are expressed as mean % cell viability relative to untreated cells ± S.D. IC50 values were determined by Prism software using non-linear regression involving log (inhibitor) vs. response (three parameters) analysis of dose-response inhibition.

2.3.10 Intracellular uptake of MTX

Dose dependent cellular uptake of free MTX and MTX loaded in SH-MSN was determined by measuring cell-associated fluorescence of MTX by flow cytometry. MDA-MB-231 cells (2.5×10^5 cells per well) were seeded in 24-well plate 12 hours before experiment. Cells were incubated with increasing concentration of free MTX and MTX/SH-MSN in RPMI/FBS for 2 hours at 37 °C. Cells were washed twice with PBS and harvested by trypsinization. Cells were resuspended in Hank's buffered salt solution (HBSS) and MTX concentration was analyzed immediately by flow cytometry at an excitation laser wavelength of 658 nm and using a 670 nm emission band pass filter. Flow cytometry analysis was performed on a BD Biosciences LSR II instrument. Ten thousand cells were collected for each measurement. Cellquest software was used for data analysis. Reported fluorescence intensity data were corrected for cell autofluorescence using untreated cells.

2.3.11 Intracellular release of MTX

Time dependent intracellular release of MTX from internalized SH-MSN particles loaded with MTX was determined by flow cytometry. MDA-MB-231 cells (3.8 x 10^5 cells per well) were seeded in 12-well plate 12 hours before experiment. Cells were incubated with 10 µg/ml of either free MTX or MTX loaded in SH-MSN in RPMI/FBS for 2 h at 37 °C. Cells were washed with PBS to remove any free drug and particles. The cells were then incubated for additional 2, 4 and 6 h in RPMI/FBS and cell-associated fluorescence intensity of MTX was measured by flow cytometry.

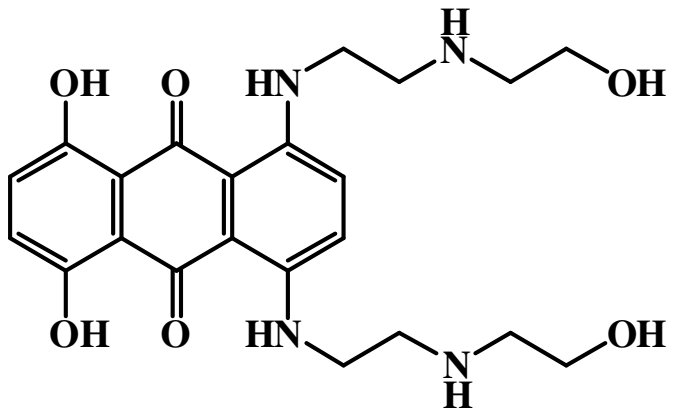

Figure 1. Chemical structure of MTX

2.4 Results

This chapter reports that a simple surface functionalization of MSN can control crystallization, loading, release and anti-cancer activity of drug molecules. Such surface modification of mesoporous structure allows encapsulation of small molecular weight, charged drugs and release of the encapsulated cargoes in a sustained as well as controlled manner. In general, such modifications were limited to encapsulating unionized, hydrophobic small molecules based on charge-charge interaction. Our hypothesis was that controlling charge of the nanoparticles at given pH will improve overall drug loading, release profile and crystallization pattern of the encapsulated molecules.

To demonstrate feasibility of such surface modifications, nanoparticles were modified with thiol, mixed thiol/amine and amine groups and surface functionality was optimized in the development of successful MTX formulation with high drug loading, controlled drug release, amorphous form of encapsulated drug and retaining anti-cancer activity.

2.4.1 Synthesis and characterization of surface-functionalized MSN

Surface-functionalized MSN were synthesized by co-condensation of TEOS with the appropriately functionalized siloxane; MPTMS to prepare SH-MSN, APTES to prepare NH_2-MSN or a mixture of MPTMS and APTES to prepare mixed SH/NH_2-MSN. The morphology and pore structure of the modified MSN were first analyzed by TEM (Figure 2). The TEM images show that all synthesized MSN had a nearly spherical shape with average diameter of 86, 87 and 138 nm for SH-MSN, mixed SH/NH_2-MSN and NH_2-MSN, respectively. The presence of mesoporous structure in SH-MSN, mixed SH/NH_2-MSN and NH_2-MSN was confirmed by porosimetry (Figure 3). The nitrogen adsorption/desorption experiments revealed that all the synthesized MSN displayed type IV isotherm, a characteristic feature of mesoporous materials.

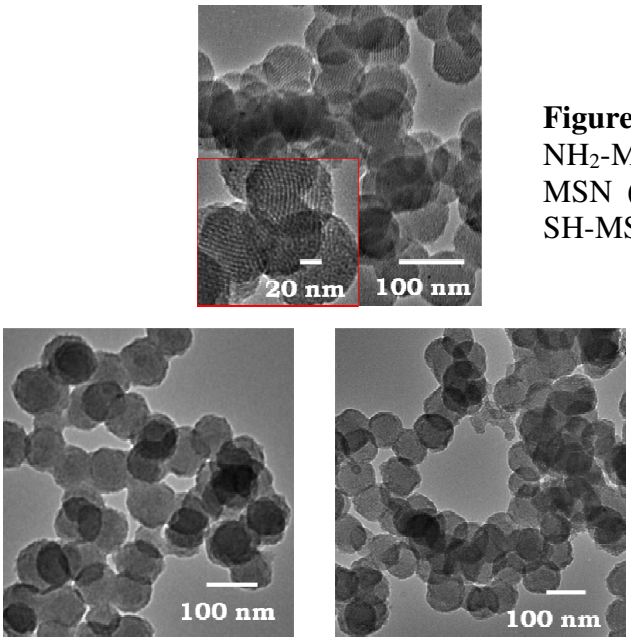

Figure 2. TEM images of SH-MSN (top), NH_2-MSN (bottom right) and mixed SH/NH_2-MSN (bottom left) (Inset: HRTEM image of SH-MSN).

The main results of the MSN characterization are summarized in Table 2. The results demonstrate that surface functionalization had only a limited effect on the pore size and pore volume of the particles. The BET surface area of the SH-MSN and SH/NH_2-MSN was higher than surface area of the NH_2-MSN particles.

Table 2. Surface properties of SH-MSN, mixed SH/NH_2-MSN and NH_2-MSN.

MSN	Pore Size (Å)	Pore Volume (cm^3/g)	BET S.A. (m^2/g)[a]
SH-MSN	37	0.51	776
SH/NH_2-MSN	28	0.53	754
NH_2-MSN	37	0.57	506

[a] BET: Brunauer-Emmett-Teller surface area measurement

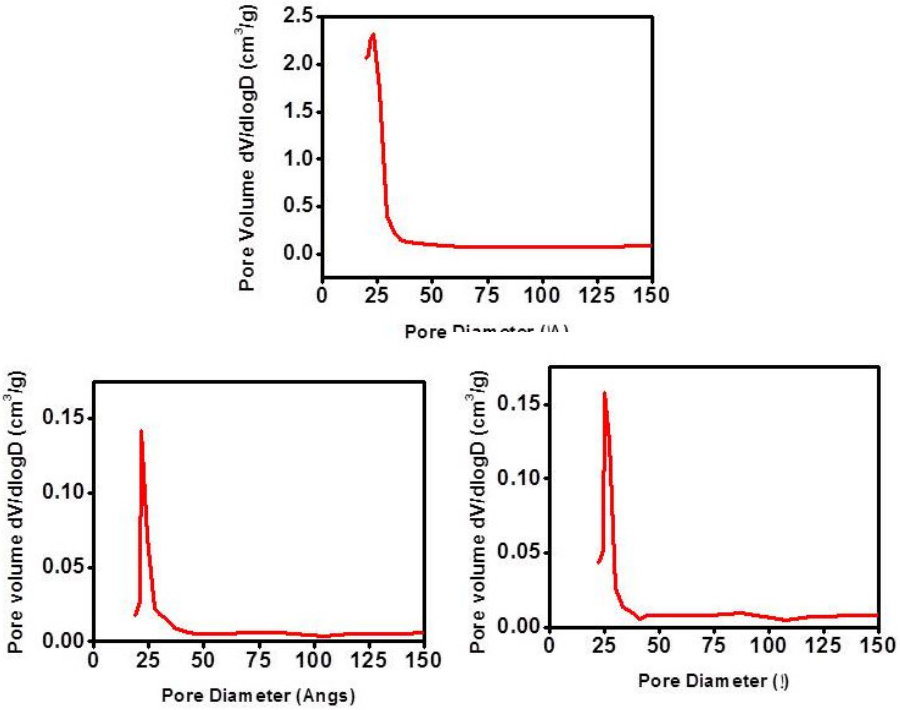

Figure 3. DFT pore size distribution of surface modified MSN. SH-MSN (top), mixed SH,NH_2-MSN (middle) and NH_2-MSN (bottom).

The presence of thiols and amines in the MSN was confirmed by elemental analysis. The elemental composition of the functionalized MSN is given in Table 3. As expected, no nitrogen

was detected in SH-MSN while no sulfur was detected in NH_2-MSN. The elemental analysis results indicate that SH-MSN contained 1.2 mmol of SH/g of MSN, mixed SH/NH_2-MSN contained 0.75 mmol SH/g of MSN and 0.8 mmol NH_2/g of MSN, and NH_2-MSN contained 1.8 mmol NH_2/g of MSN.

Table 3. Elemental analysis of surface-modified MSN.

Element	Element content (%)		
	SH-MSN	SH/NH_2-MSN	NH_2-MSN
C	4.3	6.4	8.2
H	4.9	2.2	2.8
N	0.0	1.1	2.5
S	4.0	2.4	0.0

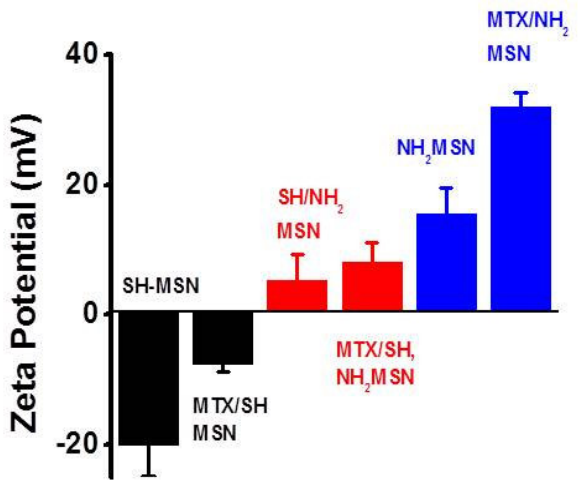

Figure 4. Effect of surface modification and MTX loading on zeta potential of MSN at pH 7.4.

The presence of the functional groups had a pronounced effect on the surface charge of MSN (Figure 4). At neutral pH, NH_2-MSN had an overall positive surface charge with zeta potential 15.6 mV, while SH-MSN exhibited a negative surface charge with zeta potential -15 mV. As expected, the mixed SH/NH_2-MSN showed intermediate zeta potential of 5.2 mV. Zeta

potential increased at pH 4.5 with NH_2-MSN, SH-MSN, and SH/NH_2-MSN showing zeta potential of 31.0 mV, -2.5 mV and 16.6 mV, respectively (data not shown).

2.4.2 MTX loading

We have encapsulated MTX into the synthesized MSN to determine the effect of surface functionalization on MTX loading. The data show that modification of MSN with amino groups limited MTX loading to 1% w/w. In contrast, modification of MSN with thiols resulted in significant enhancement of MTX loading to 18% w/w (Figure 5 Left). MSN modified with both thiols and amines exhibited intermediate MTX loading (8% w/w). Corresponding encapsulation efficiencies in SH-MSN, SH/NH_2-MSN and NH_2-MSN particles were 60%, 27% and 3.4%, respectively. The differences in MTX loading among the different functionalized MSN were confirmed by TGA (Figure 5 Right). MTX alone decomposed fully at temperatures above 600 °C. MSN that were not loaded with MTX showed weight loss in the range of 13 to 25% due to incomplete condensation of TEOS and presence of residual solvents. Comparison of the weight

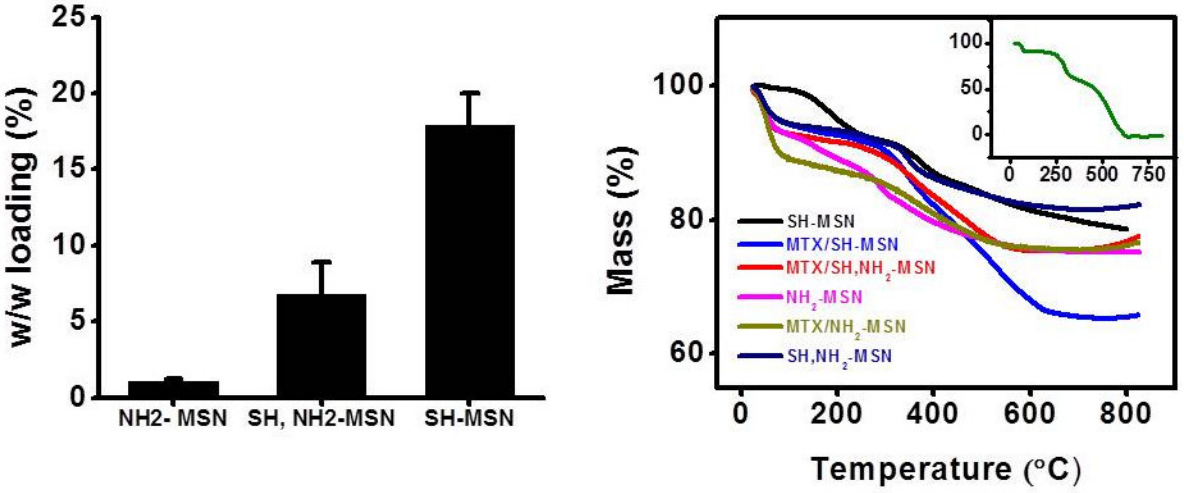

Figure 5. (Left) Effect of surface modification of MSN on MTX loading (Right) Thermogravimetric analysis of MSN loaded with MTX. (Inset: TGA of MTX).

loss of the MTX-loaded MSN with the weight loss observed for the empty particles suggested that the SH-MSN particles contained 21% w/w MTX, while the mixed SH/NH_2-MSN particles contained 8% w/w MTX and the NH_2-MSN particles contained only 1% w/w MTX.

2.4.3 Characterization of MTX-loaded MSN

MSN loaded with MTX were characterized for particle size, zeta potential, morphology, and physical state. TEM studies indicated that after MTX encapsulation, nanoparticles retained spherical morphology; however, filled pores were observed with SH-MSN (data not shown). Loading of the positively charged MTX increased the zeta potential of all the MSN (Figure 4). Upon MTX loading, the zeta potential of SH-MSN increased from -15.0 to -7 mV, while the zeta potential of the mixed SH/NH_2-MSN increased from 5.2 to 8.1 mV. Despite low MTX loading, the zeta potential of NH_2-MSN increased from 15.6 to 32.1 mV. In acidic conditions (pH 4.5), further increase in the zeta potential was observed. The zeta potential of MTX/SH-MSN was 22.0 mV, while the zeta potential of the MTX-loaded mixed SH/NH_2-MSN was 26.5 mV and the zeta potential of MTX/NH_2-MSN was 42.8 mV.

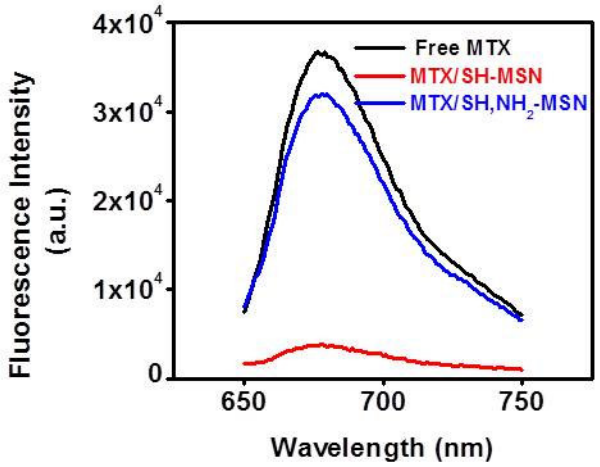

Figure 6. Fluorescence quenching of MTX loaded in MSN

MTX is a fluorescent molecule with emission maximum at 685 nm. Concentration-dependent fluorescence quenching is a well-known phenomenon that can be exploited for determining the release of fluorescent molecules from nanoparticles. We measured fluorescence of MTX loaded in the three types of functionalized MSN (Figure 6). Our result shows that the levels of loading achieved in SH-MSN are sufficient to achieve quenching of MTX fluorescence. The lower loading achieved in the two amine-containing MSN resulted in MTX fluorescence similar to that of the free drug.

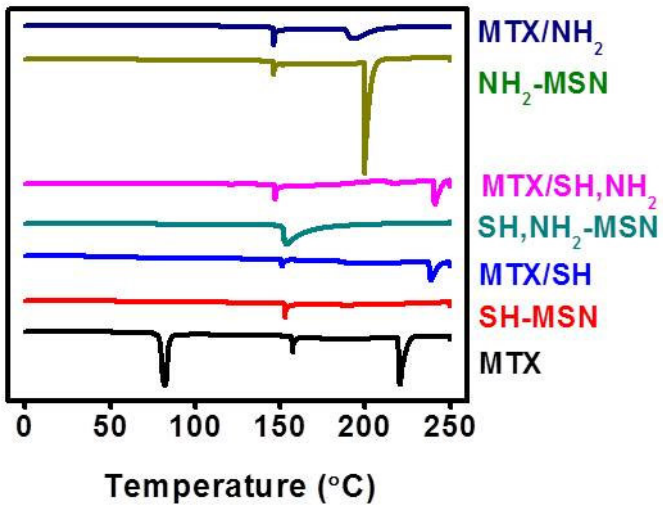

Figure 7. DSC analysis of MTX-loaded MSN

Drug crystallinity affects the rate of dissolution and release from nanoparticles. We have used DSC and XRD to evaluate crystalline/amorphous state of MTX loaded in MSN. The DSC thermograms of MTX, MTX-loaded MSN, and empty MSN are shown in Figure 7. Two endothermic peaks (75 and 220 °C) were observed in the sample of free MTX. The peak at 220 °C corresponds to the melting point of dihydrochloride of MTX. The peak at 75 °C represents residual solvent in the commercial sample of MTX. This was confirmed by TGA by observing a small weight loss at that temperature. Analysis of MTX loaded in SH-MSN showed an

endothermic peak at 232 °C, which was due to the phosphate buffer used in the loading protocol (data not shown). No signs of MTX melting point were observed in MTX-loaded SH-MSN. In contrast, a broad endothermic peak at 188 °C was observed in the sample of MTX loaded in NH_2-MSN. All empty MSN and free MTX showed endothermic signals between 156-158 °C.

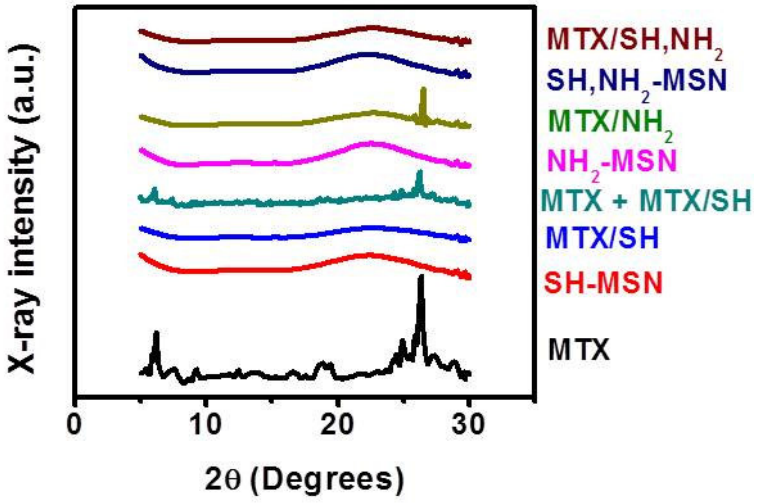

Figure 8. XRD analysis of MTX-loaded MSN

Amorphous nature of MTX loaded in SH-MSN was confirmed by XRD (Figure 8). Free MTX showed highly crystalline nature as illustrated by the numerous peaks at 5.9, 6.2, 19.4, 23.6, 24.4, 24.9, 25.9, and 26.3°. After encapsulation in SH-MSN no crystalline peaks of MTX were observed. XRD pattern of physical mixture of MTX with MTX-loaded SH-MSN showed distinct peaks corresponding to the pure MTX while XRD patterns of control SH-MSN, mixed SH/NH_2-MSN and NH_2-MSN were consistent with amorphous nature of the particles. XRD pattern of MTX loaded in mixed SH/NH_2-MSN revealed non-crystalline state of MTX. NH_2-MSN loaded with MTX showed one crystalline peak at 26.3° while other MTX crystalline peaks were not observed indicating presence of semi-crystalline MTX in NH_2-MSN.

2.4.4 Effect of pH and surface functionality on MTX release

The release behavior of MTX from the different surface functionalized MSN was investigated in PBS (pH 7.4) and in acidic conditions (0.2 M sodium acetate buffer, pH 4.5) to mimic conditions during intracellular lysosomal trafficking of the particles. Release profile of MTX as a function of pH and surface functionality of MSN are shown in Figure 9. The rate of MTX release from MSN was strongly dependent on the pH of the release media as well as surface modification of MSN. SH-MSN showed a much faster MTX release at pH 4.5 than pH 7.4. Within the first 4 h ~34% MTX was released at pH 4.5 while only ~1-2% MTX was released at pH 7.4 from SH-MSN. In contrast, a significantly faster MTX release was observed from mixed SH/NH_2–MSN with 75% and 90% of the drug released within 4 h at pH 7.4 and 4.5, respectively. MTX was released even more rapidly from NH_2-MSN, with complete release observed within 1 h.

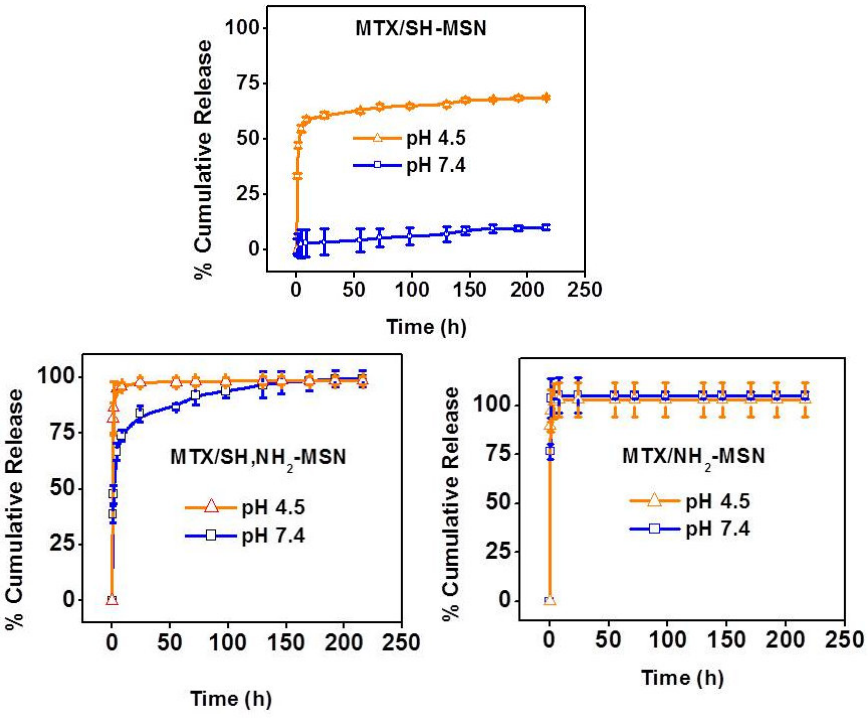

Figure 9. Effect of pH and surface functionality on the rate of MTX release. (top) SH-MSN, (bottom left) SH/NH2-MSN, (bottom right) NH2-MSN.

2.4.5 Intracellular delivery and release of MTX using SH-MSN

Dose dependent uptake of free MTX was determined using flow cytometry after 2 h incubation of MDA-MB-231 cells with increasing concentrations of MTX (Figure 10 left). The amount of free MTX in the cells increased continuously in the entire dose range studied. The same assay was used to measure cell-associated fluorescence of MTX delivered by SH-MSN. We found significantly lower fluorescence intensity in case of MTX delivered by SH-MSN when compared with free MTX. Taking advantage of the self-quenching of fluorescence of MTX loaded in SH-MSN (Figure 6), we then followed MTX fluorescence in cells that were incubated for 2 h with 10 µg/mL of either free MTX or MTX in SH-MSN (Figure 10 right). The medium containing the drug and the nanoparticles was removed and replaced with fresh drug-free medium In case of free MTX, the fluorescence intensity decreased over the 6 h of observation indicating drug efflux from the cells. During the same time period, the fluorescence intensity in cells treated with MTX/SH-MSN increased almost 3-times. Initially, the intracellular fluorescence intensity of MTX loaded in SH-MSN was low due to quenching (Figure 6) and the subsequent increase in the fluorescence indicated effective intracellular release of the drug from the internalized particles.

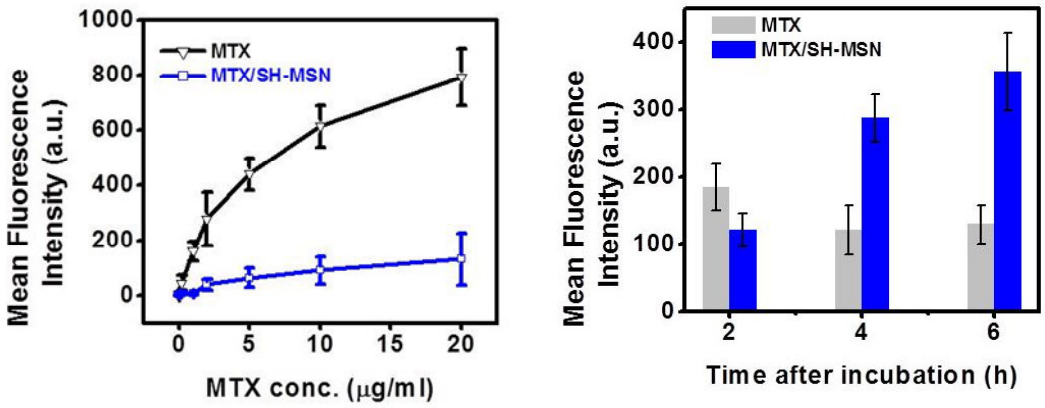

Figure 10. Flow cytometry analysis to determine (left) Effect of MTX concentration on cell uptake and (right) Effect of post-incubation time on intracellular content of free MTX

2.4.6 Cytotoxicity of MSN

We have determined the effect of surface functionalization on the cytotoxicity of MSN in MDA-MB-231 (Figure 11). Cells were incubated with increasing concentration of the different synthesized MSN (from 0.01 µg/ml to 100 µg/ml) and cell viability was assessed by MTS assay. The amine-containing particles had higher toxicity at the highest tested concentration with 83-87 % cell viability, while SH-MSN showed a lower toxicity with 92% cell viability.

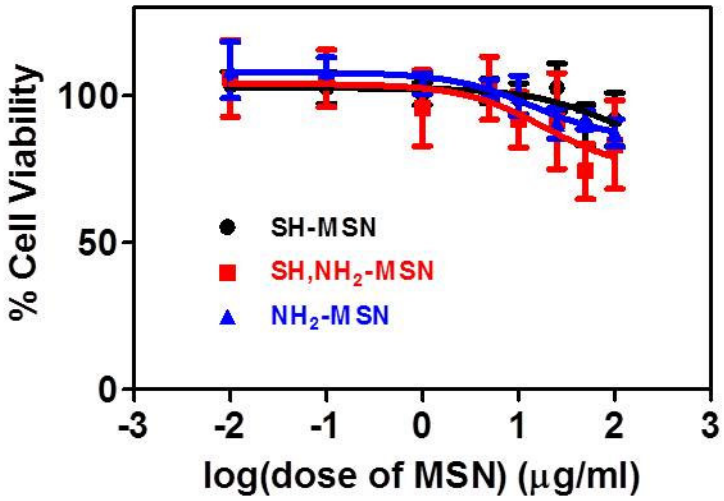

Figure 11. Effect of MSN surface modification on viability of MDA-MB-231 cells (mean ± S.D., n=3)

2.4.7 Antiproliferative activity of MTX delivered in SH-MSN.

Anti-proliferative activity of MTX loaded in SH-MSN was compared with free MTX in a human breast adenocarcinoma cells MDA-MB-231 (Figure 12). Similar activity was observed for both tested formulations. The concentration of SH-MSN at the highest tested MTX dose was 79 µg/mL. At this concentration, the cell viability of cells treated with empty SH-MSN was 94% (Figure 11).

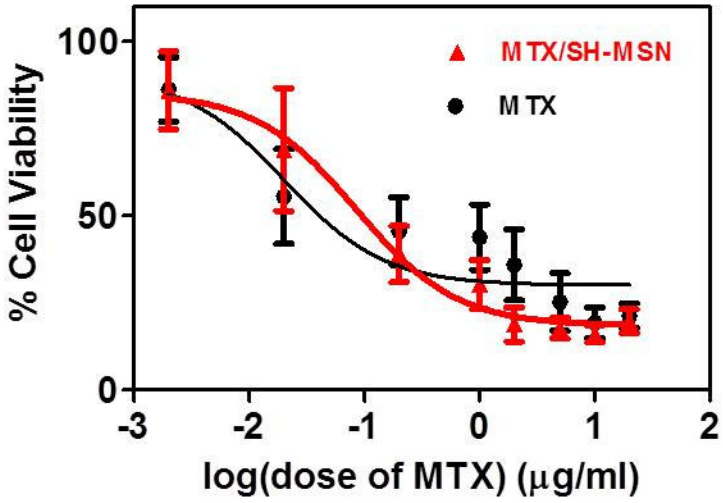

Figure 12. Anti-proliferative activity of free MTX and MTX loaded in SH-MSN in MDA-MB-231 cells. (mean ± S.D., n=3)

2.5 Discussion

Favorable properties, such as large surface area and free volume, make MSN suitable for easy loading of large amounts of a wide range of drugs. The easy way of loading often results in rapid release of drugs and in generally poor control of the drug release from the MSN, severely limiting the potential of MSN in drug delivery. Additional methods of controlling the release are thus required, especially in case of highly soluble drugs with low affinity for silica. Numerous clever and sophisticated strategies have been devised to control the rate of drug release from MSN (Knezevic et al., 2011; Liu et al., 2010; Muhammad et al., 2011; Ruiz-Hernández et al., 2011; Schlossbauer et al., 2010; Zhu et al., 2011). Many of the strategies, however, are not robust enough or compatible with physiologically relevant conditions in which drug delivery vectors must function. In this study, we focused on changes in surface functional groups as a simple way of controlling drug loading and release. We selected MTX as the drug candidate in our studies. MTX exerts antiproliferative activity in advanced breast cancer, acute leukemia, non-Hodgkin's lymphoma and chronic myeloid leukemia by interfering with DNA synthesis

through intercalation and stabilization of DNA topoisomerase II cleavable complex (Parker et al., 2004). Non-specific organ accumulation of MTX justifies development of delivery strategies that can achieve improved delivery to the tumors.

Encapsulation of drugs in MSN is governed by the interplay among drug-solvent, solvent-solvent, drug-silica and silica-solvent interactions. We have initially investigated MTX loading in organic solvents (e.g., DMSO, CH_2Cl_2, DMF, methanol) and mixtures of solvents (e.g., DMF:DMSO 1:0.1, ethanol:water 1:1, methanol:water 1:1) but none of the experiments resulted in drug loading above 4 % w/w. We have found that loading MTX in aqueous pH-controlled environment provided us with substantially higher levels of loading compared with organic solvents. MTX is a weakly basic drug with two types of secondary amines with pK_a = 5.99 and 8.13 and its loading in MSN is thus strongly affected by surface charge of MSN and the pH of the loading media. We have investigated MSN modified with thiols and amines as a way of examining the effect of surface charge on drug loading and release. Thiol-modified MSN are often used in drug delivery applications because of their compatibility with standard bioconjugation techniques to introduce additional functionality into the particles (Lai et al., 2003b). The SH-MSN particles maintained a strong negative charge observed also for the unmodified MSN and caused by the silanol and thiol surface groups. Surface modification with amines resulted in an overall positive charge of the particles. In order to be able to discern the effect of surface functionalization, we have prepared particles with similar physicochemical properties.

As expected, we have found that MTX loading was strongly influenced by the pH. Negligible MTX loading (~1 % w/w) was observed in acidic solution (pH 2.0) regardless of the type of surface functionalization of MSN. MTX loading increased with increasing pH and

reached 18 % w/w at pH 7.4 in SH-MSN. Our results are in agreement with a recent report on the effect of pH on MTX loading in MSN (Ma et al., 2011). Considering that the pK_a of mesoporous silica is ~ 7 (Ma et al., 2011), these results suggest that the pH-dependence of MTX loading is mainly controlled by the ionization of the surface silica in the particles. The importance of electrostatic interactions on silica drug loading of another weak base drug, doxorubicin, was reported previously (Meng et al., 2010b).

Surface functionalization of MSN controls drug loading as well as drug release rate. Vallet-Regi et al. found that ibuprofen loading was higher in non-functionalized MCM-41 silica compared to amine modified silica (Vallet-Regí, 2006). Similar trend was observed for erythromycin where non-functionalized silica loading was 34% compared to 15% for hydrophobically modified silica (Doadrio et al., 2006). We have investigated the effect of surface functionalization on MTX loading using PBS (pH 7.4) as the loading medium. Increasing the relative content of amines in MSN resulted in drastically decreased MTX loading. This observation is in a good agreement with the positive role of electrostatic drug-silica interactions in drug loading. MTX loading increased zeta potential of all MSN, suggesting that at least some of the drug is adsorbed on the surface of the particles. Despite negligible overall loading, the largest increase of zeta potential after MTX loading was observed in NH_2-MSN, suggesting substantial surface adsorption of the drug and thus a limited pore entry. Investigating the physical state of MTX in MSN by XRD and DSC showed that high loading in SH-MSN was not due to MTX crystallization in the pores and that MTX was present in amorphous state. Interestingly, MTX encapsulated in NH_2-MSN showed signs of crystalinity in both DSC and XRD analysis. The observed decrease in melting temperature of MTX loaded in NH_2-MSN is in accordance with the Gibbs-Thompson equation, which predicts the change of melting

temperature to vary linearly with the inverse of pore diameter (Ha et al., 2009). It is likely that electrostatic and hydrogen bond interactions of MTX with the negatively charged silica surface in the pores of SH-MSN inhibits crystallization of loaded MTX (Zhang et al., 2010b), while electrostatic repulsion between MTX and NH_2-MSN does not compete with MTX-MTX interactions and supports crystallization. Previously, crystallization of a weakly acidic drug ibuprofen was observed in MSN, supporting the notion that limited interaction between drug and silica surface is favorable for crystallization in the pores (Riikonen et al., 2009a).

Drug release from MSN can be varied from several hours to several days by altering pore size (Munoz et al., 2003), pore surface area, surface chemistry (Kapoor et al., 2009), drug loading (Song et al., 2011) and choice of drug molecule (Zhang et al., 2010b). Previously, Vallet-Regi demonstrated the feasibility of controlling the release of ibuprofen from MSN by functional groups of silica pore wall (Munoz et al., 2003). The same lab reported that mobility of ibuprofen in the porous silica confinement is dependent on surface functionalization. They found increased mobility for ibuprofen adsorbed on non-functionalized MCM-41 compared to amine–functionalized particles. They attributed faster ibuprofen release rates from non-functionalized silica to the differences in the drug mobility (Munoz et al., 2003). Based on the observed pH-dependence of MTX loading, we hypothesized that surface functionalization will provide a simple method of pH-controlled MTX release from MSN. Indeed, we observed strong pH-dependence of MTX release in SH-MSN (Figure 10 Right) with rapid release in acidic pH and very slow release in neutral pH. In comparison, we observed rapid and pH-independent MTX release from NH_2-MSN and to a large extent also from the mixed SH/NH_2-MSN. These differences in the rate of MTX release and its dependence on the pH are due to the differences in the interactions of the drug with the silica matrix. Strong charge-mediated interactions of MTX

with negatively charged SH-MSN not only increase the drug loading as discussed earlier but also decrease substantially the rate of drug release. Decrease of ionization of the silica in acidic pH weakens the interactions and facilitates rapid drug release. In the absence of the electrostatic interactions in the NH_2-MSN, the release rate is controlled mainly by the rate of drug dissolution. The strong selectivity of MTX release for acidic pH is a useful feature for drug delivery because it should limit the release in systemic circulation and contribute to rapid release of the drug either in the extracellular acidic tumor microenvironment or in the lysosomes after intracellular uptake (Webb et al., 2011).

Anticancer activity of drugs encapsulated in nanoparticles is determined by the intracellular concentration of the free drug released from the particles. The self-quenching nature of the fluorescence of MTX loaded in SH-MSN represents a suitable basis for estimating the amount of free, i.e. non-encapsulated, MTX in the cells and the rate of intracellular MTX release from MSN. As shown in Figure 10 Left, the amount of free MTX present in cells immediately after incubation is significantly larger when using free drug than when delivering the drug with the particles. The situation changes significantly, however, when the intracellular amount of free MTX is followed after the incubation is stopped and the drug removed from the media (Figure 10 Right). Intracellular content of MTX following incubation of cells with free drug declines rapidly after removal of the drug from the media. In contrast, intracellular content of free MTX delivered by the MSN continues to increase even after removal of the particles from the incubation media as the drug is being released from the internalized particles. The almost three fold increase in cell-associated fluorescence 6 h after incubation is a clear indication of intracellular release of MTX from the particles. MSN are internalized by endocytosis and sequestered in lysosomes (Slowing et al., 2006b). The intracellular release of MTX is then

triggered by the acidic pH in the lysosomes as suggested by accelerated MTX release rate in acidic pH. These findings suggest that MSN can deliver MTX into cancer cells and maintain significantly higher intracellular drug concentration than when using free drug.

Evaluation of cytotoxicity of drug delivery carrier is as important as its drug delivery efficiency. In vitro toxicity of MSN is known to be highly cell-type dependent and is controlled by the surface area and surface functionality of the particles (Yu et al., 2011). It has been reported that MSN concentration below 100 μg/ml does not induces cytotoxicity in various cancer cells while growth inhibition is observed when concentration exceeds 200 μg/ml (Lu et al., 2007b; Lu J, 2010; Slowing et al., 2006b). Our results in MDA-MB-231 cells mostly confirmed prior findings, although we observed enhanced toxicity of the amine-containing nanoparticles at 100 μg/mL when compared with SH-MSN. We then assessed the anti-cancer efficacy of MTX delivered by SH-MSN and found similar activity as free MTX. This finding is not surprising. Many drug delivery systems show little benefit in cell culture where the free drug faces no barriers to delivery, while the particles have to overcome multiple delivery barriers.

2.6 Conclusion

In summary, surface functionalization of inorganic nanoparticles serves a simple tool to develop controlled release drug formulation. Based on these results, we conclude that thiol functionality is suitable for MTX formulation development which resulted in successful MSN based MTX formulation. However, it has been shown that shape of such nanoparticles is important in improving cellular uptake and overall tumor accumulation (Arnida et al., 2011; Huang et al., 2009; Muro et al., 2008). To investigate the effect of shape of nanoparticles and their surface PEGylation, we next developed PEGylated mesoporous silica nanorods and optimized formulation parameters for MTX delivery (discussed in chapter 3).

CHAPTER 3

SURFACE PEGYLATION OF MESOPOROUS SILCIA NANORODS (MSNR): IMPLICATIONS FOR LOADING, RELEASE AND DELIVERY OF MITOXANTRONE TO HYPOXIC TUMOR CELLS

3.1 Introduction

The application of nanomaterials in drug and gene delivery has attracted much attention in recent decades (Farokhzad and Langer, 2009; Heffernan and Murthy, 2005). Various nanoparticle drug delivery systems have been developed to deliver chemotherapeutic agents to overcome drug resistance (Patil et al., 2009), to improve drug bio-availability (Shenoy et al., 2005) and to achieve selective cellular targeting with diminishing chemotherapy side effects (Dhar et al., 2008). Interestingly, it has been shown that the shape of nanoparticles has significant impact on cellular uptake (Huang et al., 2009). Ghandehari et al. have shown that PEGylated gold nanorods had higher tumor accumulation than PEGylated gold nanospheres in orthotopic ovarian tumor xenograft in mice (Arnida et al., 2011). Rod shaped particles showed increase in the total blood circulation time compared to spherical nanoparticles, confirming that shape is an important characteristic of nanoparticles in drug delivery (Arnida et al., 2011; Muro et al., 2008).

Inorganic materials such as mesoporous silicas offer a great potential as drug delivery systems due to their high drug loading, tunable pore size and pore volume, control over shape of the particles, easy surface modifications and an excellent biocompatibility. MSN have been used to deliver chemotherapeutic agents and nucleic acids *in vitro* (Chen et al., 2009b; Lin et al.,

2008; Oupicky et al., 2010). MSN can encapsulate and protect hydrophobic as well as hydrophilic molecules and allow for controlled drug delivery (Meng et al., 2011a). *In vivo* application of MSN in cancer treatment has been investigated previously with some promising activity (Meng et al., 2011a; Singh et al., 2011). However colloidal instability (Graf et al., 2012) and hemolysis (Lin and Haynes, 2010) were major drawbacks in the development of successful MSN as drug delivery systems. Lu et al. addressed the problem of colloidal instability by surface modification of MSN with phosphonate groups to prevent aggregation of the particles by electrostatic stabilization (Lu et al., 2007b). Though such surface modifications improved colloidal stability, the issue of hemolysis was not addressed. PEGylation is a frequent strategy to improve colloidal stability by providing steric surface hindrance to improve particle dispersion and to decrease hemolysis (Lin and Haynes, 2010; Meng et al., 2011a; Zhao et al., 2011). Indeed, biodistribution studies of PEG-MSN showed longer blood circulation with significantly less phagocytosis in the liver and spleen and a decrease in the capture by the capillary vessel beds in the lung (He et al., 2011). Despite this, there remains a gap in our understanding of the effect of PEGylation on drug loading, drug release and *in vitro* cell drug delivery using MSN.

Mitoxantrone (MTX) is an anthraquinoline anticancer agent that has been extensively studied and used in the treatment of breast and prostate cancer (Kostrzewa-Nowak et al., 2007; Toh and Li). MTX exerts antiproliferative activity in advanced breast cancer, acute leukemia, chronic myeloid leukemia and non-Hodgkin's lymphoma by interfering with DNA synthesis through intercalation and stabilization of DNA topoisomerase II cleavable complex (Parker et al., 2004). Cardiotoxicity, a severe side effect of anthraquinoline derivatives, may be overcome by localizing drug at the tumor site through a nanomedicine approach (Petros and DeSimone, 2010). Although MTX loaded solid lipid nanoparticles (Lu et al., 2006), PLGA nanoparticles and

liposomes (Law et al., 1996) have been developed, low loading capacity and uncontrolled MTX release prevented their use in preclinical applications. Shi et al. reported that mesoporous silica gives more control over the loading capacity and release profile of weakly basic drugs (Cui et al., 2011; Law et al., 1996; Lu et al., 2006). In our previously published study, we described the effect of surface functionalization of MSN on MTX crystallization, loading and *in vitro* drug release, and demonstrated that thiol functionalized MSN is suitable for MTX formulations, demonstrating a classic crystalline-to-amorphous transformation, high drug loading and controlled MTX release (Wani et al., 2012).

Hypoxia and acidic extracellular conditions are hallmarks of tumor microenvironments. Hypoxia is an adaptive trait of progressive cancers and efforts have been made to develop targeted therapeutics to selectively kill cancer cells (Webb et al., 2011). Poon et al. successfully demonstrated the localization of acidic-pH responsive nanoparticles in the hypoxic tumor microenvironment (Poon et al., 2011). As hypoxia and subsequent acidosis are unifying factors for tumor cells to acquire resistance to chemotherapy and radiation, such targeted technologies may be helpful to sensitize tumor cells and decrease resistance (Poon et al., 2011; Tannock, 2001). Inspired by the pH dependent release of MTX, we hypothesized that MTX formulations will be more effective in hypoxic than normoxic conditions. Inherent properties of MTX such as increased solubility in acidic conditions and facilitated increase in the cell uptake of MTX justified testing of MTX delivery by MSN in hypoxic conditions. To achieve the goal, we investigated the effect of PEGylation on MTX release in the simulated hypoxic and normoxic conditions.

In this study, we demonstrate the effect of PEGylation of mesoporous silica nanorods (MSNR) on loading of MTX and evaluate the *in vitro* release profile under simulated hypoxic

and normoxic conditions. We have synthesized PEGylated MSNR (PMSNR) and loaded MTX into MSNR and PMSNR using electrostatic adsorption. The effect of PEG on colloidal stability, hemolytic properties of MSNR, *in vitro* release of MTX and cell killing efficiency under normoxic and hypoxic conditions was studied. PEGylation decreased the overall MTX loading but increased the rate of MTX release. It was also found that MTX was more effective in the hypoxic than normoxic conditions. For the first time, we report the application of PMSNR for delivery of anti-cancer drugs under hypoxic conditions.

3.2 Materials

Tetraethylorthosilicate (TEOS), 3-mercaptopropyltrimethoxysilane (MPTMS), *N*-cetyltrimethylammonium bromide (CTAB), Sodium hydroxide, hydrochloric acid, and sulfuric acid were purchased from Sigma-Aldrich. Mitoxantrone dihydrochloride (MTX) was purchased from Santa Cruz Biotechnology Inc. (Santa Cruz, CA). PEG-silane (MW 5000) was purchased from Laysan Bio Inc. Sheep whole blood (in sodium heparin) was purchased from Lampire Biological Laboratories. Roswell Park Memorial Institute medium (RPMI), phosphate buffered saline (PBS) (0.15M, pH 7.4) and fetal bovine serum (FBS) were purchased from Invitrogen. Cell titer 96 Aqueous One solution cell proliferation assay (MTS reagent) was purchased from Promega.

3.3 Methods

3.3.1 Synthesis of mesoporous silica nanorods (MSNR)

Thiol-functionalized MSNR were synthesized by co-condensation of TEOS and MPTMS using a modified surfactant-templated base catalyzed method reported previously (Arnida et al., 2011; Giri et al., 2005; Lin et al., 2008; Oupicky et al., 2010). In a typical synthesis of SH-

MSNR, 1.0 g of CTAB was dissolved in 480 mL of de-ionized water made basic by the addition of 3.5 mL of 2.0 M NaOH, and the temperature was raised to 80 °C. To the rapidly stirred solution, 5.0 mL TEOS was injected at a rate of 1.0 mL/min using a syringe pump while stirring. The injection of TEOS was immediately followed by drop-wise addition of MPTMS (1.3 mmol), to achieve a molar ratio of TEOS: MPTMS of 8.7:1. The suspension was maintained at 80 °C for about 2 h and the final product was isolated by centrifugation. The isolated product was washed with excess deionized water and methanol and dried in vacuum. The removal of the CTAB template was carried out by refluxing the dried product in acidic methanol solution (18 mL of 12 M HCl, 20 mL of methanol) overnight. The particles were isolated by centrifugation, washed with methanol and de-ionized water, and dried overnight under active vacuum to yield a white powder.

3.3.2 Characterization of MSNR

The morphology and size of nanoparticles were characterized by transmission electron microscopy (TEM) on a JEOL 2010F Analytical Electron Microscope at 200 kV. TEM samples were prepared by placing a drop of a sonicated aqueous suspension of MSNR on a carbon-film copper grid. The surface area, average pore size, cumulative pore volume, and pore size distributions were determined from nitrogen adsorption/desorption isotherms acquired at 77 K using a 30 s equilibrium interval on an ASAP 2010 Micromeritics porosimeter or a TriSTAR II porosimeter. The surface areas were computed using the Brunauer-Emmett-Teller (BET) model. The cumulative pore volumes were obtained from the BJH (Barret-Joyner-Halenda) model and the pore size distribution was obtained from density functional theory (DFT) modeling using the DFT package of the Micromeritics V2.00 software over the entire range of the adsorption

isotherm. The content of thiol group in the MSN was determined from the sulfur content measured by elemental analysis (Atlantic Microlabs Inc.).

3.3.3 PEGylation of MSNR

Grafting of PEG-silane on the MSNR surface was achieved by using modified method reported previously (Zhao et al., 2011). The MSNR surface was modified with an increasing amount of PEG-silane targeting MSNR:PEG ratios of 1:0.2, 1:0.4, 1:1 and 1:5 (w/w). In a typical experiment, 50 mg of MSNR were suspended in 2 mL of anhydrous toluene followed by sonication for 2-3 min. The resultant MSNR suspension was heated to 110 °C and a PEG-silane solution in 4 mL anhydrous toluene was added dropwise to the stirred MSNR suspension. Particles were stirred for 12 h and isolated by centrifugation at 13,300 rpm for 5 min, followed by washing with ethanol to remove unreacted PEG-silane. PEG modified MSNR were dispersed in 2 mL of DI water and lyophilized to obtain free flowing powder. PEGylated MSNR was analyzed by elemental analysis and thermogravimetric analysis (TGA).

3.3.4 Effect of PEGylation on colloidal stability of MSNR

Colloidal stability was characterized by dispersing 1 mg of PMSNR in 1 mL of RPMI containing 10% FBS followed by analysis using a Zeta Plus particle size analyzer (Brookhaven Instrument) for 5 h. The intensity of the scattered light (kcps) at 90° was measured at the same time and plotted against time to evaluate particle sedimentation.

3.3.5 Hemolysis assay

Hemolytic properties of PMSNR were determined by a method reported previously (Vooturi et al., 2011). In a typical experiment, 2 mL of sheep whole blood was centrifuged at

3,000 rpm for 10 min and the supernatant containing plasma and white blood cells were discarded. The red blood cells (RBC) were washed with 2-3 mL of PBS until the supernatant became colorless to minimize background. The hemolysis assay was performed in triplicate in a 96-well microplate using 1% Triton-X as a positive control and PBS as the negative control. MSNR, 1:04, 1:1 and 1:5 (targeted MSNR: PEG) were selected for the hemolysis assay based on colloidal stability results. In each well, 120 µL of the RBC stock was treated with increasing concentration of the various MSNR: PEG ratios dispersed in PBS. The final volume was adjusted to 150 µL by the addition of PBS. The plate was incubated at 37 °C for 1 hr. After incubation, the plate was centrifuged at 3,800 rpm for 5 min to collect the RBC and 20 µL of supernatant was diluted to 120 µL. Final diluted supernatant was analyzed by measuring absorbance at 414 nm to determine the release of hemoglobin. The absorbance of the positive control, 1% triton X, was set to 100% hemolysis. The results are expressed as mean ± S.D of triplicate samples.

3.3.6 MTX loading

In a typical experiment, 8 mg of MTX was dissolved in 4 mL of PBS (pH 7.4) and based on the targeted MSN:MTX weight ratio (1:0.25, 1:0.5 and 1:1) various volumes of the MTX solution were added to 1 mg of dry MSN. The mixture was sonicated for 30 min and then stirred for 24 h. The drug-loaded particles were centrifuged at 14,500 rpm for 10 min. After centrifugation, MTX loaded MSN were vacuum dried overnight. The amount of MTX loaded in MSN was estimated from the MTX concentration difference in the original solution and in the supernatant after loading in MSN. The MTX concentration was determined by absorbance at 658 nm. Drug loading is expressed as % w/w = 100*(weight of MTX in MSN)/[(weight of MTX in MSN) + (weight of MSN)]. The results are expressed as mean ± S.D. (n=3).

3.3.7 Hydrodynamic radius and Zeta potential measurement

The measurement of hydrodynamic radius and zeta potential of MSNR and PMSNR with and without MTX loading was performed using a ZetaPlus Particle Size and Zeta Potential Analyzer (Brookhaven Instruments) equipped with a 35 mW solid state red laser. Scattered light was detected at 90° and the temperature was set at 25 °C. Samples were prepared by suspending 200 μg of particles in PBS (pH 7.4) at a concentration of 100 μg/ml. The mean hydrodynamic radius was calculated for size distribution by weight, assuming a lognormal distribution using the supplied algorithm and the results are expressed as mean ± S.D. of five runs.

3.3.8 *In Vitro* Release of MTX

Release of MTX from MSNR and PMSNR was analyzed by suspending a known amount of the particles in release medium (PBS, pH 7.4, or 0.2 M sodium acetate buffer, pH 4.5). At each pre-determined time point, MSN were centrifuged at 14500 rpm for 10 min. One mL of supernatant was removed and replaced with fresh 1 mL release medium to maintain sink conditions. Concentration of MTX in the supernatant was determined from absorbance at 658 nm using standard absorbance vs. concentration curve constructed for MTX in the corresponding release buffer.

3.3.9 Cell Culture

The triple negative MDA-MB-231 human breast-cancer cell line was a kind gift from Dr. Jing Li, Karmanos Cancer Institute, Detroit MI. The cells were maintained in Hyclone's RPMI medium supplemented with 2.05 mM L-glutamine, 10% FBS and 1% penicillin. The estrogen positive MCF-7 cell line was a kind gift of Dr. Malathy Shekhar, Karmanos Cancer Institute, Detroit, MI. The cells were maintained in DMEM/F12 50/50 medium supplemented with L-

glutamine, 5% FBS and 0.01% insulin. 10 μL of β-estradiol (10^{-10} M, from Sigma-Aldrich) was added during every culture. Cells were maintained in an incubator at 37 °C with 5% CO_2 for normoxic condition. For hypoxic condition, cells were maintained in an incubator installed with oxygen controller (ProOx model 110, BioSpherix) at 37 °C with 5% CO_2 and 5% oxygen.

3.3.10 Cell Viability

Cytotoxicity of drug-loaded MSNR was determined by the CellTiter 96® Aqueous Cell Proliferation Assay. Five thousand MDA-MB-231 cells per well were seeded in a 96-well plate. One day after reaching confluence, the cytotoxicity of the MTX loaded PMSNR was evaluated by incubating the cells in 100 μL of RPMI/FBS with increasing MTX concentrations. The medium was removed after 72 h and replaced with a mixture of 100 μL fresh RPMI and 20μL MTS reagent solution. The cells were incubated for 3 h at 37 °C. The absorbance of each well was then measured at 490 nm to determine cell viability. The results are expressed as mean % cell viability relative to untreated cells ± S.D. IC50 values were determined by Prism software using non-linear regression involving log (inhibitor) vs. response (three parameters) analysis of dose-response inhibition. The results are represented as mean ± S.D. (n=3)

3.4 Results

3.4.1 Synthesis and characterization of PMSNR

A representative TEM image of MSNR is shown in Figure 13 (top). The TEM image showed MSNR with a rod-like shape with dimensions ~120 nm x 25 nm (length x width). The nitrogen adsorption isotherm (Figure 13 bottom right) revealed that MSNR followed a type IV adsorption isotherm, typical of an MCM-41 type pore structure. The total surface area of the particles was determined to be (820 m^2g^{-1}). BJH analysis revealed a narrow pore size distribution

with an average pore size of 2.6 nm (Figure 13 bottom left). Various MSNR-PEG hybrids were synthesized using different MSNR: PEG ratios (w/w) 1:0.2, 1:0.4, 1:1 and 1:5. Successful PEGylation of MSNR surface was confirmed by elemental analysis (Table 4). The PEG content in PMSNR was calculated from the carbon and hydrogen content and was found to be 14.8, 24.1, 36.2 and 37.1 (w/w %) for 1:0.2, 1:0.4, 1:1 and 1:5 MSNR: PEG ratios respectively. PEG content on MSNR was also confirmed by TGA analysis (Figure 14). The results also show increasing PEG content with increasing concentration of PEG in the reaction: 15%, 22.3%, 29.5% and 33.2% for 1:0.2, 1:0.4, 1:1 and 1:5 ratios respectively. For the remainder of the text, the PMSNR will be referred to by the targeted MSNR: PEG ratios.

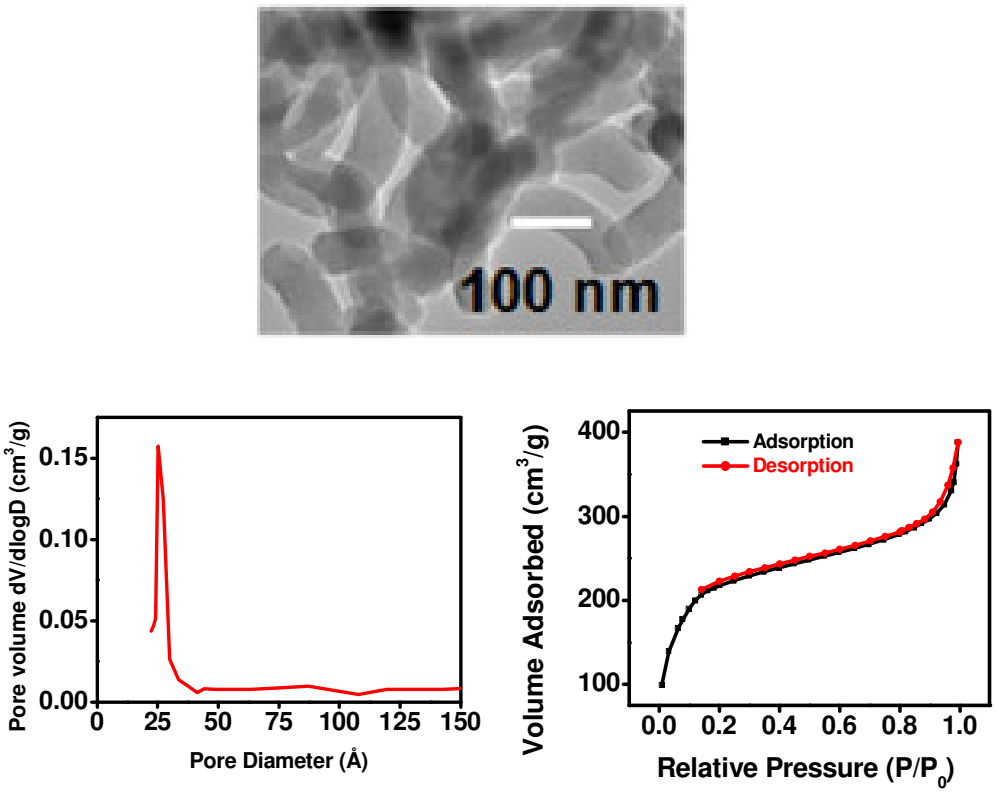

Figure 13. Physiochemical characterization of MSNR. (Top) TEM image of MSNR. (Scale Bar = 100 nm). (Bottom Right) Type IV adsorption isotherm measured by surface area analysis and (Bottom left) Pore size distribution of MSNR.

Table 4. Elemental analysis of MSNR and PEGylated MSNR (PMSNR) (1:0.2, 1:0.4, 1:1 and 1:5 w/w MSNR: PEG).

Element	Element content (%)				
	MSNR	1:0.2	1:0.4	1:1	1:5
C	10.6	17.1	18.8	22.9	23.2
H	2.7	3.7	3.9	4.5	4.5
S	8.6	7.3	7	6.1	6.1

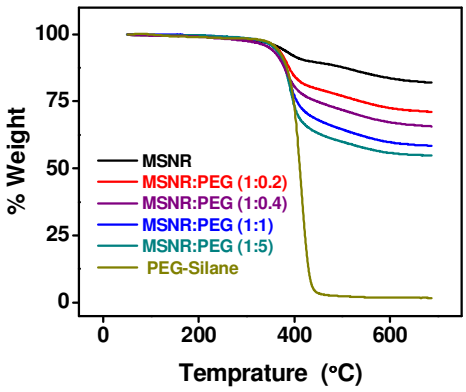

Figure 14. Thermogravimetric analysis of MSNR and PEGylated-MSNR. TGA was done under air with increase in the temperature from 0-700 °C at the rate of 10 °C/min.

MSNR and PMSNR were further characterized to determine their colloidal stability, zeta potential and hemolytic properties. Colloidal stability was examined in deionized water and RPMI containing 10% FBS. Extensive aggregation of MSNR was observed in water but MSNR-PEG (1:5) was stable during the time of study (Figure 15a). In serum -containing RPMI medium, light scattering showed that the MSNR colloidal stability was improved significantly; the particle size decreased in the first hour of incubation but stabilized afterwards, achieving a value of 550 ± 40 nm at the end of the 5 h experiment (Figure 15c). Increase in the PEG content in MSNR-PEG resulted in a decrease in average particle size and colloidally stable particles (no size change over the course of the experiment). Colloidal stability of MSNR-PEG was confirmed by sedimentation studies. The sedimentation of particles was evaluated from the combined size and scattering intensity data. Scattering intensity is directly proportional to the molecular weight and

weight concentration of the particles in solution. A change in the weight concentration with time due to sedimentation, or a decrease in the molecular weight due to silica hydrolysis, results in a decrease in the observed scattering intensity. The scattering intensity of MSNR dropped dramatically over the 5 hour experiment, whereas that of MSNR-PEG remained essentially unchanged (Figure 15b), demonstrating the role of PEG in conferring colloidal stability to MSNR. Sheep RBCs were used to determine hemolytic properties of MSNR and PMSNR (Figure 15d). The results indicate that MSNR has dose dependent hemolytic activity while the presence of PEG prevented damage to RBCs.

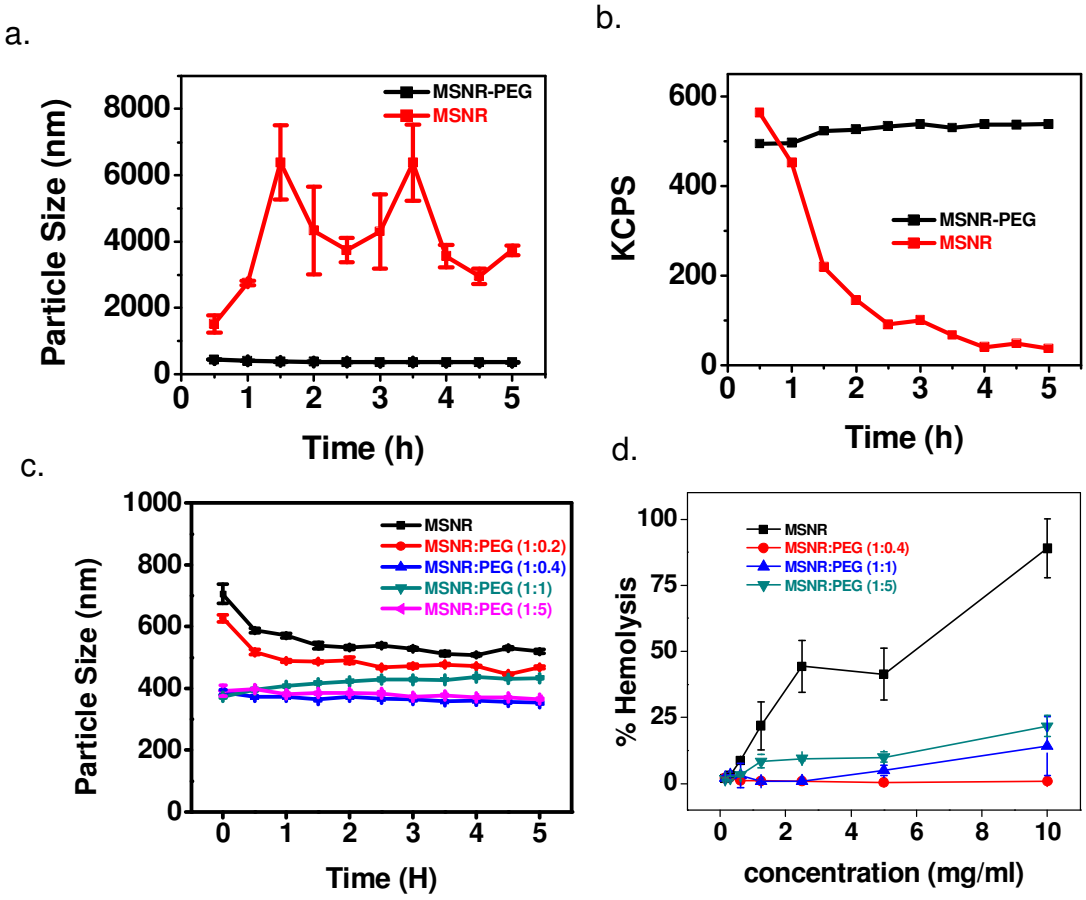

Figure 15. (a) Colloidal stability of MSNR and PEG-MSNR (1:5) in water. (b) Stabilization of MSNR by PEGylation (1:5) confirmed by KCPS data (c) Colloidal stability of MSNR and PEG-MSNR in 5% FBS and (d) Hemolysis study of MSNR and PEG-MSNR.

Zeta potential data are shown in Table 5 and Figure 16. A clear change in the zeta potential after PEGylation of MSNR was observed (Compare Figure 16 bottom left and Table 4 column 1). The result showed MSNR to have a zeta potential of -11.1±0.7 mV, while the PEGylated particles were neutral to slightly positively charged.

Table 5. Zeta potential measurement of MTX loaded various MSNR-PEG counterparts. Results are represented as a mean and standard deviation (n=5).

MSNR:PEG (w:w)	Zeta potential of MSNR:MTX (w/w) (mV)			
	1:0	**1:0.25**	**1:0.5**	**1:1**
1:0.4	4.1±1.8	2.1 ± 2.3	2.8 ± 2.8	5.1 ± 2.5
1:1	3.3±1.2	3.8 ± 1.9	2.8 ± 0.9	3.2 ± 1.7
1:5	4.2±2.1	1.6 ± 1.7	3.3 ± 1.9	4.6 ± 1.6

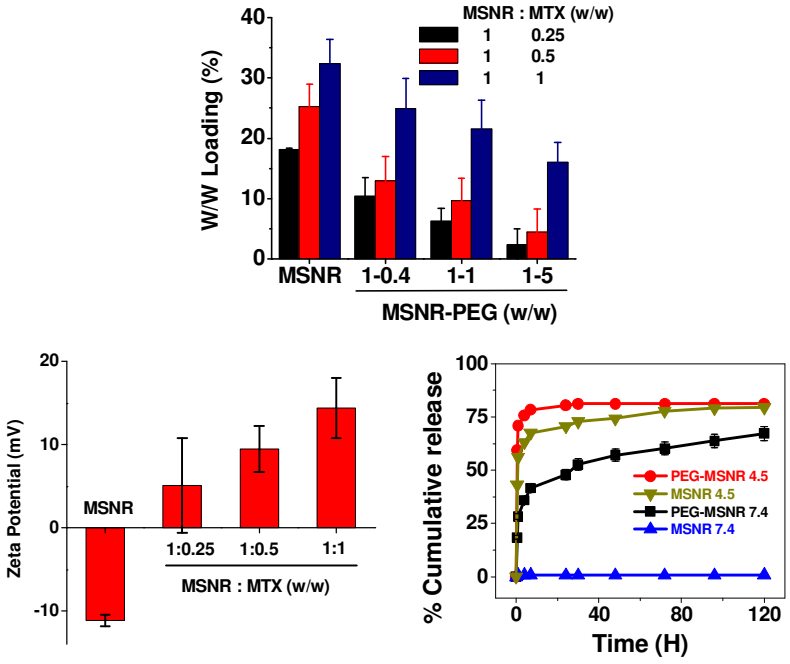

Figure 16. Effect of PEGylation of MSNR on (top) MTX loading (bottom left) zeta potential and (bottom right) *In Vitro* release of MTX. The results represented are mean ± S.D. (n=3).

3.4.2 MTX Loading

MTX loading in MSNR is a function of the electrostatic interactions between cationic MTX and anionic MSNR at pH 7.4. We have encapsulated MTX into MSNR as well as PMSNR containing different amounts of PEG in order to determine the effect of PEG content on MTX loading. Figure 16 (top) shows the effect of PEGylation on MTX loading in MSNR using increasing concentrations of MTX in the loading solution. The data showed that MTX loading in MSNR increased from 18% to 34% with the change in the MSNR:MTX ratio from 1:0.25 to 1:1. MTX loading increased in a similar way for all PMSNR but the loading decreased for all MTX feeding ratios with increasing PEG content in PMSNR. This suggests that MTX loading is hindered by the presence of PEG on the MSNR surface. We have also studied the effect of MTX loading on zeta potential of MSNR (Figure 16 bottom left). The results show that the zeta potential of particles increases as MTX content in the particles increases. The zeta potential for MSNR was -11.11 ± 0.68 mV, while zeta potential for 1:0.25, 1:0.5 and 1:1 MSNR-MTX ratio was found to be 4.5 ± 3.5mV, 8.9 ± 2.6mV and 12.3 ± 3.1 mV, respectively. However, only a negligible change in the zeta potential was observed after MTX loading in the different PMSNR (Table 4).

3.4.3 *In vitro* release of MTX

The release profile of MTX from MSNR and PMSNR (1:0.4) was investigated in PBS (0.15 M, pH 7.4) and in acetate buffer (0.2 M, pH 4.5) to mimic conditions during intracellular endo/lysosomal trafficking of particles. The effect of PEGylation on the release behavior of MTX is shown in Figure 16 (bottom right). The results indicate that MTX release was dependent on pH of the release medium as well as the degree of PEGylation of MSNR. MSNR showed a

much higher MTX release at pH 4.5 than pH 7.4. Within the first 6 h, about 55% of MTX was released from MSNR at pH 4.5, while only 1-2% was released at pH 7.4. Interestingly, PEGylation increased MTX release within the first 2 h to ~75% (pH = 7.4) and about 35% (pH =4.5).

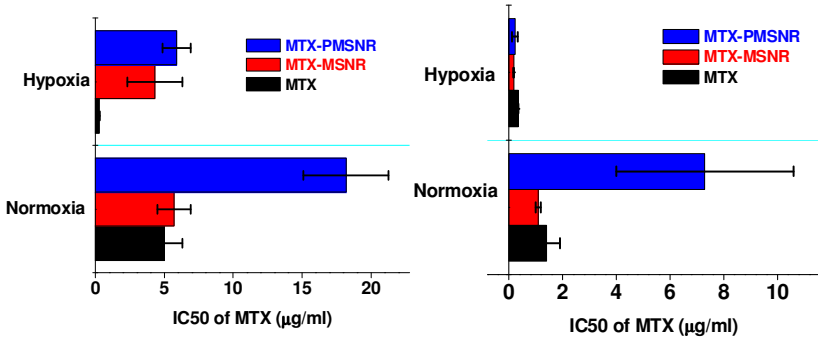

Figure 17. Effect of hypoxia on IC50 of MTX in MCF-7 cells (left) and MDA-MB-231 cells (right).

3.4.4 Effect of hypoxia on antiproliferative activity of MTX loaded in MSNR and PMSNR

Cytotoxic activity of MTX-PEGylated MSNR (MTX-PMSNR) and MTX-MSNR was compared with free MTX in MDA-MB-231 cells and in MCF-7 cells (Figure 17). The results indicate that activity of MTX was decreased under normoxic conditions than under hypoxic conditions in both MDA-MB-231 (Figure 18) and MCF-7 (Figure 19) cells. Loading of MTX in MSNR resulted in a similar anticancer activity in both cell lines under normoxic conditions, whereas under hypoxic conditions, MTX loaded in MSNR showed higher activity in MDA-MB-231 cells (IC50 = 0.18±0.01µg/ml, comparable to MTX alone) than in MCF-7 cells (IC50 = 4.3±2µg/ml, less active than MTX alone). The PEGylation of MSNR had a distinct effect on the observed anticancer activity profiles. MTX-PMSNR was less effective than MTX-MSNR and free MTX under normoxia in both cell lines. Under hypoxia, MTX-PMSNR (IC50 = 0.22µg/ml) was as effective as MTX-MSNR (IC50 = 0.18µg/ml) and free MTX (IC50 = 0.34µg/ml) in

MDA-MB-231 cells. In MCF-7, MTX-PMSNR (IC50 = 5.9µg/ml) has shown lower activity compared with MTX-MSNR (IC50 = 4.3µg/ml) and free MTX (IC50 = 0.25µg/ml). To optimize the time span for effective MTX delivery, we have compared the effect of incubating MTX formulations for 24 and 72 h. The results showed that 24 h incubation was not sufficient for MTX activity under normoxic or hypoxic conditions to level off, and cell killing increased with 72 h incubation.

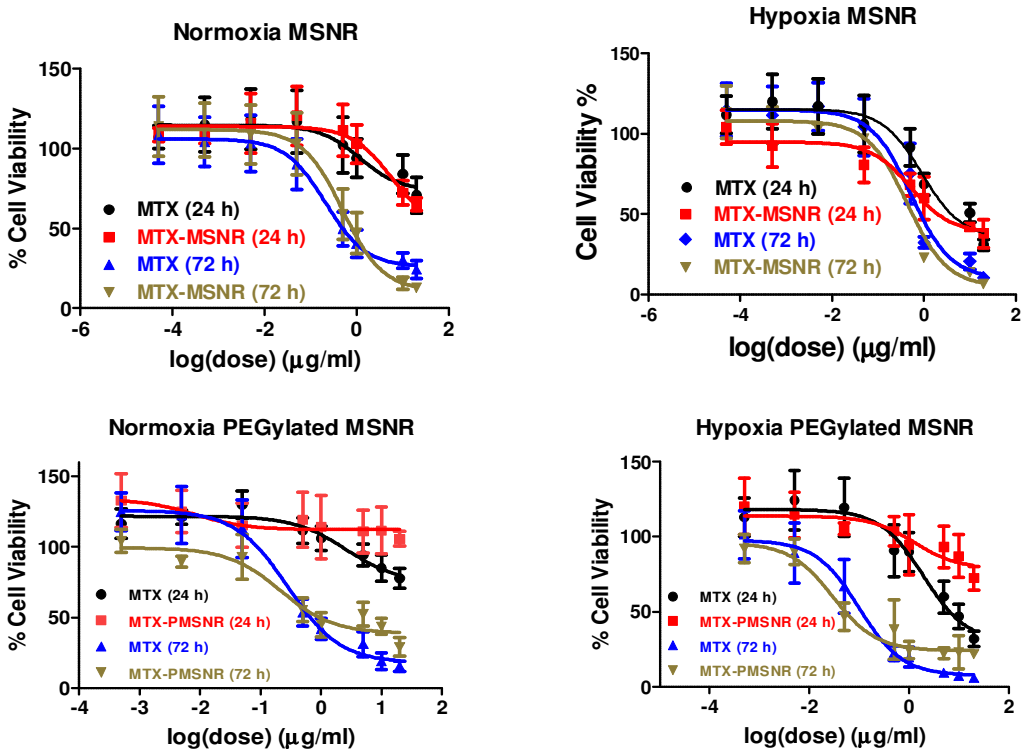

Figure 18. Effect of hypoxia on MTX driven MDA-MB-231 cell toxicity. MTX-loaded MSNR toxicity in normoxic and hypoxic condition (top left and top right respectively). MTX loaded PEGylated MSNR toxicity in normoxic and hypoxic condition (bottom left and bottom right respectively.

3.5 Discussion

Due to excellent control over particle size and shape, mesoporous silica is an attractive material for a wide range of applications ranging from drug delivery to theranostics (Ferrari,

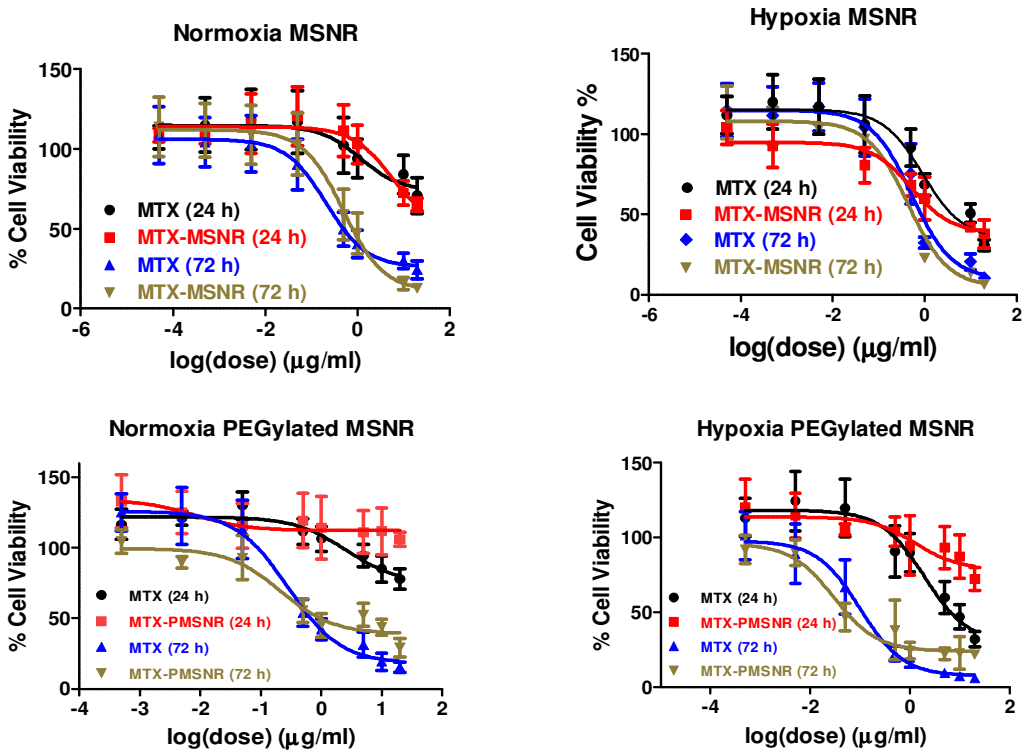

Figure 19. Effect of hypoxia on MTX driven MDA-MB-231 cell toxicity. MTX-loaded MSNR toxicity in normoxic and hypoxic condition (top left and top right respectively). MTX loaded PEGylated MSNR toxicity in normoxic and hypoxic condition (bottom left and right respectively).

2005; Park et al., 2009d). To develop MSN for controlled release applications, sophisticated techniques such as nanovalves (Meng et al., 2010a), pH sensitive polymer shells (Liu et al., 2011) and various surface polymer modifications (Oupicky et al., 2010; Singh et al., 2011) have been applied. However, only a few studies have directly reported the effect of such techniques on MSN properties such as drug loading and drug release. Meng et al. reported that polymer attachment leaves the porous interior structure free for drug binding and hence mesoporous silica can be used for drug and gene delivery application (Meng et al., 2011a). Nevertheless, the same group reported low doxorubicin loading of 2.5-3 w/w % in PEGylated MSN. We previously reported that surface modification of MSN with poly(2-(dimethylamino)ethylmethacrylate) or poly(2-(diethylamino)ethylmethacrylate) synergistically delivered chloroquine and nucleic acids

to cancer cells with decrease in the chloroquine loading from 0.73 mg/mg in unmodified MSN to 0.43 mg/mg in PEGylated MSN (Oupicky et al., 2010). However, Singh et al. have reported 40% doxorubicin loading in polymer modified MSN (Singh et al., 2011). Such discrepancies in the literature about the effect of surface modifications inspired us to fill this gap by (i) scrutinizing the effect of surface modifications on drug loading and drug release, (ii) optimizing PEG content for MTX loading and (iii) investigating the effect of PEGylation on MTX delivery *in vitro*.

In this study, we focused on rod-shaped mesoporous silica and the effect of surface PEGylation on loading and release kinetics of an anticancer drug MTX. Particle shape is known to control biological outcomes of the delivery systems due to a change in the rate of intracellular uptake (Huang et al., 2009), an increase in the blood circulation time (Arnida et al., 2011) or a decrease in the opsonization The selection of rod shaped mesoporous silica was based on our preliminary *in vitro* studies, in which it was found that cytotoxicity of MTX loaded in MSNR was similar to MTX loaded in spherical MSN (data not shown).

Non-specific organ accumulation of MTX justifies development of delivery strategies that can achieve improved delivery to the tumors. MTX is a weakly basic drug with two types of secondary amines with pK_a = 5.99 and 8.13 and its loading in MSNR is thus strongly affected by surface charge of MSNR and the pH of the loading media. This study focused on the investigation of surface modifications of MSN with PEG with regards to drug loading and release. PEGylation of nanoparticles is widely used to modify their renal clearance, to improve biodistribution and to prevent opsonization by reducing the overall surface charge of nanoparticles (He et al., 2010b; He et al., 2011; Petros and DeSimone, 2010). However, PEGylation also has a dramatic impact on the surface charge. MSNR has a negative charge caused by the silanol and thiol surface groups. Loading of MTX into MSNR produces a positive

surface charge (Figure 16) which depends on the weight-to-weight (w/w) ratio between drug and MSNR. Thus increasing the drug concentration during loading from 1 mg/ml to 10 mg/ml increases w/w loading from 18 to 34%. After PEGylation, the surface charge becomes slightly positive to neutral (Table 5, column 1) and this decrease in the charge adversely affects loading capacity of MSNR for MTX. Thus, increasing the PEG content on PMSNR from 0 to 5 % decreases the MTX loading from 18 to ~3%. This suggests optimized PEG content is necessary to develop PEGylated MSNR with acceptable colloidal stability and drug loading.

Interaction of nanoparticles with RBCs is a concern for systemic intravenous administration. MSN have been shown to be hemolytic in a dose dependent manner (Lin and Haynes, 2010; Zhao et al., 2011). It has been shown that hemolytic activity of MSN is a function of particle size, total surface area and the presence of silanol groups (Lin and Haynes, 2010; Zhao et al., 2011). PEGylation is a viable approach to counter the hemolytic nature of MSN (Lin and Haynes, 2010; Slowing et al., 2009). Our results confirm that MSNR are hemolytic in a dose dependent manner while hemolysis was prevented after PEGylation. PEGylation alters the charge of the particles, reduces interactions with RBCs, and hence enhances compatibility with blood.

In vitro drug release from MSN has been well studied with respect to varying pore size (Shi et al., 2007), pore wall functional groups (Riikonen et al., 2009b), drug loading and choice of drug molecule (Lu et al., 2007b). Based on the pH dependent solubility of MTX, we found slow release of MTX at neutral pH and faster drug release at acidic pH from MSNR. Such pH dependence is a useful feature so that after encapsulation, we can prevent the drug release during *in vivo* circulation. Then hypoxic tumor microenvironment may help to increase localization of the drug at the tumor site simply based on the solubility profile of a drug molecule. Interestingly,

after PEGylation an increase in the rate of MTX release was observed at neutral as well as acidic pH. These differences in the MTX release are most likely due to changes in the electrostatic interactions between MTX and the silica matrix caused by PEGylation. Thus, the same electrostatic repulsion that makes PMSNR difficult to load with MTX, facilitates the release.

In vitro assessment of anti-cancer agents in hypoxic conditions mimics better the tumor microenvironment than normoxic conditions. Hypoxia inducible factors (HIF) play an important role in hypoxia associated tumor development and therapeutic resistance. MTX has been shown to inhibit HIF-1α preferentially under hypoxic conditions (Toh and Li, 2011). In our study we found that MTX activity was higher in hypoxic conditions than normoxic ones in both MDA-MB-231 and MCF-7 (Figure 18 and Figure 19). Such an increase in the activity may relate to an increase in the cell uptake of MTX under hypoxia. To test this hypothesis, we treated MDA-MB-231 cells with free MTX and MTX loaded in MSNR and PMSNR. We indeed observed higher MTX cell uptake under hypoxia than normoxia for all formulations (Figure 17). However, we observed higher uptake of free MTX under both normoxic (MFI = 306) and hypoxic (MFI = 514) conditions compared to MTX-MSNR (Normoxia MFI = 161, Hypoxia MFI = 189) and MTX-PMSNR (Normoxia MFI = 196, Hypoxia MFI = 299). Higher cell uptake of free drug was not surprising as free soluble drug faces limited barriers for delivery *in vitro* while with nanoparticle formulations, the drug has to diffuse out of the particles and the particles have to overcome multiple barriers. Surprisingly, despite well-established phenomenon of decreased cell uptake of PEGylated nanoparticles (Zhu et al., 2010), we have observed higher MTX accumulation in PEGylated particles compared to non-PEGylated MSNR. This agrees well with the results from MTX *in vitro* release in which higher MTX release was observed in PEGylated MSNR relative to MSNR at both pH 7.4 and 4.5.

3.6 Conclusion

In summary, we have successfully demonstrated the effect of PEGylation of MSNR on loading and release of MTX. PEGylation of MSNR decreased overall drug loading but increased MTX release. Anticancer activity studies showed that MTX formulations were as effective as free MTX in hypoxic conditions but less effective in normoxic conditions. We conclude that further optimization of MSNR PEGylations is necessary to develop MSN as an injectable.

CHAPTER 4

IS PEGYLATION OF MSN A VIABLE APPROACH TO DELIVER HYDROPHOBIC DRUG PACLITAXEL?

4.1 Introduction

Biodegradable inorganic materials such as mesoporous silica are currently being investigated for the purpose of controlled release of hydrophilic drugs (Chen et al., 2009b; Cui et al., 2011; Wani et al., 2012), improved oral bioavailability of hydrophobic drugs (Lu et al., 2007a; Qian and Bogner, 2012) and intracellular delivery of nucleic acids such as DNA and siRNA (Bhattarai et al., 2010; Chen et al., 2009b; Lin et al., 2008). High surface area, easy surface modifications, well controlled pore size and excellent biocompatibility persuaded scientists to develop mesoporous silica for drug, gene and drug-gene combinatorial delivery applications (Bhattarai et al., 2010; Chen et al., 2009b; Meng et al., 2011a; Singh et al., 2011).

Paclitaxel (PTX), one of the most powerful chemotherapeutic drugs, has gained widespread clinical use in the treatment of breast, ovarian, non-small cell lung carcinoma, bladder, prostate, melanoma, and esophageal solid tumor cancers but its administration is still associated with significant toxicity (Sheihet et al., 2012). Paclitaxel formulations in Cremophor EL PTX (Taxol) has been used clinically to improve aqueous solubility of hydrophobic PTX (10.6 mM in water) (Mitra and Lin, 2003; ten Tije et al., 2003). Unfortunately, dose dependent inherent toxicity of Cremophor limits its use in the PTX formulation and there is thus a need for improved method of PTX solubilization. Nanotechnology holds a potential to overcome the problems of the PTX bioavailability and perhaps improve its therapeutic index (Farokhzad and

Langer, 2009). Abraxane, albumin-based nanoparticles formulation, notably improved maximum tolerated dose and toxicity profile of PTX compared to standard Cremophor formulation. But Abraxane is less effective in the treatment metastatic breast cancer and there is thus a continuing need for better carrier for PTX (Desai et al., 2006; Lammers et al., 2012; Sheihet et al., 2012).

Among variety of available nanoparticles available for PTX delivery, MSN offer several attractive features to overcome solubility problems of hydrophobic anti-cancer drugs. High porous surface area and well controlled pore size of MSN can be used as a reservoir for solubilizing hydrophobic drugs (Lu et al., 2007a) and subsequently drugs can be released in a controlled as well as sustained manner. It has been shown that drug loading and release rate from mesoporous silica is dependent on physicochemical properties of the drug molecule (Liu et al., 2012), surface functionalization of mesoporous structure (Cui et al., 2011; Wani et al., 2012), choice of solvent and partition coefficient of drug between solvent and silica matrix (Qian and Bogner, 2012). Surface modification of mesoporous silica by functional groups such as –COOH, $-NH_2$ and –SH have been shown to modulate drug release from the silica matrix (Qian and Bogner, 2012; Qu et al., 2006; Riikonen et al., 2009b; Wani et al., 2012). Similarly, mesoporous silica surface has been modified by PEG, poly(ethyleneimine), poly(methacrylate), poly(L-lysine) and chitosan to improve blood circulation time, to control drug release and to condense nucleic acid (Chen and Zhu, 2009; Hartono et al., 2012; He et al., 2010b; Meng et al., 2011a; Shen et al., 2011).

Ease of pre- and post-modifications of MSN with desirable polymers gives more temporal control over drug release. As mentioned in the second chapter, polymer attachment leaves porous interior structure free for drug binding and hence, mesoporous silica can be used for drug and gene delivery application (Meng et al., 2011a). It has also been reported that

surface-modified MSN with poly(2-(dimethylamino)ethylmethacrylate) (PDMAEMA) or poly(2-(diethylamino)ethylmethacrylate) (PDEAEMA) synergistically delivered chloroquine and nucleic acids to cancer cells (Bhattarai et al., 2010). But drug loading in this polymer pre-modified MSN might be unique for particular drug and versatility of such polymer-silica hybrids need to be investigated with different drugs. Polymer chains swell in a good solvent to maximize polymer-solvent contacts while in bad solvent polymer chains stay close to each other and collapse forming a hard sphere (Minko, 2006). Polymers can be also present in brush and mushroom conformation based on grafting density (Hak et al., 2012). The extent of grafting density and conformation of polymeric chains in a particular solvent may be important for opening of porous structure and thus, important for drug loading and release.

In this chapter, we are presenting a case of PTX formulation based on MSN with emphasis on the effect of PEG architecture on PTX loading. We hypothesized that architecture of hydrophilic PEG will affect release of PTX loaded in MSN. We have chosen six different PEGs to identify the effect of polymer architecture on PTX loading and release: (a) Linear-PEG 5kDa (b) Linear-PEG 30kDa (c) Y-shaped PEG (d) loop forming PEG (SVA-PEG-SVA) (e) 4-arm 30kDa PEG and (f) 4-arm 2kDa PEG.

4.2 Materials

Tetraethylorthosilicate (TEOS), 3-aminopropyltriethoxysilane (APTES), *N*-cetyltrimethylammonium bromide (CTAB), Fluorescein isothiocynate (FITC), hydrochloric acid, and sulfuric acid were purchased from Sigma-Aldrich. Paclitaxel (PTX) was purchased from Santa Cruz Biotechnology Inc. (Santa Cruz, CA). Dulbecco's modified Eagle's medium (DMEM), phosphate buffered saline (PBS), fetal bovine serum (FBS) were purchased from Invitrogen. Cell titer 96 Aqueous One solution cell proliferation assay (MTS reagent) was

purchased from Promega. Various methyl poly(ethylene glycol)-succinimidyl valerate (mPEG-SVA) with different architecture were purchased from Laysan Bio Inc. HPLC grade dichloromethane (DCM) and methanol were purchased from Sigma Aldrich.

4.3 Methods

4.3.1 Synthesis of FITC functionalized mesoporous silica nanoparticles (FMSN)

FMSN was synthesized in three steps: (a) synthesis of MSN (b) preparation of fluorescein-APTMS conjugate and grafting of conjugate to the synthesized MSN (c) removal of CTAB from FMSN.

(a) Synthesis of MSN. MSN was synthesized using modified surfactant-templated base-catalyzed method reported previously in Chapter 1. In a typical synthesis, 1.0 g of CTAB was dissolved in 480 mL of de-ionized water made basic by the addition of 3.5 mL of 2.0 M NaOH, and the temperature raised to 80 °C. To this solution, 5.0 mL TEOS was injected at a rate of ~1.0 mL/min using a syringe pump while stirring. The dispersion was maintained at 80 °C for about 2 h and the final product was isolated by centrifugation. The isolated product was washed with excess deionized water and methanol and dried in vacuum.

(b) Preparation of fluorescein-APTMS conjugate and grafting of conjugate on MSN. In a typical procedure, 2.5 ml of APTES was dissolved in 10 ml of ethanol containing 10 mg of fluorescein isothiocyanate (FITC). This mixture was stirred at room temperature under dark conditions overnight to form FITC-APTES conjugate. As-synthesized MSN was dispersed in 100 ml of toluene and system temperature was raised to 80 °C. The FITC-conjugate solution was injected into the MSN dispersion dropwise using a syringe pump while stirring at a rate of ~ 1 mL/min. After the injection, the system was left at 80 °C for about 20 h. The nanoparticles were

isolated by centrifugation and washed twice with methanol and then with water twice and dried under vacuum to yield a free flowing yellow powder.

(c) Removal of CTAB. The dried yellow product was dispersed in 320 mL of methanol and 18 mL of 37% HCl and refluxed overnight. The nanoparticles were isolated by centrifugation and washed twice with methanol and once with de-ionized water before drying under vacuum to yield a free flowing FMSN powder.

4.3.2 Characterization of FMSN

FMSN were characterized by TEM and micrometric porosimeter for particle size and surface area measurement respectively by a method reported previously in the chapter II (section 2.3.2). Quantitative determination of free amines after FITC conjugation, which was required for further PEG modifications was measured by colorometric method reported previously (Bhattarai et al., 2010). The procedure consisted of two parts. In first part imine linkage was formed. In a typical experiment, mixture of 65 mg of FMSN, 16 mg of 4-nitrobenzaldehyde and 1 g of Linde's agent was dispersed in 16 mL of anhydrous methanol. Two-three drops of glacial acetic acid was added to the solution. The solution was then stirred overnight under nitrogen atmosphere at 50 °C which resulted in the formation of imine linkage. The product was then isolated by centrifugation and was washed with anhydrous methanol 3 times and dried.

In the second part, the imine linkage was hydrolyzed to generate 4-nitrobenzaldehyde. The dried particles were taken along with 16 mL water and 2-3 drops of glacial acetic acid. The contents were stirred at 40 °C overnight under N_2 atm. The imine linkage was hydrolyzed and that resulted in the formation of 4-nitrobenzaldehyde. The compound absorbed at 269 nm and its concentration was monitored by UV-Vis. The concentration of the amino groups present on the surface of the MSN was then back calculated from the estimated concentration of 4-

nitrobenzaldehyde. The estimated concentration of accessible amino groups on the surface of amine functionalized MSN was found to be $1.35x10^{-3}$ moles of NH_2 / g MSN.

4.3.3 PEGylation of FMSN

Free amines on the FMSN surface were grafted with various mPEG-SVA by using modified method reported previously (Zhao et al., 2011). In a typical experiment, known amount of FMSN was dispersed in 2 ml of anhydrous toluene and mPEG-SVA containing solution was added dropwise and the mixture was heated at 110°C overnight under nitrogen. PEG-modified FMSN were isolated by centrifugation at 14,500 rpm for 10 min. Particles were washed with methanol twice to remove unreacted PEG. Subsequently, particles were dried under vacuum. Successful PEGylation was confirmed by TGA and elemental analysis.

4.3.4 Colloidal stability of PEGylated FMSN

Colloidal stability was characterized by dispersing 1 mg of various PEG-modified FMSN into 1 mL of RPMI medium containing 5% FBS. Particle suspension was sonicated for 30 sec before particle size analysis by Zeta Plus particle size analyzer (Brookhaven Instrument) for 5 h with 30 min interval.

4.3.5 PTX drug loading

In a typical drug loading experiment, known amount of PEGylated FMSN was dispersed in 500 μL of methanol or dichloromethane and the suspension was sonicated for 10 min to disperse particles. PTX solution in methanol or dichloromethane was added dropwise to FMSN suspension and the mixture was kept stirring overnight. After stirring, drug-loaded particles were centrifuged at 14,500 rpm for 10 min and supernatant was removed. Particles were dried in vacuum. Drug loading was determined by dispersing 1 mg of PTX-loaded FMSN or various

PEGylated FMSN in 2 mL ethanol. Particles were kept shaking overnight to extract PTX. Concentration of PTX was then determined by HPLC.

4.3.6 *In vitro* drug release

PTX release from FMSN was determined in PBS (0.15 M, pH 7.4) containing 0.5% (w/v) Tween 80 at 37 °C (Chavanpatil et al., 2006). Nanoparticle suspension (1 mg/ml, 1 ml) was placed in Float-A-Lyzer® dialysis tube (molecular weight cut-off 10,000 Da, Pierce), and the dialysis tube was immersed in 10 ml of the release buffer in a 15-ml centrifuge tube to maintained sink condition. The centrifuge tubes containing dialysis tubes were placed in an incubator shaker set at 100 rpm and 37 °C. At predetermined time intervals, 1 ml of the release buffer was removed from the tube and was replaced with fresh release buffer. PTX concentration in the buffer was determined by HPLC.

4.3.7 HPLC analysis

The HPLC system (Beckmann Instruments, Fullerton, CA) used consisted of a C-18 column (4.6 mm × 25 cm) with 5 μm packing (Ascentis Express, Sigma-Aldrich, St. Louis, MO). The mobile phase consisted of a mixture of water and acetonitrile in the ratio of 35:65 (v/v), and was delivered at a flow rate of 1 ml/min. A 5 μL volume of drug sample was injected using an autoinjector (Model 508, Beckmann Instruments), and PTX was detected by UV absorbance at 227 nm (System Gold 168 detector). A standard curve for PTX was prepared in ethanol and PBS containing 0.5% tween 80 and was used to determine PTX concentration for drug loading and drug release respectively.

4.3.8 Cell Culture

Triple negative MDA-MB-231 human breast cancer cell line was a kind gift from Dr. Jing Li, Karmanos Cancer Institute, Detroit MI. The cells were maintained in Hyclone's RPMI medium supplemented with 2.05 mM L-glutamine, 10% FBS and 1% penicillin. Cells were maintained in an incubator at 37 °C with 5% CO_2.

4.3.9 Cell uptake of FMSN

Cellular uptake of PEG modified FMSN was determined by measuring cell-associated fluorescence of FITC by flow cytometry. MDA-MB-231 cells (4.0 x 10^5 cells per well) were seeded in 12-well plate 12 h before experiment. Cells were incubated with 50 μg/ml of non-modified FMSN and various PEG-modified FMSN in RPMI/FBS for 2 h at 37 °C. Cells were washed twice with PBS and harvested by trypsinization. Cells were resuspended in Hank's buffered salt solution (HBSS) and particle uptake was analyzed immediately by flow cytometry at an excitation laser wavelength of 480 nm and using a 515-545 nm emission band pass filter. Flow cytometry analysis was performed on a BD Biosciences LSR II instrument. Ten thousand cells were collected for each measurement. Cellquest software was used for data analysis. Reported fluorescence intensity data were corrected for cell autofluorescence using untreated cells.

Similarly, FMSN uptake in MDA-MB-231 cells was confirmed by confocal microscopy. In a typical experiment, 50,000 cells (2 mL of RPMI/FBS medium/well) were seeded on a cover slip in a 6-well plate. After 24 h, cells were incubated with 500 μL of 25 μg/ml of FMSN suspension for 3 h to facilitate cell uptake. RPMI medium containing FMSN suspension was removed and cells were washed twice with warm PBS. Simultaneously, to determine sub-cellular distribution of FMSN, cells were incubated with RPMI containing 200nM lysotracker red and 20 μM of hoechst 33342 to stain lysosomes and nucleus respectively. Dye containing medium was

removed after 10 min and cells were fixed with 0.4% paraformaldehyde for 2 h. Slides were removed by forceps and mounted on glass slide with a mounting media. Slides were dried overnight before confocal microscopy (Leica TCS SP5 laser scanning confocal microscope, Leica Microsystems, Buffalo Grove, IL).

4.3.10 Cytotoxicity

Cytotoxicity of PTX-loaded FMSN was determined by the CellTiter 96® Aqueous Cell Proliferation Assay. In a typical experiment, five thousand MDA-MB-231 cells were seeded in a 96-well plate. One day after reaching confluence, the cytotoxicity of PTX and PTX loaded FMSN formulation was evaluated by incubating the cells in 100 μL of RPMI/FBS with increasing concentrations of drug and drug-loaded particles. Cells were incubated for 6 h and medium containing drug and drug-loaded particles were replaced with fresh RPMI medium. The time dependent cytotoxicity of free PTX and PTX-FMSN was determined after 24 h, 48 h and 72 h by replacing with MTS solution (100 μL of RPMI and 20 μL of MTS reagent per well). The cells were incubated for 3 h at 37 °C. The absorbance of each well was then measured at 490 nm to determine cell viability. The results are expressed as mean % cell viability relative to untreated cells ± S.D. IC50 values were determined by Prism software using non-linear regression involving log (inhibitor) vs. response (three parameters) analysis of dose-response inhibition.

4.4 Results and discussion

The main aims of this study were (a) to determine the ability of unmodified FMSN to load, to release and to deliver hydrophobic drug PTX and (b) to determine the effect of PEG architecture on colloidal stability, cell uptake and PTX loading in FMSN. To achieve these aims, particles were post-grafted with six PEGs. In general, polarity of solvent dictates interaction of hydrophobic molecules with silica matrix but drug solution has to surpass polymeric layer on

particles for this interaction. However, solvent should be a "good solvent" for polymer to facilitate swift passage of drug molecules towards porous structure to achieve successful drug loading. Our hypothesis was that controlling PEG architecture on the nanoparticles at a given solvent will subsequently improve overall drug loading and release profile. To demonstrate feasibility of such surface modifications, nanoparticles were modified with linear PEG (5kDa), linear PEG (30kDa), 4-arm PEG (2kDa), 4-arm PEG (40kDa), Y shaped PEG and SVA-PEG-SVA (loop that forms PEG) polymers. PEG structure was optimized in the development of successful PTX formulation by keeping in mind to achieve high drug loading, controlled drug release, high cell uptake, while retaining anti-cancer activity.

4.4.1 Synthesis and physiochemical characterization of FMSN

FMSN was synthesized by modification of a method reported previously (Lai et al., 2003a; Slowing et al., 2006b; Wani et al., 2012; You et al., 2008). A representative image of FMSN is shown in Figure 20a. A TEM image showed that particles were spherical with size of ~90 nm. The observed porous structure in the FMSN was supported by the nitrogen adsoportion/desorption isotherm (Figure 20b). It confirmed typical type IV adsorption isotherm of mesoporous materials according to International Union of Pure and Applied Chemistry classification (IUPAC). Figure 20b shows two capillary condensations steps at P/P0 ~ 0.3 -0.4 and P/P0 ~ 0.8 which represents typical mesoporosity. The average pore size of FMSN was found to be ~2.6 nm (data not shown) while BET surface area and pore volume of FMSN were determined to be 780 m^2/g and 0.46 cm^3/g, respectively. Such high surface area makes the particles suitable for efficient loading of chemotherapeutics in the porous structure.

a.

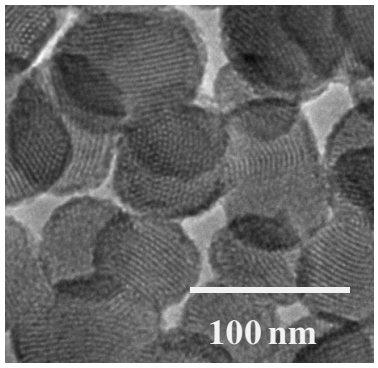

b.

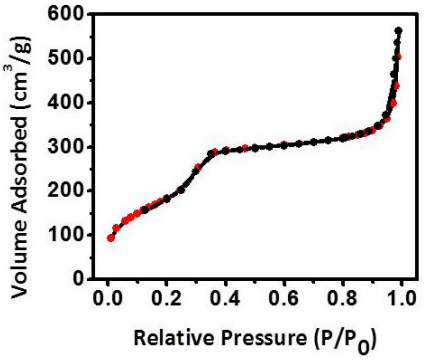

c.

solvent	Particle size (nm)
Water	1438.2 ± 110.2
PBS	2229.8 ± 163.0
RPMI/FBS	2958.7 ± 574.5
Pluronic F-127	1104.5 ± 56.7

d.

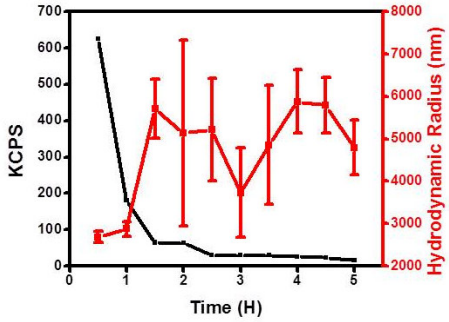

Figure 20. Physicochemical characterization of MSN. (a) TEM image of FMSN (b) Adsorption isotherm of FMSN (c) Hydrodynamic size measurement and (d) Light scattering intensity vs time (H) for FMSN. The results are expressed as mean ± S.D. (n=3)

FMSN hydrodynamic size was measured in water, PBS, RPMI/FBS and Pluronic F-127 by dynamic light scattering to determine the effect of salt, serum and surfactant on the stability of FMSN (Figure 20c). Hydrodynamic size was calculated from translational diffusional coefficient by using the Stokes-Einstein equation. The results show that FMSN were highly aggregated in all the studied media. Subsequently, time dependent colloidal stability in RPMI/FBS was also evaluated by DLS (Figure 20d). The results showed that particles were highly aggregated and sharp decrease in the scattering intensity confirmed colloidally unstable particles. Light scattering intensity sharply decreased from 600 to 100 kcps within 1 h. The results show that Pluronic F-127 surfactant was not sufficient to achieve collidally stable particles. However, it was reported that MSN can be stabilized by adsorption of serum proteins

(Xia et al., 2009a) and in the previous chapter III (section 3.3.4) we have also showed that MSN can be stabilized in the presence of FBS. Unlike those findings, however, it appears that the presence of FITC in the structure of FMSN makes the particles much more susceptible to aggregation and that serum stabilization is not effective in this case. Therefore, in order to achieve colloidal stability, we decided to use covalent PEGylation.

Efficient cell uptake of nanoparticles is necessary for intracellular delivery of therapeutics. It is thus important to monitor subcellular trafficking to understand localization of

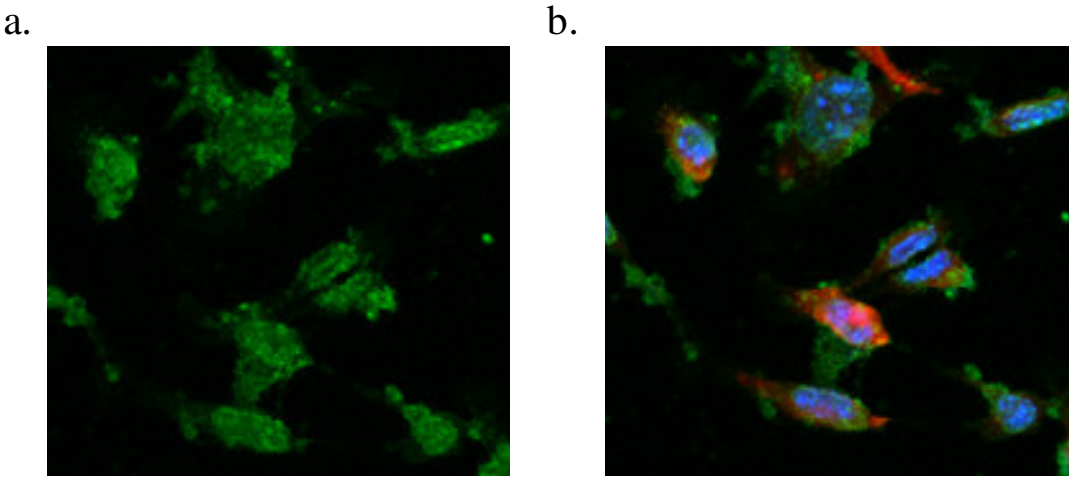

Figure 21. Cell uptake of FMSN by confocal microscopy. (a) Green FITC filter and (b) Overlay of FITC, Hoechst 33342 and lysotracker red.

nanoparticles after cell uptake. The cell uptake of FMSN was confirmed by using confocal microscopy. MDA-MB-231 cells were incubated with FMSN and then cells were washed with PBS to remove particles that were not internalized. Routing of FMSN into the lysosomes was determined by staining cells with Lysotracker red and Hoechst 33342. Lysotracker red specifically stains acidic endo-lysosomal organelles while Hoechst dye stains nucleus (Figure 21). The result suggests that FMSN were located in perinuclear regions in the cells. It was reported that FMSN are mainly taken up into the acidic organelles and trafficked to cytoplasm

with the help of an unspecified endolysosomal escaping effect (Huang et al., 2005). Our data confirm the previous findings.

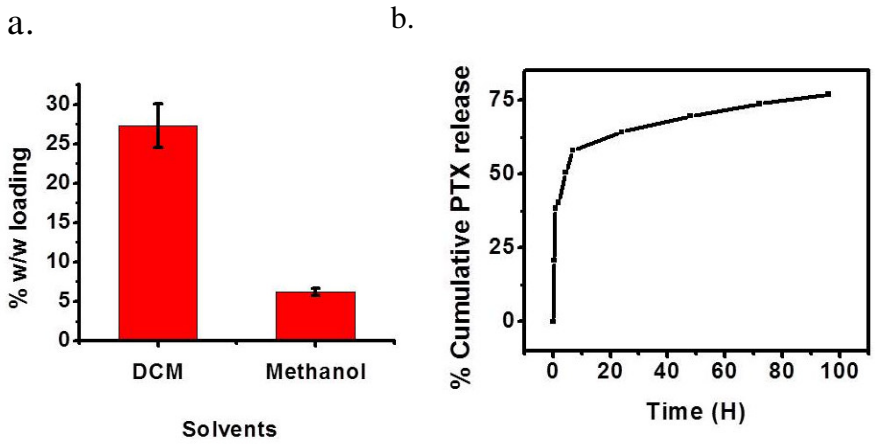

Figure 22. (a) Effect of solvent on PTX loading (b) In Vitro release of PTX. Loading and release of PTX was determined by HPLC.

4.4.2 PTX loading and *in vitro* release

In the next study, the FMSN were loaded with PTX by soaking in drug solution in DCM and methanol. We found that PTX loading in FMSN was dependent on solvent selection. We were able to achieve higher PTX loading (~24%) from DCM compared with negligible PTX loading from methanol (~4%) (Figure 22a). The difference is due to the lower polarity of DCM than methanol (dielectric constant 8.9 Vs 32.6, respectively) (Qian and Bogner, 2012). Charnay et al. and Fernandez-Nunez et al. studied range of organic solvents with different polarities for ibuprofen adsorption on silica matrix and observed that the more polar the solvent the greater the amount of ibuprofen remained in the solution and hence, less drug loading was observed (Charnay et al., 2004; Fernandez-Nunez et al., 2009; Qian and Bogner, 2012). These studies signified importance of solvent polarity for drug loading in MSN. Both studies concluded that this inverse relation of drug loading with solvent polarity is solely based on ibuprofen-solvent interactions. Preferential ibuprofen interactions with polar solvents prevent the drug from

binding to silica. In less polar solvents, greater amount of the drug was loaded into silica due to preferential interactions between ibuprofen and silica. We have also extensively studied effect of solvent polarity on drug loading and the results will be discussed in the next chapter.

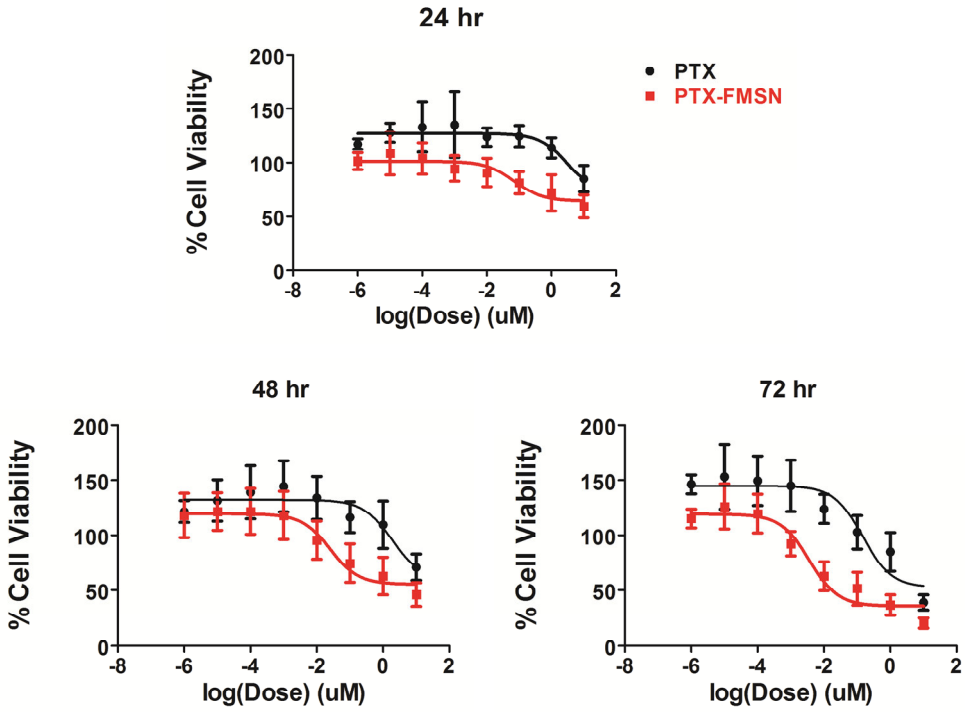

Figure 23. Time dependent toxicity of PTX delivered by FMSN. 24 h (top), 48 h (bottom left) and 72 h (bottom right). Cytotoxicity was measured by MTS assay. The results are shown as mean ± S.D. (n=3).

After drug loading, we further explored *in vitro* release of PTX in PBS containing 0.5% Tween 80 (Figure 22b). The results show that PTX release follows biphasic release behavior in which initial fast release is observed (0-10 h), which is then followed by controlled release for 4 days. It was observed that ~50% of PTX was released in the first 10 h, which we attributed to the release of PTX weakly adsorbed in the FMSN. Following the initial fast release, slower PTX release rate between 10 h and 4 days was attributed to the drugs hydrophobically interacting with the porous structure of silica. About 75% of PTX was released within 4 days. Similar biphasic

release behavior has been reported previously with silica nanoparticles, liposomes (Fatouros et al., 2001), micelles (Park et al., 2005) as well as PLGA matrices (Wang et al., 2002). Li et al. reported that release of docetaxel, a hydrophilic version of PTX, from silica nanorattles was biphasic, the 40% was released first within 10 h followed by sustained release for 5 days (Li et al., 2010).

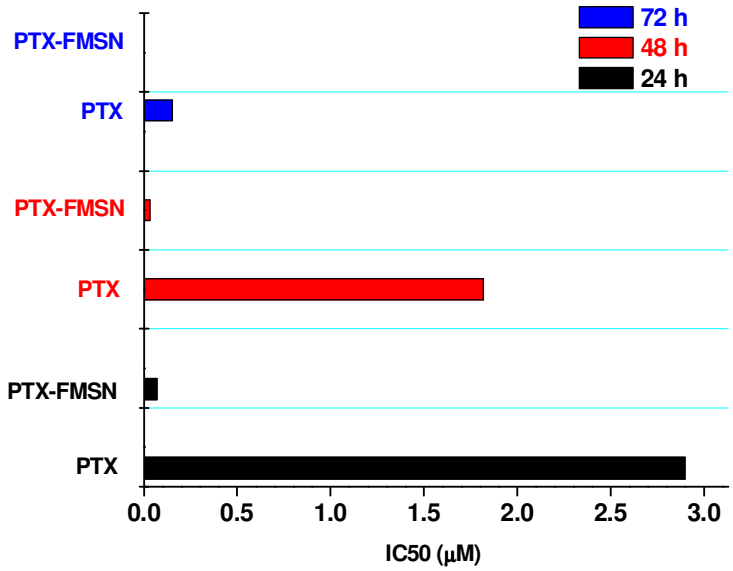

Figure 24. IC50 values of free PTX and PTX-FMSN determined by Prism software using non-linear regression involving log (inhibitor) Vs Response (three parameter) analysis of dose response inhibition.

4.4.3 Cytotoxicity study

Tumor cells develop drug resistance by overexpression of drug transporters such as P-glycoprotein (P-gp) (Milane et al., 2011b), altered expression of apoptosis associated BCL-2 protein (Manickam et al., 2008), tumor suppressor p53 protein (Martinez-Rivera and Siddik, 2012) and changes in the topoisomerase activity (Deffie et al., 1989). It is reported that dextran nanoparticles overcome P-gp mediated drug efflux by releasing and accumulating high concentration of drugs in the intracellular compartments (Susa et al., 2009). At the same time,

PTX encapsulation in PLGA nanoparticles is susceptible to P-gp efflux in drug resistant NCI/ADR-RES cells and sustained inhibition of P-gp is required to achieve high therapeutic efficiency (Chavanpatil et al., 2006). PLGA nanoparticles encapsulating PTX showed higher cell killing efficiency compared to free PTX in drug sensitive MCF-7 cells. In order to understand PTX cytotoxicity after encapsulation in FMSN, dose dependent MDA-MB-231 cell killing was evaluated and compared with free PTX by MTS assay (Figure 23 and Figure 24).

MDA-MB-231 cells were incubated with increasing concentration of free PTX and PTX-loaded FMSN for 6 h. After incubation, drug solutions were replaced with fresh RPMI medium and cytotoxicity was measured after 24 h, 48 h and 72 h. The goal of this study was to distinguish the cytotoxic effect of free PTX after cell uptake from PTX released intracellularly from FMSN The results showed that increase in the incubation time from 24 h to 72 h increased PTX toxicity in PTX-FMSN formulations as well as that of free PTX. It is worth noting that low drug doses can activate proapoptotic as well as prosurvival signaling cascades and that PTX at low concentrations enhances Bcl2 phosphorylation which leads to accumulation of survivin and X-chromosome linked inhibitor of apoptosis which leads to cell proliferation (Pushkarev et al., 2004). We have also observed that at low doses the total number of cells increased in case of free PTX compared to control cells which suggests the importance of dose selection during treatment. Within the tested range of concentrations, both free PTX and PTX-FMSN showed time dependent cell inhibition. Figure 24 shows that IC50 value of free PTX after 24 h (2.9 μM) was 41 times higher than that of PTX-FMSN (0.07 μM). After 48 h, the IC50 value decreased to 1.82 μM for free PTX and to 0.03 μM for PTX-FMSN. Similar trend was observed after 72 h with IC50 value of 0.15 μM for free PTX and 0.0004 μM for PTX-FMSN. This increased activity of PTX-FMSN at a later time points was attributed to the sustained intracellular release of PTX

from the FMSN. Similarly, Yang et al. reported that activity of PTX in A549 cells increased as the incubation time with chitosan-PLGA nanoparticles increased from 24 h to 72 h (Yang et al., 2009). We speculate that higher IC50 values for free PTX compared to PTX-loaded FMSN can be attributed to higher susceptibility of free PTX to drug efflux mechanisms.

a.

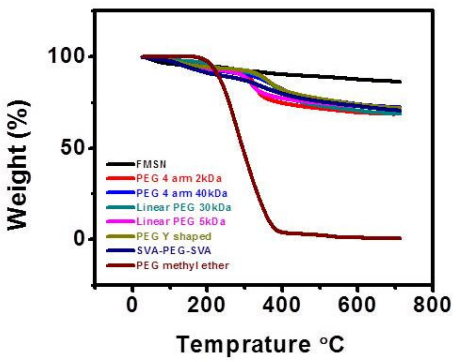

b.

Sample	w/w content (%)[a]	PEG density[b]
PEG 4 arm (2kDa)	17.6	0.4
PEG 4 arm (40kDa)	14.1	0.017
Linear PEG (5kDa)	17.7	0.028
Linear PEG (30kDa)	14.4	0.137
Y shaped PEG	14.6	0.017
SVA-PEG-SVA	15.8	0.15

Figure 25. Characterization of PEGylated FMSN. (a) TGA profile of FMSN and various PEGylated FMSN (b) Table 5 represents w/w content of PEGylated FMSN determined by TGA[a] and number of PEG molecules/nm^2 was calculated by formula present in the text[b].

4.4.4 Effect of PEGylation on cell uptake, colloidal stability and drug loading

Although FMSN encapsulation improved solubility of hydrophobic drugs and successfully delivered PTX to cancer cells, aggregation of nanoparticles still limited translation to preclinical *in vivo* application. The pharmacokinetic (PK) and biodistribution of nanoparticles are mainly governed by surface properties and hence, there is a need for a hydrophilic particle surface or surface coating for a successful intravenous administration (Hak et al., 2012). PEG is a

hydrophilic, non-toxic polymer which prevents nanoparticles aggregation by steric stabilization, shields overall charge of nanoparticles, prevents non-specific protein adsorption (opsonization), thereby delaying the removal of nanoparticles from the circulation by the ReticuloEndothelial System (RES) (Ryan et al., 2008).

To reduce aggregation of nanoparticles and to improve PK and biodistribution profile, we modified FMSN exterior surface by PEG polymers. Our goal was to develop PTX formulation with PEG-FMSN that will not only improve PK profile but also create a hydrophilic barrier for release of hydrophobic drug during blood circulation. We selected six PEG polymers: linear PEG (5kDa), linear PEG (30kDa), 4-arm PEG (2kDa), 4-arm PEG (40kDa), Y shaped like PEG and SVA-PEG-SVA (loop that forms PEG) based on molecular weight and structure. In a synthesis of PEG-FMSN, PEG-SVA (NHS ester) was reacted with primary amines on the surface of FMSN forming stable amide linkages. The content of PEG in PFMSN was quantitatively determined by TGA (Figure 25a). The first observed step in the weight loss in the range of 100-200 °C for all samples was due to the evaporation of water adsorbed in nanoparticles. The second step starting from 300°C was due to the loss of organic components of the studied sample. The results showed that FMSN were successfully modified with all selected PEGs and that 14-17% of PEG was present on FMSN surface.

Considering MSN as a perfect sphere and mesopores to be perfectly aligned as cylinders, PEG density was calculated at the silica outer surface using the following formula (Cauda et al., 2010):

$$D_{PEG}(molecule/nm^2) = N_A \frac{\rho \cdot \beta \cdot d \cdot 10^{-24}}{6MW\left[1-\frac{\rho \cdot V_p}{3}\right]}$$

Where,

D_{PEG} = Density of PEG chains (molecule / nm^2) on the exterior of MSN

ρ = Density of silica (g/cm^3)

β = Weight of PEG chains obtained by TGA data (mg/g)

d = Diameter of particles calculated from TEM images (nm)

N_A = Avogadro constant

MW = Molecular weight of PEG polymer (g/mol)

V_p = Pore volume obtained by nitrogen adsorption isotherm (cm^3/g)

10^{-24} = A factor added to convert m^2 to nm^2

The PEG density on FMSN was found to be 0.4, 0.02, 0.03, 0.14, 0.02 and 0.15 (molecules/nm^2) for 4-arm PEG (2kDa), 4-arm PEG (40kDa), linear PEG (30kDa), linear PEG (5kDa), Y shaped PEG and SVA-PEG-SVA respectively (Figure 25b). Cauda et al. reported that short chain PEG550 covered nanoparticles surface more efficiently compared to long chain PEG5000 polymer due to smaller steric hindrance (Cauda et al., 2010). In our case, we found that PEG 4-arm (40kDa), linear PEG (30kDa) and Y shaped PEG showed low PEG coverage compared to PEG 4-arm (2kDa), linear PEG (5 kDa) and SVA-PEG-SVA and these differences in the PEG density were attributed to the greater steric hindrance and coiling. The PEG density on nanoparticle surface has been found to modulate blood circulation time, non-specific cellular uptake as well as tumor targeting potential of nanoparticles (Hak et al., 2012). Studies have shown that at low PEG density, PEG chains are present in mushroom conformation while at high PEG density PEG chains transform to brush conformation (Hansen et al., 2003; Park et al., 2009c). At mushroom conformation, no lateral interaction between polymeric chains of adjacent particles occur confirming less coverage of nanoparticles surface. Polymer chains overlap with each other in case of brush conformation preventing aggregation of nanoparticles and providing

surface protection against opsonization. However, lateral interaction between polymeric chains induces chain stretching outward from nanoparticles surface, increasing overall size of surface coating layer with increasing PEG density (Hak et al., 2012). In our case, it was important to correlate PEG density to the thickness of hydrophilic layer as it may control release of hydrophobic drug during release studies.

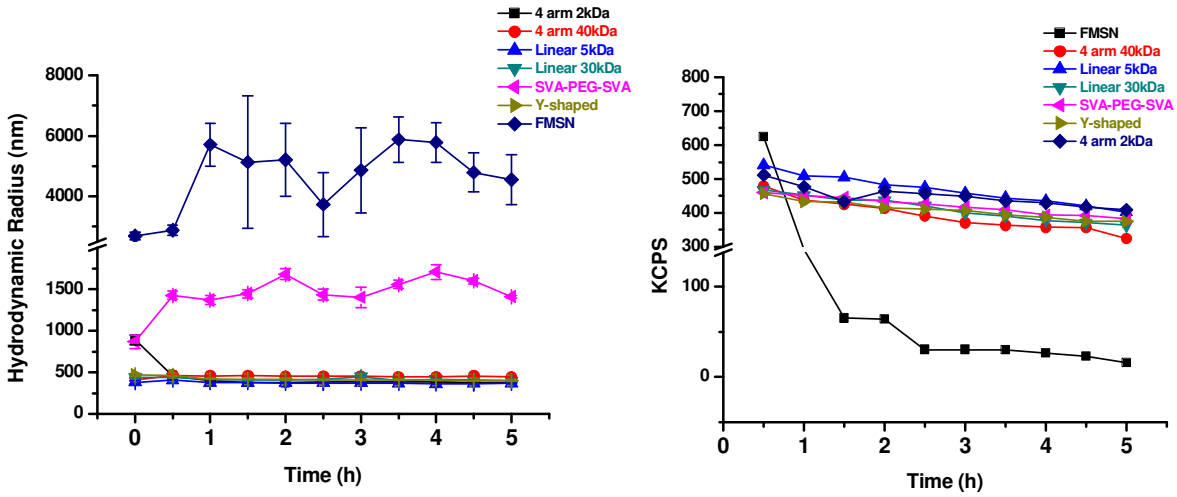

Figure 26. (a) Effect of PEG architecture on colloidal stability (b) Effect of PEG architecture on rate of sedimentation.

In order to investigate the effect of surface PEGylation on aggregation of FMSN, hydrodynamic size was measured over 5 hours by DLS in RPMI containing 10% serum (Figure 26a). The results showed that within the tested time, all PEG-FMSN were colloidally stable with particle sizes remaining below 500 nm. The only exception were FMSN coated with SVA-PEG-SVA, which were stabilized at larger hydrodynamic size (~1500 nm). We speculate that due to two reactive ester groups, the bifunctional SVA-PEG-SVA bridged adjacent particles during reaction, which resulted in covalent crosslinking. At the same time, unmodified FMSN aggregated rapidly giving particle sizes above ~4500 nm. This confirmed that covalent PEGylation of FMSN is important for improvement in the colloidal stability and potentially also

the related PK profile. Determination of sedimentation profile of nanoparticles is as important as the particle size measurement. Higher sedimentation is related to aggregation of nanoparticles which may hinder the circulation of nanoparticles and carries a risk of embolization (Kaufner et al., 2007). To investigate sedimentation of FMSN and P-FMSN, scattering intensity data were collected and plotted against time (Figure 26b). Change in the scattering intensity is dependent on the decrease in the molecular weight or a decrease in particle concentration due to their sedimentation. The results showed that unmodified FMSN aggregated and settled down at a higher sedimentation rate while all PEGylated FMSN were highly stable and hardly showed any sedimentation at the end of the 5 h study.

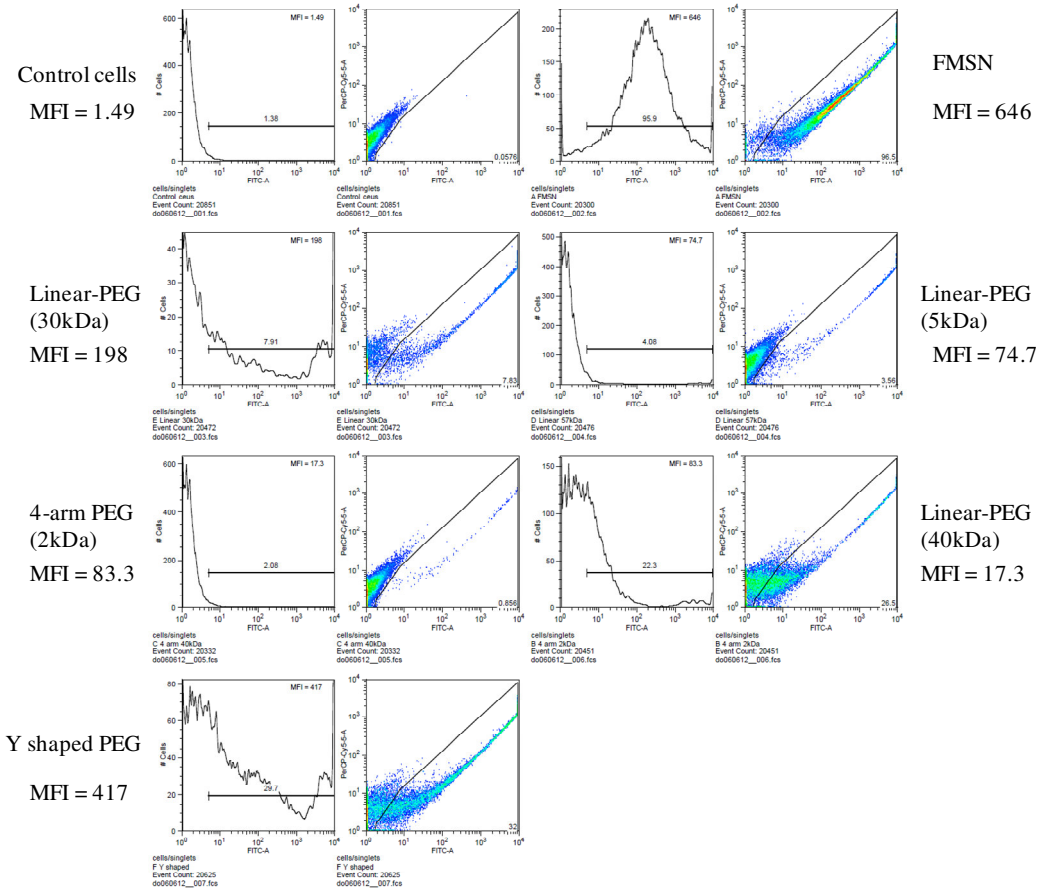

Figure 27. Effect of PEG architecture on MDA-MB-231 cell uptake determined by flow cytometry. MFI represents Mean Fluorescence Intensity.

Prolonged circulation time of nanoparticles is needed to enable extravasation at tumor sites via the enhanced permeation and retention (EPR) effect but after localization at pathophysiological site nanoparticles should deliver cargo efficiently to achieve higher therapeutic efficiency (Romberg et al., 2008). Most of the anti-cancer hydrophilic drugs, proteins as well as genes are not able to cross cell membrane and hence, nanoparticles encapsulation is required for intracellular delivery. However, polymeric surface coating interferes with the nanoparticle-cell interactions and limits nanoparticle uptake efficiency. It has been shown that PEGylation of nanoparticles decreased overall cell uptake due to loss of positive charge on nanoparticles (Romberg et al., 2008; Zhu et al., 2010). We investigated cell uptake of all PEG-FMSN formulations to identify suitable PEG architecture and molecular weight. To investigate the effect of PEG architecture on cell uptake, various PEG-FMSN were incubated with MDA-MB-231 cells for 3 h and cell uptake was determined by flow cytometry (Figure 27). The results showed that PEG architecture has significant effect on cell uptake as determined from mean fluorescence intensity (MFI) of FMSN. Cell uptake of unmodified FMSN was high while a decrease in the intensity was observed for all PEG modified FMSN. The uptake (MFI) was found to be 646, 83.3, 17.3, 74.7, 198, and 417 for FMSN, PEG 4 arm (2kDa), 4 arm (40kDa), linear PEG (5kDa), linear PEG (30kDa), and Y shaped PEG, respectively. Based on these results, we selected Y shaped PEG and linear PEG (30kDa) as suitable PEG candidates for *in vivo* studies.

In order to determine the effect of PEG coating on drug loading and release, PTX was loaded into various PEG-modified FMSN in DCM (Figure 28). The results showed that PTX loading is drastically reduced in the presence of PEG layer. In the studied conditions, PTX loading was found to be 14.5 w/w % for unmodified FMSN and between 2 to 5 w/w % for other studied PEG-modified FMSN. Such dramatic reduction in PTX loading was due to the blocking

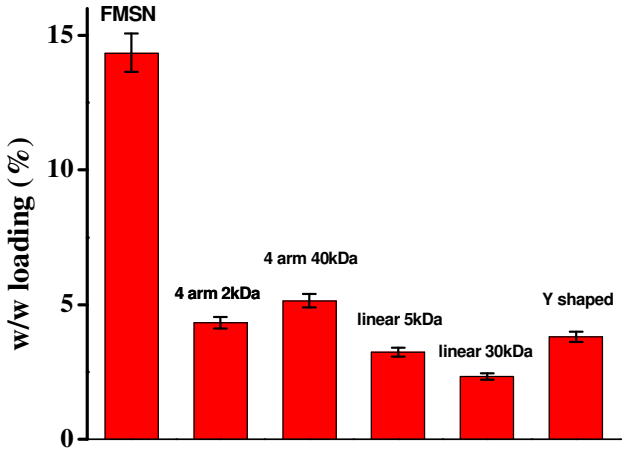

Figure 28. Effect of PEG architecture on PTX loading in dichloromethane. The PTX loading was determined by HPLC.

of entry to the porous structure of FMSN by PEG. In the previous chapter, we showed that PEGylation also decreased loading of hydrophilic drug MTX into PEG-MSNR. However, it has been reported that hydrophilic drug molecules such as doxorubicin can be loaded into pre-modified MSN with high drug loading of ~40% (Singh et al., 2011). Our study shows that PEGylation of FMSN reduces PTX loading and suggests that pre-modification of FMSN by PEG may not be a suitable approach for preparing colloidally stable MSN formulations with high loadings of hydrophobic drugs.

4.5 Conclusion

In this chapter, we have demonstrated that FMSN can solubilize hydrophobic drug PTX into porous nanoconfinement and can effectively deliver PTX to cancer cells in a time dependent manner. FMSN surface decoration with PEG improved colloidal stability of nanoparticles but decreased loading of PTX into the porous structure. This is a crucial finding for the development of MSN as systemic drug delivery systems.

CHAPTER 5

DEVELOPMENT OF MSN AS A COMBINATORIAL DELIVERY PLATFORM FOR HYDROPHILIC-HYDROPHOBIC AND HYDROPHOBIC-HYDROPHOBIC DRUG COMBINATIONS FOR CANCER THERAPY

5.1 Introduction

Combinations of chemotherapeutic agents offer a promising therapeutic approach for the treatment of multi-drug resistant tumors (Farokhzad and Langer, 2009; Lee and Nan, 2012). Various drug combinations are widely clinically used and investigated (Lee and Nan, 2012). However, there is a lack of optimal strategies for combining drugs with other emerging cancer therapies like gene therapy. Availability of suitable delivery system is one of the reasons for the limited use of such combination therapies. Nanotechnology is often implemented to deliver chemotherapeutic combinations. Amiji and co-workers formulated PTX and curcumin co-loaded nanoemulsion and observed that this combination was very effective in enhancing the cytotoxicity in wild type and resistant cells by promoting apoptosis (Ganta and Amiji, 2009). On the same note, it has been reported that combining photodynamic therapy (PDT) agent, methylene blue with doxorubicin-loaded PLGA nanoparticles successfully overcomes drug resistance and improves cytotoxicity in drug-resistant tumor cells (Khdair et al., 2009). Nevertheless, limited encapsulation of hydrophilic drugs impedes application of widely investigated polymeric nanoparticles in combining hydrophilic drugs with hydrophobic ones. Hydrophobic core of PLGA and PLA nanoparticles often restricts hydrophilic drug loading to ~4-5% w/w (Park et al., 2009b). In contrast, MSN hold promise for encapsulating hydrophilic

drugs with high drug loading, up to ~40% w/w, with enormous potential for delivery of hydrophilic-hydrophobic and hydrophobic-hydrophobic drug combinations (Liu et al., 2012; Rosenholm et al., 2010b; Singh et al., 2011).

Advantages of MSN for drug delivery include high drug loading capacity, compatibility with hydrophilic-hydrophobic drugs, amorphization of loaded drugs, high surface area, tunable pore size, and excellent biocompatibility (Qian and Bogner, 2011; Wani et al., 2012). Due to the high surface-to-volume ratio with pore size around 2-10 nm, these mesoporous silica biomaterials can hold small molecules in the cylindrical pores which have the large internal surface area. Excellent chemical and mechanical stability of MSN facilitates sequential adsorption of drug molecules and control over drug loading in MSN is possible by tuning drug-drug ratio (Liu et al., 2012; Rosenholm et al., 2010b). Drug molecules can be released in the later stage in a controlled as well as sustained manner, and release profile of drug molecules can be controlled by the choice of surface functionality, physicochemical properties of drugs and the dissolution rate of MSN (Chen et al., 2009a; Singh et al., 2011; Wani et al., 2012). Feasibility of loading drug molecules in the interior, porous nano-confinement and decorating MSN exterior surface with cationic polymers and lipids makes MSN an excellent platform in the drug-gene combinatorial delivery (Bhattarai et al., 2010). He and co-workers effectively utilized MSN for simultaneous delivery of doxorubicin and BCl-2 siRNA to multidrug resistant A2780/AD human ovarian cancer cells. They observed that such co-delivery effectively silenced Bcl-2 gene with substantial improvement in the anticancer activity of doxorubicin (Chen et al., 2009a). Such accumulating results proved that MSN is also a versatile system for combinatorial drug-drug and drug-gene delivery.

In this chapter, we focused on systematic optimization of co-loading of hydrophilic-hydrophobic and hydrophobic-hydrophobic drug combinations, effect of co-loading on crystallization and effect of co-loading on *in vitro* release profile. We also report effect of co-loading and co-mixing of anti-cancer drugs by determining cytotoxicity of breast cancer cells to evaluate advantage of co-loading of drugs over co-mixing. We have selected MTX as a hydrophilic drug and curcumin (CRM), PTX and 17-N-Allylamino-17-Demethoxygeldanamycin (17-AAG) as hydrophobic drugs based on first line drug combinations widely used in the breast cancer treatment.

5.2 Materials

Tetraethylorthosilicate (TEOS), 3-aminopropyltriethoxysilane (APTES), Mercaptopropyltrimethoxysilane (MPTMS), *N*-cetyltrimethylammonium bromide (CTAB), Fluorescein isothiocynate (FITC), hydrochloric acid, sulfuric acid and CRM were purchased from Sigma-Aldrich (St. Louis, MO). MTX and PTX were purchased from SantaCruz Biotechnology Inc. (Santa Cruz, CA). 17-AAG was purchased from LC laboratories (Woburn, MA). Roswell Park Memorial Institute medium (RPMI), phosphate buffered saline (PBS), fetal bovine serum (FBS) were purchased from Invitrogen. Cell titer 96 Aqueous One solution cell proliferation assay (MTS reagent) was purchased from Promega. HPLC grade dichloromethane (DCM) and methanol were purchased from Sigma Aldrich. Distilled water was used in the all experiments.

5.3 Methods

5.3.1 Synthesis of FITC functionalized mesoporous silica nanoparticles (FMSN)

FMSN was synthesized in three parts: (a) Synthesis of MSN (b) Preparation of fluorescein-APTMS conjugate and grafting of conjugate to the synthesized MSN (c) removal of

CTAB from FMSN as described in the chapter 4 (section 4.3.1). FMSN was used for loading of PTX/17-AAG combination based on simultaneous co-loading approach; however, thiol-functionalized MSN (SH-MSN) was used for MTX and CRM combination based on sequential co-loading strategy.

5.3.2 Characterization of FMSN

FMSN were characterized by TEM and micromeritic porosimeter for the particle size and surface area measurement respectively by a method reported previously in the Chapter 2 (Section 2.3.2). Quantitative determination of free amines after FITC conjugation, which may be required for further modification was measured by colorometric method reported previously (Bhattarai et al., 2010) and as described in the Chapter 4 (Section 4.3.2).

5.3.3 Drug loading

5.3.3.1 Sequential loading of hydrophilic-hydrophobic drug combinations

In a typical sequential drug loading experiment, known amount of MSN was dispersed in 1 mL of PBS and the mixture was sonicated for 10 min to disperse particles. MTX solution was added dropwise to MSN suspension and mixture was kept stirring overnight. After stirring, drug-loaded particles were centrifuged at 14,500 rpm for 10 min. Drug supernatant was removed and particles were vacuum dried overnight. For hydrophobic drug loading, 5 mg of CRM was dissolved in 2 mL of DCM, and 10 mg of MTX-loaded MSN were dispersed in the CRM solution followed by sonication for 30 min. MSN suspension mixture was kept stirring for 8 h. After stirring CRM/MTX-loaded MSN was isolated by centrifugation and vacuum drying as described above. Drug loading was determined by dispersing 1 mg of CRM/MTX loaded MSN in 2 mL ethanol. Particles were kept shaking overnight to extract CRM and MTX. Concentration of CRM and MTX was determined by UV-Vis spectroscopy. Drug loading was also confirmed

by thermogravimetric analysis (TGA) under air (Perkin-Elmer Pyris 1, 10 °C/min), subtracting the mass lost during analysis of empty SH-MSN particles. Similarly, individual drug loaded particles (MTX loaded MSN and CRM loaded MSN) were obtained according to the same procedure described above.

5.3.3.2 Simultaneous loading of hydrophobic-hydrophobic drug combinations

Simultaneous loading approach was utilized towards co-loading of PTX and 17-AAG instead of sequential loading due to the solubility of both drugs in the suitable solvent. In a typical loading experiment, known amount of FMSN was dispersed in 500 µL of DCM and known amount of PTX and 17-AAG was dissolved in 1 mL of DCM. Drug solution was added dropwise to FMSN suspension followed by sonication for 10 min. Particles were stirred overnight to achieve adsorption of drug molecules into the silica matrix. Drug loaded particles were recovered by centrifugation followed by vacuum drying as described above. Loaded drugs were extracted in ethanol by dispersing known amount of PTX/17-AAG loaded MSN followed by centrifugation. Drug concentrations in the supernatant were determined by HPLC method developed previously. Similarly, individual drug loaded particles (PTX loaded FMSN and 17-AAG loaded FMSN) were obtained according to the procedure described above.

5.3.4 Characterization of the physical state of loaded drugs

Crystalline state of MTX and CRM was determined by PXRD analysis as described previously in the Chapter 2 (Section 2.3.6).The physical state of PTX and CRM was determined by DSC as described previously in the Chapter 2 (Section 2.3.6).

5.3.5 *In vitro* drug release

Effect of sequential loading of CRM in MTX/MSN on MTX release was evaluated by *in vitro* release study protocol described in Chapter 2 (Section 2.3.5). In a typical experiment,

known amount of MTX/MSN and CRM/MTX-MSN were dispersed in 2 mL of release medium (sodium acetate 0.2M, pH 4.5 and PBS, 0.2M, pH 7.4) and release of content of MTX in the supernatant was determined by UV-Vis spectroscopy at 658 nm.

5.3.7 HPLC analysis

The HPLC system used consists of a C-18 column (4.6 mm × 25 cm) with 5 μm packing (Beckmann Instruments, Fullerton, CA). The mobile phase consisted of a mixture of water and acetonitrile in the ratio of 35:65 (v/v), and was delivered at a flow rate of 1 ml/min. A 5 μL volume of drug sample (PTX or 17-AAG or combination of these drugs) was injected using an autoinjector (Model 508, Beckmann Instruments), and PTX levels were quantified by UV detection at 227 nm and 17-AAG levels were quantified at 254 nm (System Gold 168 detector). A standard curve for PTX and 17-AAG was prepared in ethanol and drug loading was determined based on the standard equation.

5.3.8 Cell Culture

Triple negative MDA-MB-231 human breast cancer cell line was a kind gift from Dr. Jing Li, Karmanos Cancer Institute, Detroit MI. The cells were maintained in Hyclone's RPMI medium supplemented with 2.05 mM L-glutamine, 10% FBS and 1% penicillin. Cells were maintained in an incubator at 37 °C with 5% CO_2.

5.3.9 Cell viability study

The CellTiter 96® Aqueous Cell Proliferation Assay determined cytotoxicity of MTX, CRM, PTX and 17-AAG and their loaded MSN counterparts as described previously in the chapter 2 (Section 2.3.9) and 4 (Section 4.3.9). In a typical experiment, five thousand MDA-MB-231 cells were seeded in a 96-well plate. One day after reaching confluence, the cytotoxicity of

drugs and drugs loaded MSN formulations was evaluated by incubating the cells in 100 µL of RPMI/FBS with increasing concentrations. Cells were incubated for 72 h and medium containing drug and drug-loaded particles were replaced with MTS solution (100 µL of RPMI and 20 µL of MTS reagent per well). The cells were incubated for 3 h at 37 °C. The absorbance of each well was then measured at 490 nm to determine cell viability. The results are expressed as mean % cell viability relative to untreated cells ± S.D. IC50 values were determined by Prism software using non-linear regression involving log (inhibitor) vs. response (three parameters) analysis of dose-response inhibition.

5.4 Results and discussion

The main goal of this study was to investigate the feasibility of MSN in the development of universal multi-drug delivery system for cancer therapy. In order to develop MSN as a versatile and robust drug delivery platform, we investigated simultaneous and sequential loading strategies for combinations of hydrophobic and hydrophilic anticancer drugs.

5.4.1 Synthesis and characterization of MSN

We have selected SH-MSN for MTX and CRM sequential co-loading and FMSN for PTX and 17-AAG simultaneous co-loading. The selection of SH-MSN for hydrophilic-hydrophobic combination was based on the results in Chapter 2 where we showed that thiol functionalization is more suitable for MTX loading compared to mixed thiol/amine and amine functionalized MSN. In addition, inherent fluorescence of MTX negates need for the additional fluorescent moiety from the imaging and diagnostic point of view. However, for hydrophobic drugs combination, FMSN was utilized for two reasons: (1) FITC is a hydrophobic fluorescent marker, which helps in the imaging and (2) FITC decreases overall hydrophilicity of MSN (Yang et al., 2007), which may help in the loading of hydrophobic drugs through hydrophobic

interactions in addition to hydrogen bonding or polar interactions (Liu et al., 2012). The results and discussion about the synthesis and characterization of MSN and FMSN are described in the Chapter 2 (Section 2.4.1) and Chapter 4 (Section 4.4), respectively.

5.4.2 Drug loading

5.4.2.1 Sequential loading

During MTX/CRM co-loading, MTX was first dissolved in the aqueous medium. However, care was taken in selecting pH of the loading medium as we have previously reported that acidic pH is not suitable for MTX loading due to ionization of MTX below pH 5.3 (Wani et al., 2012). The loading of MTX was controlled by the electrostatic interaction between anionic MSN matrix and cationic MTX at pH 7.4. Detailed description of the MTX loading behavior in the MSN can be found in Chapter 2 (Section 2.5). The results showed that the adsorbed amounts of MTX and CRM were 176.4 ± 3.4 µg/mg and 76.3 ± 4.7 µg/mg, respectively. TGA analysis also confirmed the co-loading of MTX and CRM and found it to be 18% and 7%, respectively (Figure 29 left).

The selection of DCM as a hydrophobic drug loading solvent was based on (i) the insolubility of MTX in DCM and (ii) higher loading of CRM in DCM compared to other organic solvents (data not shown). This difference in the solubility pattern of MTX leads us to employ

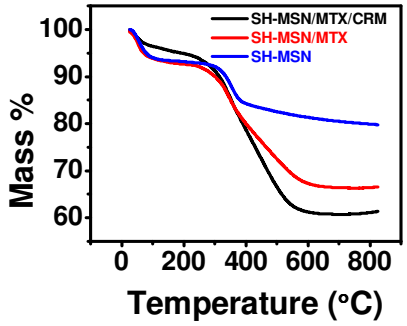

	% w/w loading		
	MTX	CRM	Total
MTX-MSN	18.3 ± 3.2	N.A.	18.3 ± 3.2
CRM-MSN	N.A.	15.4 ± 1.3	15.4 ± 1.3
MTX/CRM-MSN	14.7 ± 4.2	6.8 ± 1.5	21.5 ± 5.7

Figure 29. Sequential co-loading of MTX and CRM in SH-MSN. MTX and CRM loading was determined by (left) TGA and (right) UV-Vis spectroscopy. The results shown are mean ± S.D. (n=3).

sequential co-loading approach for hydrophilic-hydrophobic drugs. In fact, we have selected sequential loading approach due to the negligible adsorption from the simultaneous loading of MTX/CRM dissolved in organic solvents and co-solvents (data not shown). Instead of DCM, we have also tried other organic solvents such as ethanol, methanol and acetonitrile for CRM sequential loading but MTX was easily extracted during loading procedure in the loading solvent, negating advantage of high drug loading in MSN for hydrophilic drugs. We speculate that the interaction between MTX and used organic solvents was higher than the interaction MTX-MSN and MSN-organic solvent, which resulted in the higher solubility of MTX in the corresponding organic solvent. However, DCM provided us an excellent solvent for sequential hydrophilic-hydrophobic co-loading. We speculate that after MTX loading, it adsorbs in a monolayer fashion in the porous nano-confinement (Liu et al., 2012; Qian and Bogner, 2011)

DCM Acetone $CHCl_3$ Ethanol DMSO

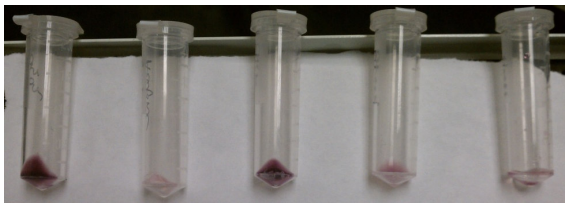

Solvent	Dielectric constant	Dipole Moment	w/w Loading (%)
DCM	8.9	1.18	13.1 ± 1.4
$CHCl_3$	4.8	1.01	11.1 ± 0.3
Acetone	20.7	2.88	ND
Ethanol	24.5	1.69	ND
DMSO	46.7	3.96	ND
water	78.5	1.85	NA

Figure 30. Effect of solvent polarity on 17-AAG loading. (top) Representation of FMSN after 17-AAG loading. Red color signifies 17-AAG loading. (bottom) Effect of polarity of solvent denoted by the dielectric constant and its effect on 17-AAG loading. (NA – Not applicable as 17-AAG was not soluble in water; ND – Not determined)

and CRM was loaded on top of the monolayers. Electrostatic interactions played an important role in the MTX loading, however, we speculate that hydrophobic moieties of adsorbed MTX molecule played a significant role in the adsorption of CRM into MSN in addition to hydrogen bonding and polar interactions. In addition to MTX/CRM co-loaded MSN, MTX and CRM was separately loaded in the MSN and at the studied condition, w/w loading was found to be ~18% and ~15% for MTX and CRM, respectively (Figure 29 right).

5.4.2.1 Simultaneous loading

Selection of solvent is very important for simultaneous co-loading, which requires desirable solubility of both drugs in the loading solvent. Our previous studies confirmed that DCM is a suitable solvent for PTX loading (Chapter 4, Section 4.3.5) and we needed to confirm 17-AAG loading in DCM. To investigate how selection of solvent affects loading efficiency, we studied the effect of polarity of solvents on 17-AAG loading (Figure 30). Based on previous studies, we selected range of solvents including DMSO, ethanol, acetone, chloroform and DCM with differences in the polarity. We found that polarity has distinct effect on 17-AAG loading, with increase in the polarity decreasing 17-AAG loading. Our results suggest that in studied conditions chlorinated solvents such as DCM and chloroform gave highest loading between ~11-13% compared to other studied solvents. This result ratifies that DCM is a suitable solvent for simultaneous co-loading of PTX and 17-AAG. Silanol groups are polar and have higher interaction with the polar solvent molecules compared to less polar solvents (Qian and Bogner, 2011). This suggests that increase in the partitioning of drug molecules into the silica matrix may occur from less polar solvents compared to high polar ones. The Figure 31 (top) shows increase in the 17-AAG loading with decrease in the polarity of solvent suggested by the darker red color of 17-AAG.

Table 6. Effect of feeding amount of 17-AAG on overall w/w loading. Drug loading was determined by HPLC.

MSN:AAG (w:w)	Amt of AAG loaded (ug)/mg of MSN	w/w loading (%)
1:0.1	26.1	2.5
1:1	43.5	4.1
1:2	136.7	12.1
1:4	237.9	19.2
1:10	432.2	30.2

After the confirmation of DCM as a common solvent, we were interested in determining the loading potential of FMSN used in the study. To investigate this, we increased the feeding amount of 17-AAG during loading experiment from 0.1 mg to 10 mg and increase in the loading capacity with increase in the MSN:17-AAG feeding ratio was observed (Table 6). In these conditions, we were able to load 432.2 µg of 17-AAG per mg of FMSN. Li and co-workers have formulated docetaxel formulation based on silica nanorattles and successfully achieved 480 µg Docetaxel/ 1 mg MSN, similar to our case. (Li et al., 2010).

Table 7. Simultaneous co-loading of PTX and 17-AAG in FMSN. Loading of PTX and 17-AAG was determined by HPLC. (Mean ± S.D. n=3)

Formulation	PTX loading (%)	17-AAG loading (%)	Total Loading (%)
PTX-FMSN	11.2 ± 0.3	NA	11.2 ± 0.3
17-AAG-FMSN	NA	12.2 ± 1.7	12.2 ± 1.7
17-AAG/PTX-FMSN	7.9 ± 0.4	6.2 ± 2.1	14.1 ± 2.5

In order to achieve simultaneous co-loading of PTX and 17-AAG, respective drugs were dissolved in DCM and adsorption of drugs into silica matrix was observed. Drug loading study showed that total 14% of drugs were loaded in the studied conditions and the particles contained 7.9% of PTX and 6.2% of 17-AAG (Table 7). At the same time, we also loaded individual drugs (PTX and 17-AAG) into FMSN under similar conditions and drug loading was found to be 11.2 ± 0.3 and 12.2 ± 1.7% for PTX and 17-AAG, respectively. Individual feeding amount of PTX and 17-AAG was similar to the feeding amount of both drugs in the co-loading experiment. We were interested in determining the effect of co-loading in comparison with individual drug loading in terms of overall drug loading capacity. Kwon and co-workers studied encapsulation of multiple drugs (PTX, 17-AAG and rapamycin) in PEG-*b*-PLA micelles and observed that co-loading of these 3 drugs increases loading capacity up to ~40% compared to ~11%, 13% and 6% of PTX, 17-AAG and rapamycin when individually loaded (Shin et al., 2011). The authors proposed that such increase in the loading capacity of PEG-*b*-PLA micelles was presumably due to intermolecular interaction among drugs in the micellar core. In our case, we didn't observe increase in the total loading of multiple drugs.

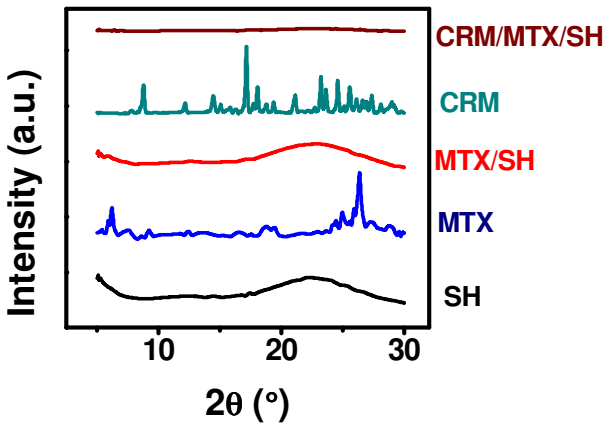

Figure 31. PXRD analysis of sequentially co-loaded CRM and MTX in MSN.

5.4.3 Characterization of drug-loaded particles

In order to determine physical state of co-loaded drug molecules in the MSN, the particles were characterized by PXRD and DSC. We previously reported that after MTX loading into MSN, the drug was present in the amorphous form (Chapter 2, Section 2.4.3). Our XRD results suggest that after sequential loading of MTX and CRM, CRM was also present in the amorphous form, confirming strong crystalline-to-amorphous transformation of molecules in the porous nano-confinement of MSN (Figure 32). The presence of strong Bragg's crystalline peaks of free CRM confirmed its crystalline form, however, such crystallization of CRM was not observed after loading into MTX-MSN.

MSN with simultaneous co-loading of PTX and 17-AAG were characterized by DSC to investigate the physical state of the drug molecules. Figure 32 shows DSC analysis of PTX, 17-AAG and the drug-loaded particles. The results show that melting point (Tm) of PTX (155.3°C), a crystalline signature, disappeared after loading into FMSN. Similarly, Tm of 17-AAG (174.1°C) was not present in the 17-AAG/FMSN formulation. We have also studied melting behavior of physical mixture of PTX and 17-AAG, and found two Tm at 146.4°C and 165.3°C for PTX and 17-AAG, respectively. After simultaneous co-loading of PTX and 17-AAG into FMSN, similar strong crystalline-to-amorphous transformation was observed without any signs of crystallinity of neither of the drugs. As reported in Chapter 2, strong Tm at 157°C from FMSN was assigned to the remaining CTAB in the particles (Section 2.4.3 and 2.5). Our preliminary study confirmed that melting point of CTAB is 171-173°C (data not shown). Decrease in the melting point from 172 to 157°C was attributed to the melting point depression, a classic phenomenon of mesoporous materials, in the porous structure as reported by the Gibbs-Thomson

Equation (Ha et al., 2009; Wani et al., 2012). Based on these observations, we assign that melting points at 183°C, 177°C and 186°C to residual CTAB present in the 17-AAG/FMSN, PTX/FMSN and 17-AAG/PTX-FMSN respectively. We believe that these variations in the Tm of CTAB were observed due to multi-steps loading process and the presence of drug molecules in the nano-confinement of particles; however, this hypothesis requires further support. For the first time, we have showed amorphization of two different molecules (hydrophilic-hydrophobic or hydrophobic-hydrophobic) in the porous silica structure suggesting potential of MSN in combinatorial drug delivery for the cancer treatment.

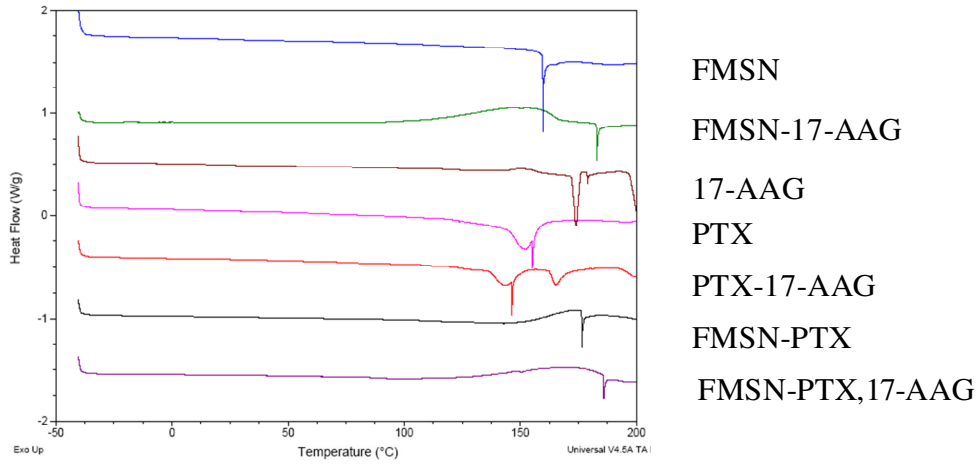

Figure 32. DSC of free PTX and 17-AAG and drug loaded FMSN counterparts

5.4.4 *In vitro* release: Effect of co-loading

In order to understand the effect of sequential loading of CRM on MTX release, time dependent *in vitro* release study was conducted in the presence of 0.2M sodium acetate pH 4.5 and 0.2M PBS pH 7.4. *In vitro* release profile of MTX is shown in the Figure 33. The results showed that MTX release from MSN containing both MTX and CRM had similar release profile as when only MTX was loaded in MSN (Section 2.4.4 and 2.5). Higher release was again

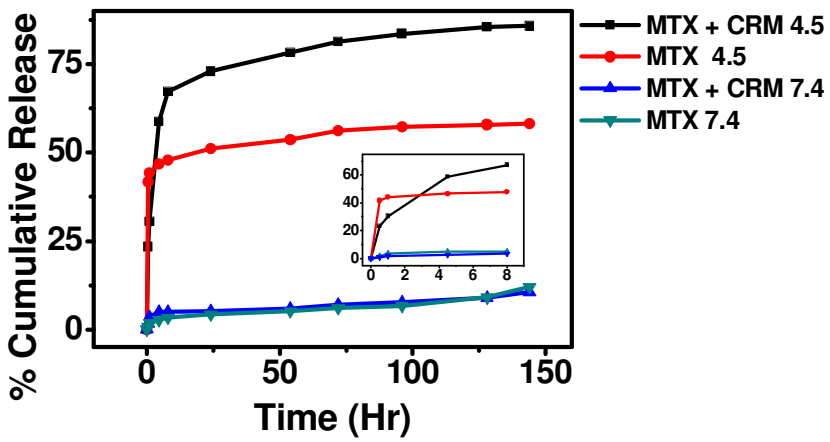

Figure 33. Effect of CRM co-loading on release of MTX. Sodium acetate (0.2M, pH 4.5) and PBS (0.2M, pH 7.4) was used for the release studies and concentration of MTX in the supernatant was determined by UV-Vis spectroscopy at 658 nm. (Inset: Initial rate of MTX in presence of CRM)

observed in acidic pH (~43% MTX at pH 4.5 in the first 2 h) and minimal release was observed at pH 7.4 (~4% MTX in the first 2 h). Interestingly, the presence of CRM in the co-loaded particles only affected the initial rate of MTX release (inset Figure 33). It was observed that ~43% of MTX was released at pH 4.5 during first 2 h in the absence of CRM; however, ~23% of MTX release was observed in presence of CRM. These results are in accordance with the study conducted by He and co-workers who observed initial decrease in the rate of doxorubicin release after PTX loading into MSN (Liu et al., 2012). Interestingly, the opposite effect of CRM on the overall release of MTX was observed at pH 4.5. The particles released ~85% of MTX in the presence of CRM vs. ~63% in the absence of CRM. Only a minimal effect of CRM co-loading was observed on MTX release at pH 7.4. Due to the poor aqueous solubility of CRM, surfactants such as tween 80 are normally used to achieve desirable water solubility required for conducting drug release experiments (Shahani and Panyam, 2011). In general, 10-15% of Tween 80 is required to achieve sink condition (Shahani et al., 2010). Because the presence of such high

amount of Tween 80 affected the pH dependance of MTX release, we could only investigate MTX release.

Drug release data can be fitted to several different kinetic models: zero-order, first-order, Hixson-Crowell, Higuchi, or Korsmeyer-Peppas models (Costa and Sousa Lobo, 2001; Huang and Brazel, 2001; Korsmeyer et al., 1983). The zero-order release describes systems where drug release rate is independent of its concentration. The first-order rate systems are concentration dependent. The Hixon-Crowell model is useful in systems where there is a change in the surface area and diameter of the drug delivery system, with progressive dissolution of the formulation as a function of time (Costa and Sousa Lobo, 2001). The Higuchi model is based on Fickian diffusion and emphasizes the release of drugs from an insoluble matrix as a square root of a time-dependent process (Costa and Sousa Lobo, 2001). The Kormeyer-Peppas model represents a comprehensive approach to describe and explain the kinetics of drug release from hydrophilic matrices (Korsmeyer et al., 1983). This model is expected to be valid up-to ~ 60% of drug release and release data should be restricted to that range. Based on the well-known dissolution

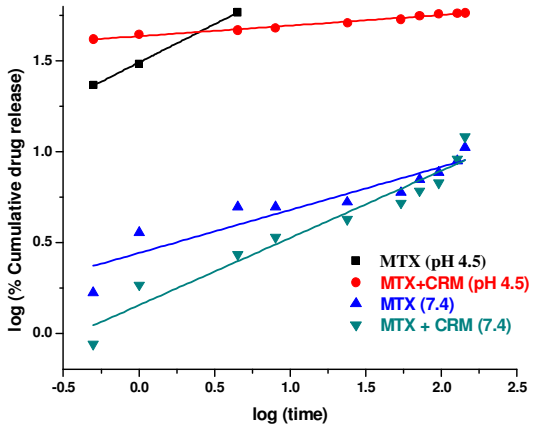

	Korsmeyer-Peppas model	Diffusional exponent (n)
MTX pH 4.5)	0.99	0.42
MTX + CRM (pH 4.5)	0.98	0.06
MTX (pH 7.4)	0.85	0.23
MTX+CRM (pH 7.4)	0.94	0.37

Figure 34. The Koresmeyer-Peppas plots. The diffusion exponent (n) determines the mechanism of drug release. $n < 0.45$ represents simple Fickian diffusion, $0.45 < n < 0.89$ represents non-Fickian diffusion.

profile of hydrophilic MSN, we selected Korsmeyer-Peppas model to understand MTX release kinetics from the silica matrix. The same approach has been reported previously in case of drug release from MSN (Liu et al., 2012). The Korsmeyer-Peppas equation is as follows:

$$\frac{M_t}{M_\infty} = kt^n$$

Where, M_t and M_∞ are the cumulative mass of drug released at a time t and infinite time, respectively; k is the kinetic constant of the drug-carrier system; and n is an exponent that characterizes the mechanism of drug release. The Korsmeyer-Peppas plots for our data are shown in Figure 34. The results indicate that up to 60% release, MTX release at pH 4.5 could be fitted into the Korsmeyer-Peppas model with good linearity and exponent n was lower than 0.45. The MTX release data at pH 7.4 could not be fitted as well with R^2 = 0.85 and 0.94 in case of release from MTX-MSN and from MTX+CRM-MSN, respectively. According to the Korsmeyer-Peppas model, the diffusional exponent (n) less than 0.45 corresponds to a simple diffusion-controlled Fickian process that involves diffusion of solvent molecules into the pores of MSN to dissolve drug molecules and the diffusion of the dissolved drug out of the mesopores. We propose that lower solubility of MTX at pH 7.4 results in the decrease of the drug diffusion out of MSN pores, which negatively affects the linearity of the fit.

It has been reported that MSN undergoes dissolution as a function of time while keeping the initial geometrical form unchanged (Bhattarai et al., 2010; Rosenholm et al., 2010b). To support this notion mathematically, we investigated the use of Hixon-Crowell model for our drug release data. This model assumes unchanged geometrical shape but a decrease in the surface area and diameter of the matrix over time. This model also assumes that the release rate is limited by the drug particles dissolution rate and not by the diffusion of drug molecules through the matrix (Costa and Sousa Lobo, 2001). The Hixon-Crowell equation is as follows:

$$M_o^{\frac{1}{3}} - M_t^{\frac{1}{3}} = K_{hc}t$$

Where, $M_o^{\frac{1}{3}}$ and $M_t^{\frac{1}{3}}$ indicate the initial amount of drug and cumulative amount of drug release at time t respectively; K_{hc} is a Hixon-Crowell release constant and *t* is time in hours. Our results indicate that MTX release from MTX-MSN and MTX+CRM-MSN at pH 4.5 did not fit well (R^2 = 0.82 and 0.51, respectively) confirming that the release of MTX from MSN is a diffusional process. It is well known that the release of hydrophilic drugs incorporated in matrix is a diffusion controlled process while for poorly soluble drugs, the erosion of the matrix is the main controlling element of the release (Costa and Sousa Lobo, 2001; Huang and Brazel, 2001).

The *in vitro* release profile of simultaneously co-loaded PTX/17-AAG-FMSN was not conducted due to the previously described practical limitations associated with the aqueous solubility of PTX and 17-AAG.

5.4.5 *In vitro* cytotoxicity

Various combinations of anti-cancer drugs have been clinically proven to give excellent tumor regression. It is important to understand whether combination therapies can benefit from drug delivery using nanoparticles (Lee and Nan, 2012). It may be possible that two drugs with clinically established synergistic effect without nanoparticles formulation will change the activity profile after encapsulation in nanoparticles. In such scenario, screening of such combinations using nanoparticles is a need of the hour and keeping this in mind, we investigated the *in vitro* cell viability study of FMSN loaded with PTX/17-AAG combination. Our goal was to answer the basic question of combinatorial drug delivery: What is the benefit of co-loading two drugs in nanoparticles over co-mixing of individually loaded nanoparticles? This fundamental question remains under-investigated in the field of combinatorial drug delivery.

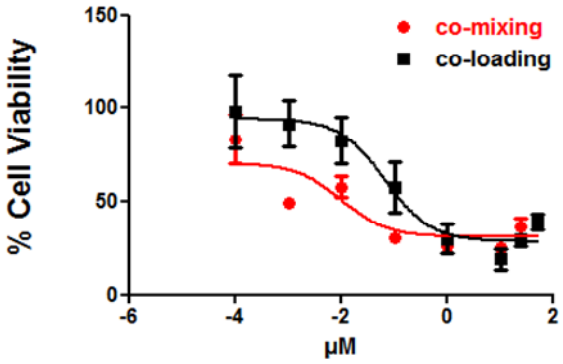

Formulation	IC50 (nM)
PTX solution	70 ± 3.4
17AAG solution	19.7 ± 4.2
PTX/17-AAG solution	44.5 ± 5.7
PTX/FMSN	17 ± 2.3
17-AAG/FMSN	33.4 ± 5.1
Co-loaded PTX/17-AAG/FMSN	68 ± 2.7
Co-mixing of PTX/FMSN & 17-AAG/FMSN	11 ± 6.3

Figure 35. Effect of co-loading and co-mixing of PTX and 17-AAG formulations on MDA-MB-231 cell viability. The results shown are mean ± S.D. (n=3)

As shown in Figure 35, IC50 values of free drugs PTX and 17-AAG in MDA-MB-231 human breast cancer cells were 70 ± 3.4 and 19.7 ± 4.2 nM, respectively. These results agree well with previously reported values (Roforth and Tan, 2008; Turturro et al., 2007). For PTX/17-AAG drug combination, the IC50 was found to be 18.5 ± 5.7 nM. However, IC50 values of PTX and 17-AAG loaded in the FMSN were found to be 17 ± 2.3 and 33.4 ± 5.1 nM, respectively. Interestingly, IC50 values for co-loaded and co-mixed PTX/17-AAG formulations were 68 ± 2.7 and 11 ± 6.3 nM, respectively. This suggests that co-mixing of PTX/FMSN and 17-AAG/FMSN is more effective than co-loading of both drugs in the same particle. Our results are in accordance with findings of Kwon and co-workers who studied anti-cancer activity of 2-in-1 combination of PTX and 17-AAG in PEG-b-PLA micelles and found that IC50 value of micellar formulation of drug combos (118 ± 1.8 nM) was higher compared to a mixture of free drugs (30 ± 4 nm) (Shin et al., 2011). On the other hand, Sasikheran and co-workers designed nanocells comprised of a nanoparticle within PEGylated-lipid envelope in which the outer lipid layer first released anti-angiogenesis agent which was then followed by a release of a chemotherapeutic agent from the nanoparticle (Sengupta et al., 2005). The authors evaluated the effect of physical

mixing of combretastatin A4 and doxorubicin over co-loading of these drugs and found that this combination was more effective in the co-loaded form compared to the physical mixture. They also reported that such temporal release of two drugs within tumor resulted in improved therapeutic index with reduced toxicity. These accumulating results suggest that there is a need to develop and optimize such combinations based on nanoparticles to treat tumor progression. The results also show that benefits of drug co-delivery using nanoparticles are strongly dependent on the specific drug combinations and disease indications.

5.5 Conclusion

In summary, we have developed a strategy to co-load hydrophilic-hydrophobic and hydrophobic-hydrophobic drug combinations in MSN. We suggest that MSN can serve as a universal delivery platform for rapid screening of potential benefits of co-delivery of a broad range of drug-drug combinations. MTX/CRM and PTX/17-AAG combinations were successfully co-loaded into MSN using either sequential or simultaneous drug loading strategy. Drug loading was found to be more than 200 μg/mg and 140 μg/mg for MTX/CRM and PTX/17-AAG combinations, respectively. Physical characterization of drug-loaded MSN by XRD and DSC confirmed that drug combinations were in the amorphous form. The drug release data confirmed that release of MTX was based on Fickian diffusion at pH 4.5, regardless of the presence or absence of CRM. In contrast, limited release was observed at pH 7.4 due to pH dependent solubility of MTX. Anticancer activity of PTX/17-AAG combination suggested that co-mixing of individually loaded nanoparticles is more effective than co-loading both drugs into the same nanoparticles. Our results show versatility and robustness of MSN as a drug delivery system in terms of delivering combinations of chemotherapeutic agents.

Future studies will further evaluate MSN formulations of hydrophilic-hydrophobic drug combinations. This research thus sets a strong foundation for future *in vivo* tumor suppression studies based on multi-drug delivery approach. In addition, MSN formulations can be developed to improve oral bioavailability of hydrophobic drug combinations considering its ability to improve aqueous solubility. Thus, these results would facilitate therapeutic applications of MSN as a combinatorial platform for multidrug chemotherapy.

REFERENCES

Arnida, Janat-Amsbury, M.M., Ray, A., Peterson, C.M., Ghandehari, H., 2011. Geometry and surface characteristics of gold nanoparticles influence their biodistribution and uptake by macrophages. Eur J Pharm Biopharm 77, 417-423.

Bauer, J., Spanton, S., Henry, R., Quick, J., Dziki, W., Porter, W., Morris, J., 2001. Ritonavir: An Extraordinary Example of Conformational Polymorphism. Pharm Res 18, 859-866.

Bergman, L., Rosenholm, J., st, A.-B., Duchanoy, A., Kankaanp, Pasi, Heino, J., Lind, n, M., 2008. On the Complexity of Electrostatic Suspension Stabilization of Functionalized Silica Nanoparticles for Biotargeting and Imaging Applications. Journal of Nanomaterials

Bhattarai, S.R., Muthuswamy, E., Wani, A., Brichacek, M., Castaneda, A.L., Brock, S.L., Oupicky, D., 2010. Enhanced Gene and siRNA Delivery by Polycation-Modified Mesoporous Silica Nanoparticles Loaded with Chloroquine. Pharmaceutical Research 27, 2556-2568.

Brannon-Peppas, L., 1995. Recent advances on the use of biodegradable microparticles and nanoparticles in controlled drug delivery. International Journal of Pharmaceutics 116, 1-9

Brigger, I.n., Dubernet, C., Couvreur, P., 2002. Nanoparticles in cancer therapy and diagnosis. Advanced Drug Delivery Reviews 54, 631-651.

Cauda, V., Argyo, C., Bein, T., 2010. Impact of different PEGylation patterns on the long-term bio-stability of colloidal mesoporous silica nanoparticles. Journal of Materials Chemistry 20, 8693-8699.

Charnay, C., Begu, S., Tourne-Peteilh, C., Nicole, L., Lerner, D.A., Devoisselle, J.M., 2004. Inclusion of ibuprofen in mesoporous templated silica: drug loading and release property. European Journal of Pharmaceutics and Biopharmaceutics 57, 533-540.

Chavanpatil, M.D., Patil, Y., Panyam, J., 2006. Susceptibility of nanoparticle-encapsulated PTX to P-glycoprotein-mediated drug efflux. International Journal of Pharmaceutics 320, 150-156.

Chen, A.M., Zhang, M., Wei, D., Stueber, D., Taratula, O., Minko, T., He, H., 2009a. Co-delivery of Doxorubicin and Bcl-2 siRNA by Mesoporous Silica Nanoparticles Enhances the Efficacy of Chemotherapy in Multidrug-Resistant Cancer Cells. Small 5, 2673-2677.

Chen, F., Zhu, Y., 2009. Chitosan enclosed mesoporous silica nanoparticles as drug nano-carriers: Sensitive response to the narrow pH range. Microporous and Mesoporous Materials 150, 83-89.

Chen, H.L., Yang, W.Z., Chen, H., Liu, L.R., Gao, F.P., Yang, X.D., Jiang, Q., Zhang, Q.Q., Wang, Y.S., 2009c. Surface modification of Mitoxantrone-loaded PLGA nanospheres with chitosan. Colloids Surf., B. 73, 212-218.

Costa, P., Sousa Lobo, J.M., 2001. Modeling and comparison of dissolution profiles. European Journal of Pharmaceutical Sciences 13, 123-133.

Cui, J.H., Ma, Y.H., Zhou, L., Zheng, H.Q., Xing, L., Li, C.G., Che, S.A., 2011. pH-responsive mitoxantrone (MX) delivery using mesoporous silica nanoparticles (MSN). Journal of Materials Chemistry 21, 9483-9486.

Davis, M.E., Brewster, M.E., 2004. Cyclodextrin-based pharmaceutics: past, present and future. Nat Rev Drug Discov 3, 1023-1035.

Davis, M.E., Chen, Z., Shin, D.M., 2008. Nanoparticle therapeutics: an emerging treatment modality for cancer. Nat. Rev. Drug Discov. 7, 771-782.

Deffie, A.M., Batra, J.K., Goldenberg, G.J., 1989. Direct correlation between DNA topoisomerase II activity and cytotoxicity in Adriamycin-sensitive and -resistant P388 leukemia cell lines. Cancer Research 49, 58-62.

Depan, D., Saikia, L., Singh, R.P., 2010. Ultrasound-Triggered Release of Ibuprofen from a Chitosan-Mesoporous Silica Composite- a Novel Approach for Controlled Drug Release. Macromolecular Symposia 287, 80-88.

Desai, N., Trieu, V., Yao, Z., Louie, L., Ci, S., Yang, A., Tao, C., De, T., Beals, B., Dykes, D., Noker, P., Yao, R., Labao, E., Hawkins, M., Soon-Shiong, P., 2006. Increased antitumor activity, intratumor paclitaxel concentrations, and endothelial cell transport of cremophor-free, albumin-bound paclitaxel, ABI-007, compared with cremophor-based paclitaxel. Clinical Cancer Research 12, 1317-1324.

Dhar, S., Gu, F.X., Langer, R., Farokhzad, O.C., Lippard, S.J., 2008. Targeted delivery of cisplatin to prostate cancer cells by aptamer functionalized Pt(IV) prodrug-PLGAâ€“PEG nanoparticles. Proceedings of the National Academy of Sciences 105, 17356-17361.

Di Pasqua, A.J., Sharma, K.K., Shi, Y.-L., Toms, B.B., Ouellette, W., Dabrowiak, J.C., Asefa, T., 2008. Cytotoxicity of mesoporous silica nanomaterials. Journal of Inorganic Biochemistry 102, 1416-1423.

Doadrio, J.C., Sousa, E.M.B., Izquierdo-Barba, I., Doadrio, A.L., Perez-Pariente, J., Vallet-Regi, M., 2006. Functionalization of mesoporous materials with long alkyl chains as a strategy for controlling drug delivery pattern. J. Mater. Chem. 16, 462-466.

Dobrovolskaia, M.A., Aggarwal, P., Hall, J.B., McNeil, S.E., 2008. Preclinical Studies To Understand Nanoparticle Interaction with the Immune System and Its Potential Effects on Nanoparticle Biodistribution. Molecular Pharmaceutics 5, 487-495.

Douglas, S.J., Illum, L., Davis, S.S., 1985. Particle size and size distribution of poly(butyl 2-cyanoacrylate) nanoparticles. II. Influence of stabilizers. Journal of Colloid and Interface Science 103, 154-163.

Ensign, L.M., Cone, R., Hanes, J., 2012. Oral drug delivery with polymeric nanoparticles: The gastrointestinal mucus barriers. Advanced Drug Delivery Reviews 64, 557-570.

Etienne, M., Walcarius, A., 2003. Analytical investigation of the chemical reactivity and stability of aminopropyl-grafted silica in aqueous medium. Talanta 59, 1173-1188.

Farokhzad, O.C., Langer, R., 2009. Impact of Nanotechnology on Drug Delivery. ACS Nano 3, 16-20.

Fatouros, D.G., Hatzidimitriou, K., Antimisiaris, S.G., 2001. Liposomes encapsulating prednisolone and prednisoloneâ€“cyclodextrin complexes: comparison of membrane integrity and drug release. European Journal of Pharmaceutical Sciences 13, 287-296.

Fernandez-Nunez, M., Zorrilla, D., Montes, A., Mosquera, M.J., 2009. Ibuprofen Loading in Surfactant-Templated Silica: Role of the Solvent According to the Polarizable Continuum Model. Journal of Physical Chemistry A 113, 11367-11375.

Ferrari, M., 2005. Cancer nanotechnology: Opportunities and challenges. Nature Reviews Cancer 5, 161-171.

Finnie, K., Waller, D., Perret, F., Krause-Heuer, A., Lin, H., Hanna, J., Barbé, C., 2009. Biodegradability of sol–gel silica microparticles for drug delivery. J. Sol-Gel Sci. Technol. 49, 12-18.

Fox, M.E., Szoka, F.C., FreÌ chet, J.M.J., 2009. Soluble Polymer Carriers for the Treatment of Cancer: The Importance of Molecular Architecture. Accounts of Chemical Research 42, 1141-1151.

Galarneau, A., Nader, M., Guenneau, F., Di Renzo, F., Gedeon, A., 2007. Understanding the Stability in Water of Mesoporous SBA-15 and MCM-41. J. Phys. Chem. C 111, 8268-8277.

Ganta, S., Amiji, M., 2009. Coadministration of Paclitaxel and Curcumin in Nanoemulsion Formulations To Overcome Multidrug Resistance in Tumor Cells. Molecular Pharmaceutics 6, 928-939.

Gao, F., Botella, P., Corma, A., Blesa, J., Dong, L., 2009. Monodispersed Mesoporous Silica Nanoparticles with Very Large Pores for Enhanced Adsorption and Release of DNA. The Journal of Physical Chemistry B 113, 1796-1804.

Geng, J., Li, M., Wu, L., Chen, C., Qu, X., 2012. Mesoporous Silica Nanoparticle-based H2O2 Responsive Controlled-Release System Used for Alzheimer's Disease Treatment. Advanced Healthcare Materials 1, 332-336.

Giri, S., Trewyn, B.G., Stellmaker, M.P., Lin, V.S.Y., 2005. Stimuli-Responsive Controlled-Release Delivery System Based on Mesoporous Silica Nanorods Capped with Magnetic Nanoparticles. Angewandte Chemie International Edition 44, 5038-5044.

Graf, C., Gao, Q., Schutz, I., Noufele, C.N., Ruan, W., Posselt, U., Korotianskiy, E., Nordmeyer, D., Rancan, F., Hadam, S., Vogt, A., Lademann, J.r., Haucke, V., Ruhl, E., 2012. Surface Functionalization of Silica Nanoparticles Supports Colloidal Stability in Physiological Media and Facilitates Internalization in Cells. Langmuir 28, 7598-7613.

Greish, K., 2007. Enhanced permeability and retention of macromolecular drugs in solid tumors: A royal gate for targeted anticancer nanomedicines. Journal of Drug Targeting 15, 457-464.

Ha, J.-M., Hamilton, B.D., Hillmyer, M.A., Ward, M.D., 2009. Phase Behavior and Polymorphism of Organic Crystals Confined within Nanoscale Chambers. Crystal Growth & Design 9, 4766-4777.

Hak, S., Helgesen, E., Hektoen, H.H., Huuse, E.M., Jarzyna, P.A., Mulder, W.J.M., Haraldseth, O., Davies, C.d.L., 2012. The Effect of Nanoparticle Polyethylene Glycol Surface Density on Ligand-Directed Tumor Targeting Studied in Vivo by Dual Modality Imaging. ACS Nano 6, 5648-5658.

Hansen, P.L., Cohen, J.A., Podgornik, R., Parsegian, V.A., 2003. Osmotic Properties of Poly(Ethylene Glycols): Quantitative Features of Brush and Bulk Scaling Laws. Biophysical Journal 84, 350-355.

Hartono, S.B., Gu, W.Y., Kleitz, F., Liu, J., He, L.Z., Middelberg, A.P.J., Yu, C.Z., Lu, G.Q., Qiao, S.Z., 2012. Poly-L-lysine Functionalized Large Pore Cubic Mesostructured Silica Nanoparticles as Biocompatible Carriers for Gene Delivery. Acs Nano 6, 2104-2117.

He, Q., Shi, J., Zhu, M., Chen, Y., Chen, F., 2010a. The three-stage in vitro degradation behavior of mesoporous silica in simulated body fluid. Microporous and Mesoporous Materials 131, 314-320.

He, Q., Zhang, J., Shi, J., Zhu, Z., Zhang, L., Bu, W., Guo, L., Chen, Y., 2010b. The effect of PEGylation of mesoporous silica nanoparticles on nonspecific binding of serum proteins and cellular responses. Biomaterials 31, 1085-1092.

He, Q., Zhang, Z., Gao, F., Li, Y., Shi, J., 2011. In vivo Biodistribution and Urinary Excretion of Mesoporous Silica Nanoparticles: Effects of Particle Size and PEGylation. Small 7, 271-280.

Heffernan, M.J., Murthy, N., 2005. Polyketal Nanoparticles:â€‰ A New pH-Sensitive Biodegradable Drug Delivery Vehicle. Bioconjugate Chemistry 16, 1340-1342.

Hu, Y., Zhi, Z., Zhao, Q., Wu, C., Zhao, P., Jiang, H., Jiang, T., Wang, S., 2012. 3D cubic mesoporous silica microsphere as a carrier for poorly soluble drug carvedilol. Microporous and Mesoporous Materials 147, 94-101.

Huang, D.-M., Hung, Y., Ko, B.-S., Hsu, S.-C., Chen, W.-H., Chien, C.-L., Tsai, C.-P., Kuo, C.-T., Kang, J.-C., Yang, C.-S., Mou, C.-Y., Chen, Y.-C., 2005. Highly efficient cellular labeling of mesoporous nanoparticles in human mesenchymal stem cells: implication for stem cell tracking. The FASEB Journal 19, 2014-2016.

Huang, X., Brazel, C.S., 2001. On the importance and mechanisms of burst release in matrix-controlled drug delivery systems. Journal of Controlled Release 73, 121-136.

Huang, X., Teng, X., Chen, D., Tang, F., He, J., 2009. The effect of the shape of mesoporous silica nanoparticles on cellular uptake and cell function. Biomaterials 31, 438-448.

Hudson, S.P., Padera, R.F., Langer, R., Kohane, D.S., 2008. The biocompatibility of mesoporous silicates. Biomaterials 29, 4045-4055.

Jabr-Milane, L.S., van Vlerken, L.E., Yadav, S., Amiji, M.M., 2008. Multi-functional nanocarriers to overcome tumor drug resistance. Cancer treatment reviews 34, 592-602.

Jackson, C.L., McKenna, G.B., 1996. Vitrification and Crystallization of Organic Liquids Confined to Nanoscale Pores. Chem. Mat. 8, 2128-2137.

Jugdaohsingh, R., Reffitt, D.M., Oldham, C., Day, J.P., Fifield, L.K., Thompson, R.P.H., Powell, J.J., 2000. Oligomeric but not monomeric silica prevents aluminum absorption in humans. Am. J. Clin. Nutr. 71, 944-949.

Kapoor, S., Hegde, R., Bhattacharyya, A.J., 2009. Influence of surface chemistry of mesoporous alumina with wide pore distribution on controlled drug release. J. Controlled Release 140, 34-39.

Kaufner, L., Cartier, R., Wustneck, R., Fichtner, I., Pietschmann, S., Bruhn, H., Schutt, D., Thunemann, A.F., Pison, U., 2007. Poly(ethylene oxide)-block-poly(glutamic acid) coated maghemite nanoparticles: in vitro characterization and in vivo behaviour. Nanotechnology 18.

Kawakami, K., 2012. Modification of physicochemical characteristics of active pharmaceutical ingredients and application of supersaturatable dosage forms for improving bioavailability of poorly absorbed drugs. Advanced Drug Delivery Reviews 64, 480-495.

Khdair, A., Handa, H., Mao, G., Panyam, J., 2009. Nanoparticle-mediated combination chemotherapy and photodynamic therapy overcomes tumor drug resistance in vitro. European Journal of Pharmaceutics and Biopharmaceutics 71, 214-222.

Kim, H., Kim, S., Park, C., Lee, H., Park, H.J., Kim, C., 2010. Glutathione-Induced Intracellular Release of Guests from Mesoporous Silica Nanocontainers with Cyclodextrin Gatekeepers. Advanced Materials 22, 4280-4283.

Knezevic, N.Z., Trewyn, B.G., Lin, V.S.Y., 2011. Functionalized mesoporous silica nanoparticle-based visible light responsive controlled release delivery system. Chem. Commun. 47, 2817-2819.

Korsmeyer, R.W., Gurny, R., Doelker, E., Buri, P., Peppas, N.A., 1983. Mechanisms of solute release from porous hydrophilic polymers. International Journal of Pharmaceutics 15, 25-35.

Kostrzewa-Nowak, D., Paine, M.J.I., Korytowska, A., Serwatka, K., Piotrowska, S., Wolf, C.R., Tarasiuk, J., 2007. Bioreductive activation of mitoxantrone by NADPH cytochrome P450 reductase. Implications for increasing its ability to inhibit the growth of sensitive and multidrug resistant leukaemia HL60 cells. Cancer Letters 245, 252-262.

Kotsuchibashi, Y., Ebara, M., Aoyagi, T., Narain, R., 2012. Fabrication of doubly responsive polymer functionalized silica nanoparticles via a simple thiol-ene click chemistry. Polymer Chemistry 3, 2545-2550.

Lai, C.-Y., Trewyn, B.G., Jeftinija, D.M., Jeftinija, K., Xu, S., Jeftinija, S., Lin, V.S.Y., 2003a. A Mesoporous Silica Nanosphere-Based Carrier System with Chemically Removable CdS Nanoparticle Caps for Stimuli-Responsive Controlled Release of Neurotransmitters and Drug Molecules. Journal of the American Chemical Society 125, 4451-4459.

Lai, C.Y., Trewyn, B.G., Jeftinija, D.M., Jeftinija, K., Xu, S., Jeftinija, S., Lin, V.S.Y., 2003b. A mesoporous silica nanosphere-based carrier system with chemically removable CdS nanoparticle caps for stimuli-responsive controlled release of neurotransmitters and drug molecules. J. Am. Chem. Soc. 125, 4451-4459.

Lammers, T., Kiessling, F., Hennink, W.E., Storm, G., 2012. Drug targeting to tumors: Principles, pitfalls and (pre-) clinical progress. Journal of Controlled Release 161, 175-187.

Law, S.L., Ho, C.K., Jang, T.F., Chang, P., Lin, F.M., 1996. Antitumor effect of mitoxantrone-containing liposomes. Int. J. Pharm. 128, 139-143.

Lee, J.H., Nan, A., 2012. Combination Drug Delivery Approaches in Metastatic Breast Cancer. Journal of Drug Delivery 2012, 17.

Li, L., Tang, F., Liu, H., Liu, T., Hao, N., Chen, D., Teng, X., He, J., 2010. In Vivo Delivery of Silica Nanorattle Encapsulated Docetaxel for Liver Cancer Therapy with Low Toxicity and High Efficacy. ACS Nano 4, 6874-6882.

Lin, V.S.Y., Slowing, I.I., Vivero-Escoto, J.L., Wu, C.W., 2008. Mesoporous silica nanoparticles as controlled release drug delivery and gene transfection carriers. Advanced Drug Delivery Reviews 60, 1278-1288.

Lin, Y.-S., Haynes, C.L., 2010. Impacts of Mesoporous Silica Nanoparticle Size, Pore Ordering, and Pore Integrity on Hemolytic Activity. Journal of the American Chemical Society 132, 4834-4842.

Liong, M., Lu, J., Kovochich, M., Xia, T., Ruehm, S.G., Nel, A.E., Tamanoi, F., Zink, J.I., 2008. Multifunctional Inorganic Nanoparticles for Imaging, Targeting, and Drug Delivery. ACS Nano 2, 889-896.

Liu, Q., Zhang, J.X., Sun, W., Xie, Q.R.B., Xia, W.L., Gu, H.C., 2012. Delivering hydrophilic and hydrophobic chemotherapeutics simultaneously by magnetic mesoporous silica nanoparticles to inhibit cancer cells. International Journal of Nanomedicine 7, 999-1013.

Liu, R., Liao, P., Liu, J., Feng, P., 2011. Responsive Polymer-Coated Mesoporous Silica as a pH-Sensitive Nanocarrier for Controlled Release. Langmuir 27, 3095-3099.

Liu, R., Zhang, Y., Zhao, X., Agarwal, A., Mueller, L.J., Feng, P.Y., 2010. pH-Responsive Nanogated Ensemble Based on Gold-Capped Mesoporous Silica through an Acid-Labile Acetal Linker. J. Am. Chem. Soc. 132, 1500-1501.

Lu, B., Xiong, S.B., Yang, H., Yin, X.D., Chao, R.B., 2006. Solid lipid nanoparticles of mitoxantrone for local injection against breast cancer and its lymph node metastases. European Journal of Pharmaceutical Sciences 28, 86-95.

Lu, J., Liong, M., Zink, J.I., Tamanoi, F., 2007a. Mesoporous Silica Nanoparticles as a Delivery System for Hydrophobic Anticancer Drugs. Small 3, 1341-1346.

Lu, J., Liong, M., Zink, J.I., Tamanoi, F., 2007b. Mesoporous silica nanoparticles as a delivery system for hydrophobic anticancer drugs. Small 3, 1341-1346.

Lu J, L.M., Li Z, Zink JI, Tamanoi F., 2010. Biocompatibility, Biodistribution, and Drug-Delivery Efficiency of Mesoporous Silica Nanoparticles for Cancer Therapy in Animals. Small 6, 1794-1805.

Ma, Y.H., Zhou, L., Zheng, H.Q., Xing, L., Li, C.G., Cui, J.H., Che, S.A., 2011. pH-responsive mitoxantrone (MX) delivery using mesoporous silica nanoparticles (MSN). J. Mater. Chem. 21, 9483-9486.

Manickam, D.S., Hirata, A., Putt, D.A., Lash, L.H., Hirata, F., OupickÃ½, D., 2008. Overexpression of Bcl-2 as a proxy redox stimulus to enhance activity of non-viral redox-responsive delivery vectors. Biomaterials 29, 2680-2688.

Martens, J.A., Mellaerts, R., Jammaer, J.A.G., Van Speybroeck, M., Chen, H., Van Humbeeck, J., Augustijns, P., Van den Mooter, G., 2008. Physical state of poorly water soluble therapeutic molecules loaded into SBA-15 ordered mesoporous silica carriers: A case study with itraconazole and ibuprofen. Langmuir 24, 8651-8659.

Martinez-Rivera, M., Siddik, Z.H., 2012. Resistance and gain-of-resistance phenotypes in cancers harboring wild-type p53. Biochemical Pharmacology 83, 1049-1062.

Matsumura, Y., Maeda, H., 1986. A New Concept for Macromolecular Therapeutics in Cancer Chemotherapy: Mechanism of Tumoritropic Accumulation of Proteins and the Antitumor Agent Smancs. Cancer Research 46, 6387-6392.

Mellaerts, R., Aerts, C.A., Humbeeck, J.V., Augustijns, P., den Mooter, G.V., Martens, J.A., 2007. Enhanced release of itraconazole from ordered mesoporous SBA-15 silica materials. Chemical Communications, 1375-1377.

Mellaerts, R., Jammaer, J.A.G., Van Speybroeck, M., Chen, H., Humbeeck, J.V., Augustijns, P., Van den Mooter, G., Martens, J.A., 2008a. Physical State of Poorly Water Soluble Therapeutic Molecules Loaded into SBA-15 Ordered Mesoporous Silica Carriers: A Case Study with Itraconazole and Ibuprofen. Langmuir 24, 8651-8659.

Mellaerts, R., Mols, R., Jammaer, J.A.G., Aerts, C.A., Annaert, P., Van Humbeeck, J., Van den Mooter, G., Augustijns, P., Martens, J.A., 2008b. Increasing the oral bioavailability of the poorly water soluble drug itraconazole with ordered mesoporous silica. European Journal of Pharmaceutics and Biopharmaceutics 69, 223-230.

Meng, H., Xue, M., Xia, T., Ji, Z., Tarn, D.Y., Zink, J.I., Nel, A.E., 2011a. Use of Size and a Copolymer Design Feature To Improve the Biodistribution and the Enhanced Permeability and Retention Effect of Doxorubicin-Loaded Mesoporous Silica Nanoparticles in a Murine Xenograft Tumor Model. ACS Nano 5, 4131-4144.

Meng, H., Xue, M., Xia, T., Zhao, Y.-L., Tamanoi, F., Stoddart, J.F., Zink, J.I., Nel, A.E., 2010a. Autonomous in Vitro Anticancer Drug Release from Mesoporous Silica Nanoparticles by pH-Sensitive Nanovalves. Journal of the American Chemical Society 132, 12690-12697.

Meng, H., Yang, S., Li, Z., Xia, T., Chen, J., Ji, Z., Zhang, H., Wang, X., Lin, S., Huang, C., Zhou, Z.H., Zink, J.I., Nel, A.E., 2011b. Aspect Ratio Determines the Quantity of Mesoporous Silica Nanoparticle Uptake by a Small GTPase-Dependent Macropinocytosis Mechanism. ACS Nano 5, 4434-4447.

Meng, H.A., Liong, M., Xia, T.A., Li, Z.X., Ji, Z.X., Zink, J.I., Nel, A.E., 2010b. Engineered Design of Mesoporous Silica Nanoparticles to Deliver Doxorubicin and P-Glycoprotein siRNA to Overcome Drug Resistance in a Cancer Cell Line. Acs Nano 4, 4539-4550.

Milane, L., Duan, Z., Amiji, M., 2011a. Development of EGFR-Targeted Polymer Blend Nanocarriers for Combination Paclitaxel/Lonidamine Delivery To Treat Multi-Drug Resistance in Human Breast and Ovarian Tumor Cells. Molecular Pharmaceutics 8, 185-203.

Milane, L., Ganesh, S., Shah, S., Duan, Z.-f., Amiji, M., 2011b. Multi-modal strategies for overcoming tumor drug resistance: Hypoxia, the Warburg effect, stem cells, and multifunctional nanotechnology. Journal of Controlled Release 155, 237-247.

Minko, S., 2006. Responsive polymer brushes. Polymer Reviews 46, 397-420.

Mitra, A., Lin, S., 2003. Effect of surfactant on fabrication and characterization of paclitaxel-loaded polybutylcyanoacrylate nanoparticulate delivery systems. Journal of Pharmacy and Pharmacology 55, 895-902.

Mortera, R., Fiorilli, S., Garrone, E., Verne, E., Onida, B., 2010. Pores occlusion in MCM-41 spheres immersed in SBF and the effect on ibuprofen delivery kinetics: A quantitative model. Chemical Engineering Journal 156, 184-192.

Muhammad, F., Guo, M., Qi, W., Sun, F., Wang, A., Guo, Y., Zhu, G., 2011. pH-Triggered Controlled Drug Release from Mesoporous Silica Nanoparticles via Intracelluar Dissolution of ZnO Nanolids. J. Am. Chem. Soc. 133, 8778–8781.

Munoz, B., Ramila, A., Perez-Pariente, J., Diaz, I., Vallet-Regi, M., 2003. MCM-41 organic modification as drug delivery rate regulator. Chem. Mater. 15, 500-503.

Muro, S., Garnacho, C., Champion, J.A., Leferovich, J., Gajewski, C., Schuchman, E.H., Mitragotri, S., Muzykantov, V.R., 2008. Control of Endothelial Targeting and Intracellular Delivery of Therapeutic Enzymes by Modulating the Size and Shape of ICAM-1-targeted Carriers. Mol Ther 16, 1450-1458.

Napierska, D., Thomassen, L.C.J., Rabolli, V., Lison, D., Gonzalez, L., Kirsch-Volders, M., Martens, J.A., Hoet, P.H., 2009. Size-Dependent Cytotoxicity of Monodisperse Silica Nanoparticles in Human Endothelial Cells. Small 5, 846-853.

Nasongkla, N., Bey, E., Ren, J., Ai, H., Khemtong, C., Guthi, J.S., Chin, S.-F., Sherry, A.D., Boothman, D.A., Gao, J., 2006. Multifunctional Polymeric Micelles as Cancer-Targeted, MRI-Ultrasensitive Drug Delivery Systems. Nano Letters 6, 2427-2430.

Oupicky, D., Bhattarai, S.R., Muthuswamy, E., Wani, A., Brichacek, M., Castaneda, A.L., Brock, S.L., 2010. Enhanced Gene and siRNA Delivery by Polycation-Modified Mesoporous Silica Nanoparticles Loaded with Chloroquine. Pharmaceutical Research 27, 2556-2568.

Pan, L., He, Q., Liu, J., Chen, Y., Ma, M., Zhang, L., Shi, J., 2012. Nuclear-Targeted Drug Delivery of TAT Peptide-Conjugated Monodisperse Mesoporous Silica Nanoparticles. Journal of the American Chemical Society 134, 5722-5725.

Panyam, J., Labhasetwar, V., 2003. Sustained Cytoplasmic Delivery of Drugs with Intracellular Receptors Using Biodegradable Nanoparticles. Molecular Pharmaceutics 1, 77-84.

Panyam, J., Williams, D., Dash, A., Leslie-Pelecky, D., Labhasetwar, V., 2004. Solid-state solubility influences encapsulation and release of hydrophobic drugs from PLGA/PLA nanoparticles. Journal of Pharmaceutical Sciences 93, 1804-1814.

Park, C., Oh, K., Lee, S.C., Kim, C., 2007. Controlled Release of Guest Molecules from Mesoporous Silica Particles Based on a pH-Responsive Polypseudorotaxane Motif. Angewandte Chemie International Edition 46, 1455-1457.

Park, E.K., Kim, S.Y., Lee, S.B., Lee, Y.M., 2005. Folate-conjugated methoxy poly(ethylene glycol)/poly(β)-caprolactone) amphiphilic block copolymeric micelles for tumor-targeted drug delivery. Journal of Controlled Release 109, 158-168.

Park, J.-H., Gu, L., von Maltzahn, G., Ruoslahti, E., Bhatia, S.N., Sailor, M.J., 2009a. Biodegradable luminescent porous silicon nanoparticles for in vivo applications. Nat. Mater. 8, 331-336.

Park, J., Fong, P.M., Lu, J., Russell, K.S., Booth, C.J., Saltzman, W.M., Fahmy, T.M., 2009b. PEGylated PLGA nanoparticles for the improved delivery of doxorubicin. Nanomed Nanotech Biol Med. 5, 410-418.

Park, J., Fong, P.M., Lu, J., Russell, K.S., Booth, C.J., Saltzman, W.M., Fahmy, T.M., 2009c. PEGylated PLGA nanoparticles for the improved delivery of doxorubicin. Nanomedicine: Nanotechnology, Biology and Medicine 5, 410-418.

Park, J.H., Gu, L., von Maltzahn, G., Ruoslahti, E., Bhatia, S.N., Sailor, M.J., 2009d. Biodegradable luminescent porous silicon nanoparticles for in vivo applications. Nature Materials 8, 331-336.

Parker, B.S., Buley, T., Evison, B.J., Cutts, S.M., Neumann, G.M., Iskander, M.N., Phillips, D.R., 2004. A molecular understanding of mitoxantrone-DNA adduct formation - Effect of cytosine methylation and flanking sequences. Journal of Biological Chemistry 279, 18814-18823.

Patil, Y., Sadhukha, T., Ma, L., Panyam, J., 2009. Nanoparticle-mediated simultaneous and targeted delivery of paclitaxel and tariquidar overcomes tumor drug resistance. Journal of Controlled Release 136, 21-29.

Petros, R.A., DeSimone, J.M., 2010. Strategies in the design of nanoparticles for therapeutic applications. Nat Rev Drug Discov 9, 615-627.

Poon, Z., Chang, D., Zhao, X., Hammond, P.T., 2011. Layer-by-Layer Nanoparticles with a pH-Sheddable Layer for in Vivo Targeting of Tumor Hypoxia. ACS Nano 5, 4284–4292.

Popat, A., Liu, J., Lu, G.Q., Qiao, S.Z., 2012. A pH-responsive drug delivery system based on chitosan coated mesoporous silica nanoparticles. Journal of Materials Chemistry 22, 11173-11178.

Pushkarev, V.M., Starenki, D.V., Saenko, V.A., Namba, H., Kurebayashi, J., Tronko, M.D., Yamashita, S., 2004. Molecular Mechanisms of the Effects of Low Concentrations of Taxol in Anaplastic Thyroid Cancer Cells. Endocrinology 145, 3143-3152.

Qian, K.K., Bogner, R.H., 2011. Application of mesoporous silicon dioxide and silicate in oral amorphous drug delivery systems. Journal of Pharmaceutical Sciences 101, 444-463.

Qu, F., Zhu, G., Huang, S., Li, S., Qiu, S., 2006. Effective Controlled Release of Captopril by Silylation of Mesoporous MCM-41. ChemPhysChem 7, 400-406.

Riikonen, J., Makila, E., Salonen, J., Lehto, V.P., 2009b. Determination of the Physical State of Drug Molecules in Mesoporous Silicon with Different Surface Chemistries. Langmuir 25, 6137-6142.

Roforth, M.M., Tan, C., 2008. Combination of rapamycin and 17-allylamino-17-demethoxygeldanamycin abrogates Akt activation and potentiates mTOR blockade in breast cancer cells. Anti-Cancer Drugs 19, 681-688.

Romberg, B., Hennink, W., Storm, G., 2008. Sheddable Coatings for Long-Circulating Nanoparticles. Pharmaceutical Research 25, 55-71.

Rosenholm, J.M., Peuhu, E., Bate-Eya, L.T., Eriksson, J.E., Sahlgren, C., Lindén, M., 2010a. Cancer-Cell-Specific Induction of Apoptosis Using Mesoporous Silica Nanoparticles as Drug-Delivery Vectors. Small 6, 1234-1241.

Rosenholm, J.M., Sahlgren, C., Linden, M., 2010b. Towards multifunctional, targeted drug delivery systems using mesoporous silica nanoparticles - opportunities & challenges. Nanoscale 2, 1870-1883.

Ruiz-Hernández, E., Baeza, A., Vallet-Regí, M.a., 2011. Smart Drug Delivery through DNA/Magnetic Nanoparticle Gates. ACS Nano 5, 1259-1266.

Ryan, S.a.M., Mantovani, G., Wang, X., Haddleton, D.M., Brayden, D.J., 2008. Advances in PEGylation of important biotech molecules: delivery aspects. Expert Opinion on Drug Delivery 5, 371-383.

Salonen, J., Paski, J., Vaha-Heikkila, K., Heikkila, T., Bjorkqvist, M., Lehto, V.P., 2005. Determination of drug load in porous silicon microparticles by calorimetry. Physica Status Solidi a-Applications and Materials Science 202, 1629-1633.

Schadlich, A., Caysa, H., Mueller, T., Tenambergen, F., Rose, C., Gopferich, A., Kuntsche, J., Mader, K., 2011. Tumor Accumulation of NIR Fluorescent PEG-PLA Nanoparticles: Impact of Particle Size and Human Xenograft Tumor Model. ACS Nano 5, 8710-8720.

Schlossbauer, A., Warncke, S., Gramlich, P.M.E., Kecht, J., Manetto, A., Carell, T., Bein, T., 2010. A Programmable DNA-Based Molecular Valve for Colloidal Mesoporous Silica. Angew. Chem., Int. Ed. Engl. 49, 4734-4737.

Schroeder, A., Heller, D.A., Winslow, M.M., Dahlman, J.E., Pratt, G.W., Langer, R., Jacks, T., Anderson, D.G., 2012. Treating metastatic cancer with nanotechnology. Nat Rev Cancer 12, 39-50.

Sengupta, S., Eavarone, D., Capila, I., Zhao, G., Watson, N., Kiziltepe, T., Sasisekharan, R., 2005. Temporal targeting of tumour cells and neovasculature with a nanoscale delivery system. Nature 436, 568-572.

Serajuddin, A.T.M., 1999. Solid dispersion of poorly water-soluble drugs: Early promises, subsequent problems, and recent breakthroughs. Journal of Pharmaceutical Sciences 88, 1058-1066.

Shahani, K., Panyam, J., 2011. Highly loaded, sustained-release microparticles of curcumin for chemoprevention. Journal of Pharmaceutical Sciences 100, 2599-2609.

Shahani, K., Swaminathan, S.K., Freeman, D., Blum, A., Ma, L., Panyam, J., 2010. Injectable Sustained Release Microparticles of Curcumin: A New Concept for Cancer Chemoprevention. Cancer Research 70, 4443-4452.

Sheihet, L., Garbuzenko, O.B., Bushman, J., Gounder, M.K., Minko, T., Kohn, J., 2012. Paclitaxel in tyrosine-derived nanospheres as a potential anti-cancer agent: In vivo evaluation of toxicity and efficacy in comparison with paclitaxel in Cremophor. European Journal of Pharmaceutical Sciences 45, 320-329.

Shen, S.-C., Ng, W., Shi, Z., Chia, L., Neoh, K., Tan, R., 2011. Mesoporous silica nanoparticle-functionalized poly(methyl methacrylate)-based bone cement for effective antibiotics delivery. Journal of Materials Science: Materials in Medicine 22, 2283-2292.

Shenoy, D., Little, S., Langer, R., Amiji, M., 2005. Poly(ethylene oxide)-Modified Poly(β-amino ester) Nanoparticles as a pH-Sensitive System for Tumor-Targeted Delivery of Hydrophobic Drugs. 1. In Vitro Evaluations. Molecular Pharmaceutics 2, 357-366.

Shi, J.L., Li, X., Zhang, L.X., Dong, X.P., Liang, J., 2007. Preparation of mesoporous calcium doped silica spheres with narrow size dispersion and their drug loading and degradation behavior. Microporous and Mesoporous Materials 102, 151-158.

Shin, H.-C., Alani, A.W.G., Cho, H., Bae, Y., Kolesar, J.M., Kwon, G.S., 2011. A 3-in-1 Polymeric Micelle Nanocontainer for Poorly Water-Soluble Drugs. Molecular Pharmaceutics 8, 1257-1265.

Singh, N., Karambelkar, A., Gu, L., Lin, K., Miller, J.S., Chen, C.S., Sailor, M.J., Bhatia, S.N., 2011. Bioresponsive Mesoporous Silica Nanoparticles for Triggered Drug Release. Journal of the American Chemical Society 133, 19582-19585.

Slowing, I., Trewyn, B.G., Lin, V.S.Y., 2006b. Effect of surface functionalization of MCM-41-type mesoporous silica nanoparticleson the endocytosis by human cancer cells. J. Am. Chem. Soc. 128, 14792-14793.

Slowing, I.I., Trewyn, B.G., Lin, V.S.Y., 2007. Mesoporous silica nanoparticles for intracellular delivery of membrane-impermeable proteins. Journal of the American Chemical Society 129, 8845-8849.

Slowing, I.I., Vivero-Escoto, J.L., Wu, C.-W., Lin, V.S.Y., 2008. Mesoporous silica nanoparticles as controlled release drug delivery and gene transfection carriers. Adv Drug Deliv Rev. 60, 1278-1288.

Slowing, I.I., Wu, C.-W., Vivero-Escoto, J.L., Lin, V.S.Y., 2009. Mesoporous Silica Nanoparticles for Reducing Hemolytic Activity Towards Mammalian Red Blood Cells. Small 5, 57-62.

Song, M.R., Li, Y.Y., Fai, C.L., Cui, S.M., Cui, B.A., 2011. The controlled release of tilmicosin from silica nanoparticles. Drug Dev. Ind. Pharm. 37, 714-718.

Susa, M., Iyer, A., Ryu, K., Hornicek, F., Mankin, H., Amiji, M., Duan, Z., 2009. Doxorubicin loaded Polymeric Nanoparticulate Delivery System to overcome drug resistance in osteosarcoma. BMC Cancer 9, 399.

Takano, R., Furumoto, K., Shiraki, K., Takata, N., Hayashi, Y., Aso, Y., Yamashita, S., 2008. Rate-Limiting Steps of Oral Absorption for Poorly Water-Soluble Drugs in Dogs; Prediction from a Miniscale Dissolution Test and a Physiologically-Based Computer Simulation. Pharmaceutical Research 25, 2334-2344.

Tannock, I.F., 2001. Tumor Physiology and Drug Resistance. Cancer and Metastasis Reviews 20, 123-132.

Tao, Z., Toms, B.B., Goodisman, J., Asefa, T., 2009. Mesoporosity and Functional Group Dependent Endocytosis and Cytotoxicity of Silica Nanomaterials. Chemical Research in Toxicology 22, 1869-1880.

ten Tije, A.J., Verweij, J., Loos, W.J., Sparreboom, A., 2003. Pharmacological Effects of Formulation Vehicles: Implications for Cancer Chemotherapy. Clinical Pharmacokinetics 42, 665-685.

Thomas, M.J.K., Slipper, I., Walunj, A., Jain, A., Favretto, M.E., Kallinteri, P., Douroumis, D., 2010. Inclusion of poorly soluble drugs in highly ordered mesoporous silica nanoparticles. International Journal of Pharmaceutics 387, 272-277.

Toh, Y.-M., Li, T.-K., Mitoxantrone Inhibits HIF-1Î± Expression in a Topoisomerase IIâ€“Independent Pathway. Clinical Cancer Research 17, 5026-5037.

Turturro, F., Von Burton, G., Friday, E., 2007. Hyperglycemia-Induced Thioredoxin-Interacting Protein Expression Differs in Breast Cancerâ€“Derived Cells and Regulates Paclitaxel IC50. Clinical Cancer Research 13, 3724-3730.

Vallet-Regí, M., 2006. Ordered Mesoporous Materials in the Context of Drug Delivery Systems and Bone Tissue Engineering. Chemistry – A European Journal 12, 5934-5943.

Vallet-Regi, M., Ramila, A., del Real, R.P., Parez-Pariente, J., 2000. A New Property of MCM-41: A Drug Delivery System. Chemistry of Materials 13, 308-311.

Van Dalen, E.C., van der Pal, H.J.H., Bakker, P.J.M., Caron, H.N., Kremer, L.C.M., 2004. Cumulative incidence and risk factors of mitoxantrone-induced cardiotoxicity in children: a systematic review. Eur. J. Cancer 40, 643-652.

Van Speybroeck, M., Barillaro, V., Thi, T.D., Mellaerts, R., Martens, J., Van Humbeeck, J., Vermant, J., Annaert, P., Van den Mooter, G., Augustijns, P., 2009. Ordered mesoporous silica material SBA-15: A broad-spectrum formulation platform for poorly soluble drugs. Journal of Pharmaceutical Sciences 98, 2648-2658.

Van Vlerken, L., Vyas, T., Amiji, M., 2007. Poly(ethylene glycol)-modified Nanocarriers for Tumor-targeted and Intracellular Delivery. Pharmaceutical Research 24, 1405-1414.

Viitala, R., Jokinen, M., Tuusa, S., Rosenholm, J.B., Jalonen, H., 2005. Adjustably bioresorbable sol-gel derived SiO2 matrices for release of large biologically active molecules. J. Sol-Gel Sci. Technol. 36, 147-156.

Vinu, A., Murugesan, V., Tangermann, O., Hartmann, M., 2004. Adsorption of Cytochrome c on Mesoporous Molecular Sieves: An Influence of pH, Pore Diameter, and Aluminum Incorporation. Chemistry of Materials 16, 3056-3065.

Vooturi, S.K., Dewal, M.B., Firestine, S.M., 2011. Examination of a synthetic benzophenone membrane-targeted antibiotic. Organic & Biomolecular Chemistry 9, 6367-6372.

Wang, J., Wang, B.M., Schwendeman, S.P., 2002. Characterization of the initial burst release of a model peptide from poly(d,l-lactide-co-glycolide) microspheres. Journal of Controlled Release 82, 289-307.

Wani, A., Muthuswamy, E., Savithra, G., Mao, G., Brock, S., Oupický, D., 2012. Surface Functionalization of Mesoporous Silica Nanoparticles Controls Loading and Release Behavior of Mitoxantrone. Pharmaceutical Research, 1-12.

Webb, B.A., Chimenti, M., Jacobson, M.P., Barber, D.L., 2011. Dysregulated pH: a perfect storm for cancer progression. Nat Rev Cancer 11, 671-677.

Willart, J.F., Descamps, M., 2008. Solid State Amorphization of Pharmaceuticals. Molecular Pharmaceutics 5, 905-920.

Xia, T., Kovochich, M., Liong, M., Meng, H., Kabehie, S., George, S., Zink, J.I., Nel, A.E., 2009a. Polyethyleneimine Coating Enhances the Cellular Uptake of Mesoporous Silica Nanoparticles and Allows Safe Delivery of siRNA and DNA Constructs. ACS Nano 3, 3273-3286.

Xia, T.A., Kovochich, M., Liong, M., Meng, H., Kabehie, S., George, S., Zink, J.I., Nel, A.E., 2009b. Polyethyleneimine Coating Enhances the Cellular Uptake of Mesoporous Silica Nanoparticles and Allows Safe Delivery of siRNA and DNA Constructs. Acs Nano 3, 3273-3286.

Xie, H., Smith, J., 2010. Fabrication of PLGA nanoparticles with a fluidic nanoprecipitation system. Journal of Nanobiotechnology 8, 18.

Yang, R., Yang, S.-G., Shim, W.-S., Cui, F., Cheng, G., Kim, I.-W., Kim, D.-D., Chung, S.-J., Shim, C.-K., 2009. Lung-specific delivery of paclitaxel by chitosan-modified PLGA nanoparticles via transient formation of microaggregates. Journal of Pharmaceutical Sciences 98, 970-984.

Yang, S.C., Ge, H.X., Hu, Y., Jiang, X.Q., Yang, C.Z., 2000. Formation of positively charged poly(butyl cyanoacrylate) nanoparticles stabilized with chitosan. Colloid & Polymer Science 278, 285-292.

Yang, T.-H., Yee, C.K., Amweg, M.L., Singh, S., Kendall, E.L., Dattelbaum, A.M., Shreve, A.P., Brinker, C.J., Parikh, A.N., 2007. Optical Detection of Ion-Channel-Induced Proton Transport in Supported Phospholipid Bilayers. Nano Letters 7, 2446-2451.

You, Y.Z., Kalebaila, K.K., Brock, S.L., Oupicky, D., 2008. Temperature-controlled uptake and release in PNIPAM-modified porous silica nanoparticles. Chemistry of Materials 20, 3354-3359.

Yu, L., 2001. Amorphous pharmaceutical solids: preparation, characterization and stabilization. Advanced Drug Delivery Reviews 48, 27-42.

Yu, T., Greish, K., McGill, L.D., Ray, A., Ghandehari, H., 2012. Influence of Geometry, Porosity, and Surface Characteristics of Silica Nanoparticles on Acute Toxicity: Their Vasculature Effect and Tolerance Threshold. ACS Nano 6, 2289-2301.

Yu, T., Malugin, A., Ghandehari, H., 2011. Impact of Silica Nanoparticle Design on Cellular Toxicity and Hemolytic Activity. Acs Nano 5, 5717-5728.

Zhang, Y., Zhi, Z., Jiang, T., Zhang, J., Wang, Z., Wang, S., 2010a. Spherical mesoporous silica nanoparticles for loading and release of the poorly water-soluble drug telmisartan. Journal of Controlled Release 145, 257-263.

Zhang, Z., Wang, L., Wang, J., Jiang, X., Li, X., Hu, Z., Ji, Y., Wu, X., Chen, C., 2012. Mesoporous Silica-Coated Gold Nanorods as a Light-Mediated Multifunctional Theranostic Platform for Cancer Treatment. Advanced Materials. **24**, 1418-1423.

Zhao, Y., Sun, X., Zhang, G., Trewyn, B.G., Slowing, I.I., Lin, V.S.Y., 2011. Interaction of Mesoporous Silica Nanoparticles with Human Red Blood Cell Membranes: Size and Surface Effects. ACS Nano. **5**, 1366-1375.

Zhu, C.-L., Lu, C.-H., Song, X.-Y., Yang, H.-H., Wang, X.-R., 2011. Bioresponsive Controlled Release Using Mesoporous Silica Nanoparticles Capped with Aptamer-Based Molecular Gate. J. Am. Chem. Soc. **133**, 1278–1281.

Zhu, S., Hong, M., Zhang, L., Tang, G., Jiang, Y., Pei, Y., 2010. PEGylated PAMAM Dendrimer-Doxorubicin Conjugates: In vitro Evaluation and & in vivo Tumor Accumulation. Pharmaceutical Research. **27**, 161-174.

ABSTRACT

FORMULATION DEVELOPMENT OF MESOPOROUS SILICA NANOPARTICLES AS AN INJECTABLE DELIVERY SYSTEM

by

AMIT WANI

May 2013

Advisor: Dr. David Oupický

Major: Pharmaceutical Sciences

Degree: PhD

Our ***long term goal*** is to develop a versatile and robust injectable carrier based on Mesoporous Silica Nanoparticles (MSN) for drug/drug combination therapies. The ***objective*** of my dissertation was to optimize surface functionality, particle shape and methods of colloidal stabilization of mesoporous silica by PEG for delivery of drug/drug combinations. This was achieved by pursuing the following three aims:

1. Optimize surface functionality of MSN for high drug loading and controlled release
2. Investigate the effect of particle shape and PEGylation on drug delivery in hypoxic tumor cells
3. Develop MSN capable of delivering drug/drug combinations

To investigate the effect of surface functionalization of MSN on crystallization, loading, release and activity of mitoxantrone (MTX), we synthesized thiol (SH), mixed thiol/amine (SH/NH_2) and amine (NH_2) functionalized MSN by sol-gel process. We observed that NH_2 modification of MSN has limited MTX loading. In contrast, modifications of MSN with SH resulted in significant enhancement of MTX loading. MTX loading was controlled by pH of the loading media and surface charge of MSN. The SH-MSN particles maintained a strong negative

charge due to silanol and thiol surface groups while amine modified MSN resulted in an overall positive charge. Differences in the loading were due to decrease in the electrostatic interaction between MTX and MSN. Based on the observed pH-dependence of MTX loading, we hypothesized that surface functionalization will provide a simple method of pH controlled MTX release from MSN. Indeed, we observed strong pH-dependence of MTX release in SHMSN with rapid release in acidic pH and very slow release in neutral pH. In comparison, MTX was released rapidly from NH_2-MSN regardless of the pH. Similar to loading, the differences in the release behavior are due to differences in interactions of the drug with the silica matrix. Another important aspect of mesoporous silica is amorphization or crystalline-to-amorphous transformation of drugs in the porous nanoconfinement. We found strong effect of surface functionalization of MSN on crystallization of MTX. In SH-MSN particles, MTX was found to be in the amorphous form while semi-crystalline MTX was present in the NH_2-MSN. This is a very interesting feature as surface functionalization serves as a simple tool to allow control over MTX loading, its crystallization and release profile.

After optimizing surface functionality, we investigated the effect of surface PEGylation and particle shape on loading and release profile of MTX in hypoxic tumor cells. We synthesized thiol functionalized mesoporous silica nanorods (MSNR) and stabilized them with different amount of covalently attached PEG. The focus on rod-shaped particles was based on studies showing beneficial properties of nanorods for increased blood circulation and tumor accumulation compared with spherical particles. We found that PEGylation decreased zeta potential of MSNR with improved colloidal stability but reduced overall MTX loading as a function of PEG content. PEGylation also increased the rate of MTX release compared to release from non PEGylated MSNR. We found that MTX had better anticancer activity in hypoxic than

normoxic conditions, while no clear effect of particle shape was observed. Flow cytometry study confirmed that increased activity of MTX formulations in hypoxic conditions was due to increased cell uptake and retention of the drug in the cells.

To achieve our long-term goal of developing a robust and versatile drug delivery carrier, we investigated feasibility of co-loading of hydrophilic hydrophobic and hydrophobic-hydrophobic drug combinations in MSN. We found that loading of hydrophobic molecules such as PTX and 17-AAG depends on the polarity of solvent, with less polar solvents improving drug loading. We have successfully co-loaded PTX and 17-AAG into the same particles. We observed that PEGylation decreases loading of hydrophobic molecules. We hypothesize that this decrease in the drug loading was due to blocking of access to the pores. This is a new observation and we are currently investigating alternative ways to stabilize co-loaded MSN without compromising drug loading.

Inorganic particles like MSN offer an interesting alternative to organic drug delivery systems like polymeric nanoparticles, micelles and liposomes due to high drug loading capacity and biocompatibility. We demonstrated the effect of surface functionalization and PEGylation of MSN on crystallization, drug loading and release, and colloidal stability. We showed effective delivery of MTX using PEGylated MSN in hypoxic conditions that has significant promise in the treatment of clinically important triple negative as well as estrogen positive breast cancers. We also showed MSN are capable of delivering drug-drug combinations for cancer treatment.

AUTOBIOGRAPHICAL STATEMENT

Education

2001-2005 Bachelor of Pharmacy; University of Pune, Maharashtra, India.

2007-2008 MS Pharmaceutical Sciences; Wayne State University, Detroit, MI.

2009-2013 Ph.D. Pharmaceutical Sciences; Wayne State University, Detroit, MI

Publications

1. A.Wani, E. Muthuswamy, L.H.G. Savitra, Dr. S. Brock, Dr. D. Oupicky. Surface functionalized Mesoporous Silica Nanoparticles (MSN) Controls Loading and Release of Mitoxantrone. Pharmaceutical Research, 29 (2012) page: 2407-2418.
2. M.B. Dewal, A. Wani, D. Oupicky, M.J. Rybak, S.M. Firestine. Thieno [2, 3-d] pyrimidinedione derivatives as potential antibacterial agents. European Journal of Medicinal Chemistry, 51 (2012) page: 145-153
3. S. Bhattarai, E. Muthuswamy, A. Wani, M. Brichacek, A. L. Castañeda, S. Brock, D. Oupicky Enhanced gene and siRNA delivery by polycation-modified mesoporous silica nanoparticles loaded with chloroquine Pharmaceutical Research 27 (2010) page 2556-2563.
4. R. Regmi, S. R. Bhattarai, C. Sudakar, A. Wani, R. Cunningham, P. P. Vaishnava, R. Naik, D. Oupický and G. Lawes Hyperthermia Controlled Rapid Drug Release from Thermosensitive Magnetic Microgels. Journal of Materials Chemistry, 20 (2010) page: 6158-6163.
5. A.Wani, L.H.G. Savitra, Dr. S. Brock, Dr. D. Oupicky. PEGylated Mesoporous Silica Nanorods (MSNR) for Mitoxantrone delivery to hypoxic tumor cells. To be submitted.
6. A. Wani, E. Muthuswamy, Dr. S. Brock, Dr. D. Oupicky. Is PEGylation of Mesoporous Silica Nanoparticles (MSN) a viable approach to deliver paclitaxel? To be submitted.

Awards

2010 GlaxoSmithKline (GSK) travel award for FIP-AAPS, New Orleans, LA.
2011 Graduate Student Professional Travel Award for AAPS conference, Washington D.C. from Wayne State University
2012 AAPS-IPEC Foundation Excipient Graduate Student Scholarship award
2012 AAiPS Student Scholars Award